STRONG GROUND MOTIONS FROM TWO HISTORICAL EARTHQUAKES: ARE THE SOILS TO BLAME?

by

JONATHAN P. MCKENNA

(under the direction of Robert B. Hawman)

ABSTRACT

Strong ground motions recorded throughout the San Francisco Bay Area from the Loma Prieta earthquake (1989) and the San Francisco earthquake (1906) show high correlations with sediment/soil characteristics. Transverse, radial and vertical acceleration compiled by the Strong Motion Database (SMDB) and shake maps produced by the Association of Bay Area Governments (ABAG) have been used to analyze the relationship between ground motion and the subsurface. Modified Mercalli Intensity (MMI) reveals better results than peak ground acceleration (pga). Pearson's correlation coefficient reveals general trends including a positive relationship between ground motion and depth to bedrock, drainage class, clay content, and texture and a negative relationship for age of deposit. Both cumulative logistic and multiple regression models show no simple relationship between MMI and distance from the earthquake epicenter as predicted by the Joyner-Boore model, suggesting other variables play a greater role in ground motion. Probabilistic seismic hazard maps and strong ground motion susceptibility maps are produced for a repeat of both earthquakes.

INDEX WORDS: 1906 San Francisco earthquake, 1989 Loma Prieta, peak ground acceleration, strong ground motion, modified Mercalli intensity.

STRONG GROUND MOTIONS FROM TWO HISTORICAL EARTHQUAKES: ARE THE SOILS TO BLAME?

by

JONATHAN P. MCKENNA

B.S., The University of Georgia, 1997

A Thesis Submitted to the Graduate Faculty of The University of Georgia in Partial Fulfillment of the Requirements for the Degree

MASTER OF SCIENCE

Athens, Georgia

2002

STRONG GROUND MOTIONS FROM TWO HISTORICAL EARTHQUAKES:

ARE THE SOILS TO BLAME?

by

JONATHAN P. MCKENNA

Approved:

Major Professor: Robert B. Hawman

Committee: E. Lynn Usery
Paul A. Schroeder

Electronic Version Approved:

Gordhan L. Patel
Dean of the Graduate School
The University of Georgia
May 2002

ACKNOWLEDGMENTS

I would like to thank Robert B. Hawman for his support and guidance during the course of my undergraduate and graduate career at The University of Georgia. I am very grateful to Jaxk H. Reeves, Stephen L. Rathbun, QiQi Lu and Zhi Wang for their interest, suggestions, help, and creativity toward my research in the field of statistics. I am also thankful for E. Lynn Usery's technical help with geographic information systems and Paul A. Schroeder's suggestions and guidance toward the completion of this thesis. I am forever in debt to Beatrice Stephens for her strong support and encouragement for me to complete this study. Most of all, I love my family for their moral and spiritual support as I traveled on this arduous adventure toward the completion of the degree: Master of Science.

TABLE OF CONTENTS

Page

LIST OF TABLES

LIST OF FIGURES

INTRODUCTION

The Loma Prieta, California, earthquake (Magnitude~7.1) of October 18, 1989, induced excessive ground motions causing "at least 63 deaths, more than 3,757 injuries, and damage estimated to exceed $5.9 billion" (Borcherdt et al. 1994). Amplified ground motions caused severe damage to unreinforced masonry buildings, highway overpasses, and bridges and caused liquefaction of soils, severe ground failure, and induced landsliding. Unbelievably, much of this damage occurred at distances greater than 100 km from the epicenter of the earthquake. An understanding of ground characteristics that caused this devastation is imperative when attempting to reduce the damage associated with earthquakes. This paper addresses different aspects of soils and unconsolidated sediments that may have been attributed to strong ground motions.

Damage varied with distance from faults and underlying geologic structures. Nevertheless, the majority of destruction and hence loss of life occurred over "soft soils"(Borcherdt, et al., 1995). Holmes et al., (1990) concluded that within the San Francisco Bay area, unreinforced masonry building damage was highest for sites with the greatest potential for amplification. The great San Francisco earthquake of 1906 also affected many of the same areas and the level of damage was observed to depend primarily on the underlying ground characteristics (Wood, 1908). The dynamic role geological deposits play on amplification of local and regional S-waves has been reemphasized by multiple devastating earthquakes of the 1980's in other parts of the world, including Mexico City and Leninakan, Armenia (Borcherdt, 1994).

A local assessment of the strong-motion recordings throughout the San Francisco Bay region reveals distinct variations in ground-motion characteristics dependant on local geologic deposits. A comparison of studies has shown that higher horizontal amplification occurs on soft sediment (Borcherdt and Glassmoyer, 1992; Cassidy et al., 1997; Aguire and Kjioro, 1997; and Hartzell 1998), and on soil or unconsolidated sediment (Boore and Joyner, 1991; Aguirre and Kjioro, 1997).

Quantifying the effects of amplified ground motion is essential for understanding the destruction that was focused in Santa Cruz and the Marina and Embarcadero Districts of San Francisco. Larger earthquakes will inevitably occur. The U.S. Geological Survey and other scientists predict that there is a "70% probability of at least one magnitude 6.7 or greater quake, capable of causing widespread damage, striking the San Francisco Bay region before 2030" (Michael et al., 1999). A better understanding of site amplification will result in more accurate earthquake hazard maps.

GEOLOGIC SETTING OF THE SAN FRANCISCO BAY

The San Francisco Bay basin is a northwest-trending graben bounded by the Hayward fault on the northeast and the San Andreas Fault on the southwest. The San Francisco Bay Area lies at the center of the graben. Bay mud, artificial fill, marshes, alluvial deposits, and coastal ranges surround the bay. The geology is complex in that a vast number of geological units reside in close proximity to one another. The geologic units range from Mesozoic plutonic and sedimentary rocks in the Coastal Ranges, to Holocene estuarine mud and alluvium on the perimeter of the bay. Mesozoic and Tertiary sedimentary rock sequences consisting of older bay sediments overlain by younger bay sediments underlie the graben (Borcherdt and Glassmoyer, 1992).

The geology can be generalized into six main units: Holocene Bay mud, Quaternary alluvium, Tertiary and Quaternary sedimentary rocks of the Santa Clara and Merced Formations, Mesozoic and Tertiary sedimentary rocks, Cretaceous granitic rocks, and the Cretaceous and Jurassic Franciscan Complex (Helly and Lajoie, 1979). These six generalized units can be further subdivided into 28 units on the basis of composition and physical properties.

Quaternary deposits occur in five general settings: (1) northwest trending deposits generally following structural features of the valley, (2) alluvial pediments that slope southwest from the eastern San Francisco Bay area hills and slope northwest from the San Francisco Peninsula hills, (3) dune deposits of Holocene and late Pleistocene age in the northern San Francisco Peninsula and Oakland area, (4) beach and terrace deposits trending along the Pacific Coast, and (5) estuarine deposits engulfing the San Francisco

Bay. The northwest trending deposits found on the large valley floors consist of alluvial sediments deposited by rivers on alluvial fans, flood plains, and basins. Thinner sedimentary deposits can be found in the smaller inter-montane valleys. Inter-fingering alluvial fans form a broad alluvial pediment along the eastern San Francisco Bay hills. Eolian deposits envelope the northern San Francisco Peninsula and coalesce with bay muds along the shoreline near Oakland. Coastal and estuarine areas contain deltaic sediment where rivers enter the San Francisco Bay and Pacific Ocean (Atwater et al, 1977; Rogers and Figures, 1991; Knudsen et al, 1997).

PREVIOUS RESEARCH

There are two basic approaches for estimating strong ground motions from earthquakes. The first is waveform modeling of a synthetic seismogram (e.g. Spudich and Hartzell, 1985; Aki et al., 1995), which can be applied to models that account for shaking duration and building response. The second is probabilistic seismic hazard analysis, (PSHA) (Cornell, 1968; Reiter, 1990) which uses a relatively simple parameter such as peak ground acceleration, spectral response, or intensity (e.g. Modified Mercalli Intensity, Rossi-Forel, or Aries Intensity). Both methods are valid and may be used to estimate earthquake hazards. The final output of a PSHA study oftentimes depicts the most destructive earthquake scenarios for specific sites. Waveform modeling results in hypothetical seismograms for the different scenarios. However, both PSHA and waveform modeling are usually reserved for point analyses and used to estimate site effects.

Site effects can be thought of as residual earthquake responses at a specific point on the earth after removing ground motions within the underlying bedrock. This is not a new concept. In fact, much of the current thinking stems back to 1815 when Daniel Drake observed that most of the ground shaking from the New Madrid earthquakes (1811-1812) occurred along the Mississippi and Ohio rivers. He even gave a valid explanation in saying, “the strata in both valleys are loose” (Drake, 1815, appendix p. 238). After the 1906 San Francisco earthquake, H.O. Wood (1908) concluded, “…the amount of damage produced by the earthquake…depended chiefly upon the geological

character of the ground. Where the surface was of solid rock, the shock produced little damage; whereas upon made land great violence was manifested…"

Despite these pioneering studies, it wasn't until 1970 that Borcherdt (1970) expanded on these ideas and introduced the sediment-to-bedrock spectral ratio to more clearly define site effects. Measurements of nuclear explosions from 37 sites in Nevada were analyzed. Peak ground acceleration for sites on "soil" (alluvium, fill / Bay mud) divided by sites on "hard rock" (sandstone, shale, Franciscan Complex) collectively became known as "spectral amplification" and it was shown that amplification is consistently greater on soil sites (Borcherdt, 1970).

Rogers et al. (1985) applied Borcherdt's spectral ratio technique to 157 three-component recordings of the 1971 San Fernando earthquake. This empirical study indicates that Quaternary thickness or depth to basement is a controlling factor in site amplification.

A major problem with identifying site effects using Borcherdt's technique is that many sites located on soil lack the necessary near-by bedrock site for calculating spectral amplification. Bonilla et al. (1997) used ratios of the horizontal to vertical component of strong ground motion with a path-effect correction to simultaneously solve for source and site effects for the 1994 Northridge earthquake. This method maps any differences between true and predicted source variations into the overall site response.

Joyner and Fumal (1985) recognized the importance of shallow geologic deposits to surficial ground motion. Excluding response due to scattering, reflections and attenuation, Joyner and Fumal propose that "energy along a tube of arrays is conserved, and the amplitude [of ground motion] is proportional to:

$$\frac{1}{\sqrt{\rho\beta}}$$

where ρ is density and β is shear-wave velocity of the material being analyzed. This spurred Tinsley and Fumal (1985) to take on the task of mapping the Quaternary geology of Los Angeles paying special attention to geologic age and soil texture.

Assuming that density does not vary with depth and assuming that shear-wave velocity averaged across the depth of a formation is equal to one-quarter the wavelength of the period of interest (as suggested by Joyner and Boore 1981), Fumal and Tinsley (1985) developed the first 1-Hz shear wave velocity hazard maps for Los Angeles. However, due to geotechnical shortcomings, a maximum depth of 30 m was all that could be achieved when attempting to estimate shear wave velocities at depth. In fact, only 33 drill holes were used to construct the initial 1-Hz shear wave velocity maps. Tinsley and Fumal had to reduce their model to a shear wave velocity averaged over the uppermost 30 m, thus increasing their borehole samples from 33 to 84. The 30-m shear wave velocity (V_{30}) for characterizing near surface ground effects was born. This is the current method for classifying sites in the 1994 National Earthquake Hazard Reduction Program (NEHRP) building code provisions (BSSC, 1995). Nevertheless, the inclusion of site effects in hazard analysis remains rudimentary. In fact, current building codes utilize rock-site hazard maps that employ a correction factor at a later stage.

OBJECTIVES OF STUDY

It is apparent that unconsolidated sediments and soils play a role in the amount of ground shaking felt at the surface. The purpose of this study was to address the following questions: (1) What are soil characteristics are responsible for amplified ground motion? (2) Can the variations within the soils be used to model ground motions? (4) Are the current soils maps detailed enough to model ground shaking? (5) Is the seismic monitoring network complete enough to learn how soils contribute to this phenomenon? (6) Can Modified Mercalli Intensity be used as input to model strong ground motions?

METHODS

To model strong ground motions, it is necessary to have several different types of data: (1) a study area in a seismically active area with a reliable and sufficiently sized seismic network, (2) recordings of strong ground motions from large historical earthquakes, (3) current soils maps that are spatially complete and contain reliable geotechnical information, (4) maps showing depth to the bedrock surface, (5) detailed information on the age of formation for Quaternary deposits, and (6) supplemental information such as spatially continuous maps showing Modified Mercalli Intensity, Arias Intensity or Rossi-Forrel Intensity.

The San Francisco Bay Area is located in a highly seismically active region and is subject to countless earthquakes from numerous faults including the San Andreas, Hayward, and Calaveras Faults. The Bay Area has been studied for decades and as a result, a number of geotechnical and geophysical maps have been created and are available to the public. For these reasons, the San Francisco Bay Area was chosen as the site for this study.

Earthquake Data

The Loma Prieta earthquake occurred on October 18, 1989 along a fault with a strike of 130°, a rake of 140°, and a dip of 70°. The quake, measuring magnitude 7.0, surface magnitude 7.1, and local magnitude 7.0 occurred at -121.88 longitude, and 37.04 latitude at a depth of 17.6 km, with a seismic moment of 3.0E+26 dyne-cm (Strong Motion Database, (1997).

Eighty-seven seismographs deployed by the United States Geological Survey (USGS), California Strong Motion Program (CSMP), University of California Berkeley (UCB), California Division of Transportation (CDOT), Stanford University (SU), and the Department of Veteran's Affairs (VA) recorded the earthquake. The Strong Motion Database (SMDB) has compiled all of these readings into one website (Strong Motion Database (1997). Figure 1 shows the location of each of these stations. Only the stations in and around the San Francisco Bay area were compiled for this study and are shown in Table 1.

Records of strong ground motion (Figure 2) contain valuable information about the ground shaking in 87 different sites throughout the San Francisco Bay Area. Information collected from each station includes peak ground acceleration (pga), component of ground motion (vertical, radial, or transverse), and orientation of the seismograph (azimuth) during the Loma Prieta earthquake. The coordinates of each station are obtained from the Strong Motion Database (SMDB). The criteria for seismic station location is as follows:

> "Stations in the SMDB are labeled as Free-Field (FF), Structure (STR), or Mixed (MIX). Free-Field stations are defined as either: (1) sensors located in specially designed instrument shelters and not in any other structure; (2) sensors located on the ground floor of 1-story or 2-story light structure buildings. Wood frame is preferable, but reinforced masonry is acceptable. Building is generally less than ~4000 sq. ft. in plan; (3) sensors located at the embankment, toe, or downstream from dams; or (4) sensors located at the embankment of bridges. Structure recordings (STR) are defined as either (1) sensors located in buildings that do not

conform to the above definition; or sensors located on bridge spans or dam crests" (Strong Motion Database (1997).

Recordings from FF seismographs were chosen over STR or MIX stations when available. Otherwise, recordings were used from the ground floor or basement. This information was used to devise two types of surfaces to spatially represent peak radial, transverse, and vertical surfaces: raw data, and soil/bedrock (divides out the effect of ground acceleration within the bedrock from ground acceleration due to soil effects).

Three continuous surfaces that reflect vertical, transverse and radial acceleration (the latter two comprise the horizontal components) were constructed from SMDB data for the Loma Prieta earthquake. These components were calculated as follows:

Radial (t) = ch2 (t)*cos(θ) + ch3 (t)*sin(θ)

Transverse (t) = -ch2 (t)*sin (θ) + ch3 (t) *cos(θ)

Where:

θ = phich2 –phirad

And ch2 (t) , and ch3 (t) are input accelerations in the horizontal component and ch1 (t) is the input acceleration in the vertical component.

Where:

ch2 = azimuth of ch2 (measured clockwise from North)

phirad = azimuth, shot to station, measured clockwise from North.(adopted from Robert Hawman, University of Georgia, Geology).

71 Stations were used to interpolate vertical, transverse, and radial surfaces for the San Francisco Bay Area (Table1). The surface area for this study area is more than 3600

km and interpolation between stations is only approximate at best. Surfer 5.0 was used to interpolate peak ground acceleration between stations. The different interpolation methods investigated were kriging, inverse distance to a power, and cubic convolution (Golden Software Inc., 1999). After agonizing debate and comparison, inverse distance to a power was chosen as the interpolation method. The result shows tighter peaks in the data as anomalies rather than smoothing the data between stations. Although kriging uses a more mathematical formula for interpolation, it smoothed the data to a greater degree. The resulting grids were assigned to the Geographic Lat/Long Coordinate system using the North American Datum 1927 (NAD27), and Clarke 1866 Spheroid. Figures 3, 4, and 5 show the vertical, transverse, and radial acceleration grids respectively.

Soil Data

The United States Department of Agriculture surveyed San Francisco and San Mateo counties in 1991 (Kashiwagi and Hokholt, 1991) and Oakland in 1981 (Welch, 1981). This information is grouped together into a package, which describes the soils. (For a complete description of the different soils, refer to Appendix A.). The soil maps for this study (Figs. 6-14) cover the 7.5-minute quadrangles of San Francisco North, San Francisco South, Palo Alto, San Mateo, Redwood, Woodside and Oakland. The maps were scanned as black and white tagged image file format (TIFF) files, georefrenced to their respective Digital Raster Graphics (DRGs) using Imagine, and saved as image files. Each DRG for the specific quadrangle can be downloaded from GIS Data Depot (1995) Each DRG was re-projected to the Geographic Lat/Long coordinate system using the North American Datum 1927 (NAD27), which is cast on the Clarke 1866 Spheroid. This is consistent with the USDA soil maps. These image files then were displayed in

ArcView and digitized as a polygon coverage (a coverage is defined as "a digital analog of a single map sheet forming the basic unit of data storage in Arc/Info. In a coverage, map features are stored as primary features, such as arcs, nodes, polygons, and label points, and secondary features, such as tics, extent, links, and annotation" (Environmental Systems, 1990)). The different fields added to the database table reflect clay content, drainage class, liquid limit, organic content, permeability, plasticity index, texture, and available water capacity. All the coverages were then merged together .

The attributes of the soil coverage are defined as:

Clay: Class variable representing percent clay in soil (1 = 0-5%, 2 = 5-10%, 3 = 10-15%, 4 = 15-20%, 5 = 20-25%, 6 = 25-30%, 7 = 30-35%, 8 = 35-40%, 9 = 40-45%, 10 = 45-50%, 11 = 50-55%, 12 = 55-60%, and 13 = >60%).

Drain: Class variable measuring drainage (1 indicates excessively drained and 7 indicates very poorly drained soils).

Liquid Limit: Water content (percentage) of a soil at the arbitrarily defined boundary between the liquid and plastic states.

Org: Organic content in soil (1 = <1%, 2 = 1-2%, 3 = 1-3%, 4 = 1-4%, 4 = 1-4%, 5 = 1-5%, 6 = 2-6%, 7 = 2-10%, 8 = 4-10%).

Perm: Permeability of water through soil, measured in inches/hour.

Plasticity Index: Water content (percentage) of a soil at the boundary between the plastic and brittle states.

Texture: Particle size of soil texture, measured on the Wentworth scale (10 = fine clay and –8 indicates boulders and variable sized particles)

Watcont: Water capacity of the soil, measured in inches/hour.

Intensity Maps

Because the goal of this study was to better understand which variables within soils and subsurface quaternary geology are responsible for strong ground motion variations, it was necessary to find a way to analyze the data at a large scale (1:24 000).

Modified Mercalli Intensity (MMI) is often calculated for destructive earthquakes and displayed as contoured intensity. All MMI maps used for this study were obtained from the Association of Bay Area Governments (ABAG) (ABAG Online, 1995). Two different types of maps are produced by ABAG. First, a computer model generates intensity maps for future earthquake scenarios. For a complete discussion of these models refer to Perkins and Boatwright (1995). The second type of map available from ABAG is an intensity map for two historical earthquakes: the Great San Francisco Earthquake (1906) and the Loma Prieta Earthquake (1989). These maps are produced by combining Modified Mercalli Intensity (MMI) information plus building destruction patterns and interpolated to a 100-meter grid. MMI is mapped by sending out pamphlets to people who experienced the quakes. These pamphlets contain questions about how the quake was felt by the people. Based on the public's response, a MMI Roman numeral (I-XII) is assigned to the mailing address of the person responding. Definitions for each intensity interval for the MMI can be found in Table 2.

In order to incorporate these maps into the GIS database, they had to be digitized. Each map displayed intensity values along with major and minor roads. These maps were purchased from ABAG and scanned as color TIFF files. These TIFF files were georeferenced to the roads of their respected DRG using Imagine software and saved as image files. The lat/long-referenced images were displayed in ArcView and digitized as

a polygon coverage using the MMI scale as attributes. These shapefiles were merged, then converted to a single grid with 100-meter pixels. Figures 15 and 16 show MMI for the 1906 and 1989 earthquakes respectively. ABAG maps were only available on a city-by-city basis, therefore, there are some gaps in the data.

Geologic Maps

An inherent problem in this study is deciding whether areas within the San Francisco are covered by soil/sediment material or if the area is a geologic outcrop. Soil scientists group areas with little rock outcrop as a specific soil type whereas geologists will classify the same area as a specific rock formation. The digital atlases used in this study are as follows: (1) Quaternary Geology and Liquefaction Susceptibility, San Francisco, California 1:100,000 Quadrangle: A digital database (Figure 17) (Knudsen et al., 1997), (2) Geology of the onshore part of San Mateo County, California: A digital database (Brabb et al., 1998), (3) Geologic Map and Map Database of Parts of Marin, San Francisco, Alameda, Contra Costa, and Sonoma Counties, California (Blake et al., 2000), and (4) Preliminary geologic map of the San Francisco South 7.5' quadrangle and part of the Hunters Point 7.5' quadrangle, San Francisco Bay area, California: A digital database (Bonilla, 1998).

The information derived from the first geologic database (Figure 17), is the age of formation for each deposit. Although all bedrock formations are grouped into one class called “br” (bedrock), the relative ages and descriptions of the unconsolidated deposits are more specific and detailed than the other geologic databases.

The relative ages of each deposit were calculated by dividing the average age of the deposit (years) by 10,000 years. Each geologic deposit was assigned an age

according to Table 3. This information was used to create a coverage called “Age” and used to relate each deposit by time period of formation. Figure 18 shows the age of formation for the study area.

The latter three coverages (2, 3 and 4) were merged. This new coverage named “geology” was used to derive a new map called NEHRP. NEHRP is the classification scheme devised by the National Earthquake Hazards Reduction Program and reflects the current codes that buildings must follow. This classification is based on the 30-m shear wave velocity (V_{30}) for characterizing near surface ground effects. Coverage’s 2,3 and 4 were recoded to match the NEHRP building codes (Borcherdt et. al., 1994) and the classification scheme of Wills *et* al. (2000) as a guide. Bedrock locations are shown in Figures 3-5. Figure 19 shows the NEHRP classification for San Francisco.

Soil/Bedrock Grids

Soil/bedrock grids refers to three different grids: radial/bedrock, transverse/bedrock and vertical/bedrock. These surfaces reflect the peak ground acceleration of soil/unconsolidated sediments with the acceleration due to the bedrock removed. They can be considered normalized acceleration grids because the effect of strong ground motions due to the bedrock is removed. These grids were created using the raw data grids (radial, transverse, and vertical acceleration), the bedrock map and the Loma Prieta epicenter point coverage (consisting of one point that lies on the epicenter of the Loma Prieta earthquake). First, the Loma Prieta point source was buffered at 2 km intervals out to a radial distance of 110 km. The process for creating a soil/bedrock began at the outermost ring (110-108 km interval) and ended at the innermost ring that coincided with the soil coverage extent (64-66 km). For each 2 km interval and each

acceleration component (radial, transverse, and vertical), the same process was performed. An example of how to create a soil/bedrock grid for radial acceleration occurring within the 110-108 km interval range (referred to as 110) can be referenced in Appendix B, example 1.

Depth to Bedrock

A very important aspect of my thesis involves the depth to the bedrock. Although not all deposits that lie above the bedrock are unconsolidated sediments and soils, this parameter is extremely important in my analyses because it represents the outer limit of the model. If soils and unconsolidated sediments do play a role in strong ground motions, then as the depth to bedrock goes to zero, the influence of these materials will also go to zero.

The only bedrock contour maps readily available to the public are "Bedrock-Surface Map of the San Francisco North Quadrangle" (Schlocker, 1961) and "Bedrock-Surface Map of the San Francisco South Quadrangle" (Bonilla, 1964). Although the maps are a product of two different geophysical studies, the elevations match up fairly well at the common boundary between the north and south quadrangles. The elevation contours are relative to mean sea level. Therefore, many contours have negative elevations. In order to preserve positive values, a dummy elevation of +10,000 feet was added to all elevations. Example 2 in Appendix B shows the method for creating a depth to bedrock grid. Figure 20 shows the final depth to bedrock grid.

ANALYSIS

Statistics Part I: Pearson's Correlation Coefficient

The main objective in this study is to evaluate correlations between strong ground motion and various characteristics of unconsolidated sediments and soils. In order to accomplish this task, correlations between the following variables were investigated:

Soil Characteristics vs. Raw Acceleration (Radial, Transverse, and Vertical)

Soil Characteristics vs. Soil/Bedrock Acceleration (Radial, Transverse, and Vertical)

Soil Characteristics vs. 1989 Loma Prieta Modified Mercalli Intensity

Soil Characteristics vs. 1906 San Francisco Modified Mercalli Intensity

Age vs. Raw Acceleration (Radial, Transverse, and Vertical)

Age vs. Soil/Bedrock Acceleration (Radial, Transverse, and Vertical)

Age vs. 1989 Loma Prieta Modified Mercalli Intensity

Age vs. 1906 San Francisco Modified Mercalli Intensity

Depth to bedrock vs. Raw Acceleration (Interpolated)

Depth to bedrock vs. Soil/Bedrock Acceleration (Interpolated)

Depth to bedrock vs. 1989 Loma Prieta Modified Mercalli Intensity

Depth to bedrock vs. 1906 San Francisco Modified Mercalli Intensity

Before beginning a statistical analysis, it is important to choose the appropriate test for the data. Parametric statistical tests are more powerful than non-parametric

statistical tests. However, they cannot be applied to all data sets. The assumptions behind parametric tests are that the dataset must be from un-biased, continuous, random samples from a population that is normally distributed.

There are many problems with this data set. Firstly, most of the soil data is ordinal or ranked data. Clay content is expressed as a soil that contains an amount of clay that falls within a range of values (i.e. clay content is reported in five percent intervals or 1-5%, 5-10%, 10-15% and so on). Because exact clay content could not be inferred from the data set, the data was recoded to reflect the relative magnitude of clay content with respect to one another (1 = 1-5%, 2 = 5-10%, 3 = 10-15%, etc.) This ranking of data results in an ordinal data set that can only be analyzed using a non-parametric statistical test. Table 4 is a list of the soil data and data type.

The use of modified Mercalli intensity grids is an obvious violation of the assumptions for parametric tests. This scale is a ranked description of local accounts and observations made during an individual earthquake event. Only a non-parametric test can be used when using this type of data.

Another inherent problem with these data (and thus many gis studies) is sampling from a population. Because continuous data contains an individual value for each pixel, and each pixel with a value is incorporated into the analyses, the entire population is analyzed as opposed to a subset of the population. The population is therefore not randomly sampled. Because this is a violation of the basic assumptions of parametric statistical tests, a non-parametric test is required when analyzing the entire population.

Due to the multiple violations of assumptions for parametric tests, a non-parametric correlation statistic, Spearman's Rank Correlation Coefficient (Zar, 1996) was

chosen for this analysis. Pearson's correlation coefficient was also calculated but was just used only for comparison against the results from Spearman's test. All significance values for Pearson's test are taken from Zar, 1996.

Example 3 in Appendix B demonstrates the method for calculating Spearman's Rank Correlation Coefficient for age and shaking intensity for the 1989 Loma Prieta quake at a distance from the epicenter between 70 and 80 km. The same technique is performed by replacing age with different soil variables (texture, organic content, percent clay, drainage class, plasticity index, liquid limit, available water content, and permeability) and depth and replacing Shaking Intensity (1989) with Shaking Intensity (1906), raw acceleration (vertical, transverse, and radial), and acceleration normalized by bedrock effects.

The objective of this analysis is six-fold.

1) Identify significant correlation coefficients at the 95% confidence level.
2) Identify positive or negative relationships.
3) Identify patterns that show significant correlation throughout the study range (10-110 km from the epicenter).
4) Identify patterns that show significant correlation for each different analytical method.
5) Identify which variables show consistent positive or negative relationships, have consistent correlation throughout the study range, and have significant correlation for each different analytical method.
6) Out of all the variables chosen from step 5, determine how important each variable is for predicting ground shaking.

In order to empirically calculate the effects that various ground parameters have on ground motions, a method for analyzing the statistics was necessary. First, all statistics are arranged in tables. These tables are grouped according to different categories: soil characteristics, depth to bedrock, and age. Each category is broken up to reflect the parameter tested: raw acceleration, normalized acceleration, and mercalli intensity shaking. Each table lists the correlation coefficient, p-value, and number of samples (N). All significant correlation's are in boldface. Next, the significant correlations are looked at separately and two yes/no questions are asked for each test.

1) Do at least half the tests reflect significant correlations?
2) Of the significant correlation's, are the slopes consistent (+/-)?

These questions are asked for each of the tests. The tables are arranged as follows:

Tables 5a-c: Depth to bedrock vs. Raw Acceleration (Radial, Transverse, and Vertical)

Tables 6a-b: Depth to bedrock vs. Soil/Bedrock Grids (Radial and Transverse)

Tables 7a-b: Depth to bedrock vs. Intensity Grids (1906 San Francisco, 1989 Loma Prieta)

Tables 8a-c: Soils vs. Raw Acceleration (Radial, Transverse, Vertical)

Tables 9a-b: Soils vs. Soil/Bedrock Acceleration (Radial, Transverse)

Tables 10a-b: Soils vs. Intensity Grids (1906 San Francisco, 1989 Loma Prieta)

Tables 11a-c: Age vs. Raw Acceleration (Radial, Transverse, Vertical)

Tables 12a-b: Age vs. Soil/Bedrock Acceleration (Radial, Transverse)

Tables 13a-b: Age vs. Intensity Grids (1906 San Francisco, 1989 Loma Prieta)

For each variable, the number of yes's and no's are tabulated and compared with each other. Statistics for the vertical component are included in the raw acceleration part of the analysis but were not used when adding the number of yes's and no's. Amplification of peak ground acceleration has been demonstrated for soils in the horizontal component, but not in the vertical component (Borcherdt and Glassmoyer 1992). A summary of these statistics is provided in Table 14.

Table 14 shows that the variables that show the highest correlation with ground shaking (in order of importance) are age, depth to bedrock, drainage class, clay content, and texture (with clay content and texture tying for fourth place). The statistics indicate that as the soils and sediments become older, less acceleration or ground shaking is observed. Also, a positive relationship is observed for depth to bedrock, drainage class, clay content and texture. So, the thicker, poorly drained, fine grained soils and sediments with high clay content exhibit excessive ground shaking and greater horizontal acceleration.

The statistics from this section reveal only general trends in the soils and sediments that are responsible for strong ground motions but what exactly is the contribution from each variable? Can one just look at individual variables contributing solely to amplified ground shaking or do some variables collectively excite seismic waves as they propagate through the subsurface. To answer these questions, the data were analyzed using multivariate statistical tests.

Statistics Part II: Multivariate Analysis

Exploratory Analysis of Modified Mercalli Intensity Data

Data were randomly collected from 310 sites in the San Francisco Bay Area (Figure 21). All of these sites have some records of Modified Mercalli Intensity for both the great San Francisco Earthquake (1906) and the Loma Prieta Earthquake (1989). Each site record was scanned to insure that each field contained a variable. If a site record did not contain data for each field, it was eliminated from the dataset. The final total number of sites used for this analysis is 89. For each of the 89 sites (Table 15), the following 12 variables were collected:

Site	Sk06	Sk89	Texture	Watcont	Perm	Org	Drain	Clay	Age	Depth	Ds06	Ds89
6	9	5	7.5	0.175	6	1	2	1	20570	911	6299	97670

where:

Site: 3 digit code

Sk06: A measurement on the Modified Mercalli Intensity scale of the 1906 quake. (7-10, with higher number being more damaging).

Sk89: A measurement on the Modified Mercalli Intensity scale of the 1989 quake. (5-8, with higher number being more damaging).

Texture: Particle size of soil texture, measured on the Wentworth scale.

Watcont: Water capacity of the soil, measured in inches/hour.

Perm: Permeability of water through soil, measured in inches/hour.

Org: Class Variable measuring % of organic matter in the soil (large is more).

Drain: Class variable measuring drainage (1 indicates excessively drained and 7 indicates very poorly drained soils).

Clay: Class variable representing percent clay in soil (larger numbers indicate higher percentage).

Age: Estimated age of deposit in 10,000 years.

Depth: Distance below surface to bedrock (feet).

Dist06: Distance in meters from site to 1906 epicenter.

Dist89: Distance in meters from site to 1989 epicenter.

There are several inherent problems with the data:

- The sites are all closer to the epicenter of the 1906 earthquake than they are to the epicenter of the 1989 earthquake.
- The six soil/sediment variables (texture, water content, permeability, organic content, drainage class, clay content) are all taken from USDA reports issued in 1981 and 1995. There is no guarantee that such measurements would be consistent for both 1989 and 1906. However, because geologic conditions change at a slow rate, these estimates are probably reasonable.
- There are 5 discrete predictor variables. But fortunately, permeability, organic content, drainage class, and clay content are ordered class variables and can be treated as continuous variables. The age variable is recoded to age = 1 if age = 20570; age = 0 otherwise. Therefore, age is an indicator variable and the other variables are treated as continuous.
- There is an outlier (site # 140) from a multiple regression model. Figures 22

through 25 show that site # 140 is a leveraged point with respect to organic content and clay content. The circled 'A' in these figures has much different clay and organic values than the other X-variables and could introduce error when determining the best fit of the regression model. This leveraged point is deleted from the database. In each figure, 'A' represents a site that occurred 1 time, 'B' represents a site that occurred 2 times,…'U' represents a site that occurred 21 times.

Experimental Design

The response variables are sk06 and sk89, measured in Modified Mercalli Intensity (MMI). There is a well-known formula which relates earthquake intensity and magnitude. The equation, called the *Joyner-Boore* (J-B) (Joyner and Boore, 1981) model is:

$$\ln(I)_j = A + B * Z - \ln(\sqrt{d_j^2 + X}) - C * \sqrt{d_j^2 + X} + e_j$$

Where I_j is the intensity of the earthquake at site j,

A and B are independent normally distributed random effects for the earthquake,

Z is the magnitude of the earthquake at the epicenter,

d_j is the distance from the epicenter to site j,

x is a non-linear 'adjustment' factor to make the fit better,

e_j's are random errors. They are independently normally distributed.

In this analysis, the response variable ln(I) is replaced by (MMI) since they have a strong linear relationship (Wald et al., 1999). The problem is that MMI is discrete. That makes the analysis complicated. However, since the response variable MMI is ordered

and it is constrained only by the values {7,8,9,10} in 1906 and {5,6,7,8} in 1989, the variables can still be treated as continuous.

The goal of this analysis is to obtain a significant improvement to the J-B model by including the 8 soil variables. First we fit the J-B model without the soil variables. In this case, the MMI variable is treated as continuous. Three models are implemented for each quake ($x = 0$).

$$MMI = b_0 + b_1 Z - \ln(\sqrt{d^2 + x}) + b_3 \sqrt{d^2 + x} + e \qquad \text{------ Model(*)}$$

$$MMI = b_0 + b_1 Z - b_2 \ln(\sqrt{d^2 + x}) + b_3 \sqrt{d^2 + x} + e \qquad \text{------ Model(**)}$$

$$MMI = b_0 + b_1 Z + b_3 \sqrt{d^2 + x} + e \qquad \text{------ Model(***)}$$

- In the above models, b_1 cannot be estimated from either series separately, since there is no variability in Z (it is either 7.9 or 7.1, respectively, for 1906 and 1989). However, the b_0's can be estimated separately for the three models and then the equations solved for a common b_0, b_1.

$$\text{Intercept (06)} = b_0 + b_1 * 7.9$$

$$\text{Intercept (89)} = b_0 + b_1 * 7.1$$

- In the above models, one would expect b_3 to be negative. This makes sense, since one would believe that as distance increases, the shaking would diminish. Whether the relationship is linear or not, one would certainly expect a negative

relationship between *MMI* and distance. The results are presented in Tables 16 and 17.

However, from Pearson correlation (Table 18) for 1906, the correlation between MMI and distance, although negative, is essentially zero. For the 1989 event, there is a strong correlation ($r = + 0.60$), but it is in the wrong direction. This says that the further one is from the epicenter, the worse the shaking will be!

Different x values were also tried, but the results are similar to $x = 0$. So, distance does not seem to predict Modified Mercalli Intensity at all as expected by the J-B equation. The reason for this may be that the sites are all close to the epicenter. The general epicentral region is within 50 kilometers of the epicenter. Figure 26 shows that all the sites for the 1906 event are located within 20 kilometers of the epicenter. Within this region, it is possible that distance is not important and geological conditions at the sites play an important role.

For the 1989 quake (Figure 27), much of the damage occurred at distances greater than 100 km from the epicenter. This is apparently due to artificial fill in the Marina District. In these areas the *MMI* is amplified and does not follow the typical relationship proposed by Joyner and Boore (1981). Therefore, distance is dropped from equation and the other 8 soil variables are used to try to explain *MMI* using the cumulative logistic model and a multiple regression model. *MMI* must be treated as a discrete variable for the cumulative logistic model and must be treated as continuous for the multiple regression models.

Cumulative Logit Models (with same slope)

The logistic regression model is simply a non-linear transformation of the linear regression. The "logistic" distribution is an S-shaped distribution function, which is similar to the standard-normal distribution (which results in a probit regression model) but easier to work with in most applications (the probabilities are easier to calculate). The logit distribution constrains the estimated probabilities to lie between 0 and 1 (Stockburger, 1998).

1906 San Francisco Earthquake

⇒ Choose the best model using the cumulative logit procedure at the 95% confidence level. This procedure shows that the variables (watercont, ages, and depth to bedrock) are significant at the $\alpha = 0.05$ level for the 1906 event. The most significant variable is age and the least significant is texture.

the least significant $\rightarrow \rightarrow \rightarrow \rightarrow \rightarrow$						*the most significant*
texture	clay	drainage	organic	permeability	**depth**	**watercontent**	**age**

⇒ Test the null hypothesis that it is permissible to reduce the full model to a three-variable (watercontent, ages, depth) model.

Test statistic = deviance(reduced)-deviance(full)

= 172.552 – 166.523

= 6.032

The critical value is X^2 (0.05,5) = 11.07.

Since T.S. = 6.032 < 11.07, we can not reject the null hypothesis (i.e. it is permissible to drop from the full model to the reduced model.

$\Rightarrow$ Cumulative logit models for 1906 are as follows:

$\ln(p_7 / p_8 + p_9 + p_{10}) = -3.0559 + 0.1126*watcont + 2.5876*age - 0.00119*depth$

$\ln(p_7 + p_8 / p_9 + p_{10}) = -1.1035 + 0.1126*watcont + 2.5876*age - 0.00119*depth$

$\ln(p_7 + p_8 + p_9 / p_{10}) = 2.4776 + 0.1126*watcont + 2.5876*age - 0.00119*depth$

Where the p_7 is the probability of the MMI = 7;

the p_8 is the probability of the MMI = 8;

the p_9 is the probability of the MMI = 9;

the p_{10} is the probability of the MMI = 10.

These models indicate that the lower the water capacity of the soil the greater the amplification of ground shaking; the younger (less consolidated deposits) the soil, the more amplification of ground shaking; the greater the bedrock depth, the more amplification of ground shaking.

To show the effects of the combination of water content, age, and depth to bedrock, the distribution estimates from these combinations are compared to the original (marginal) distribution (Fig. 28). The typical distribution (Fig. 29) is similar to the original distribution since the typical combination is from the medians of water content, age, and depth. Fig. 30 shows the most dangerous respondent and Fig. 31 shows the least

dangerous respondent (where the maximums and minimums of water content, age, and depth are plugged into the probability formulas respectively).

Table 19 suggests that (8 + 10 + 37 + 0) / 88 = 62.5% of all sampled sites were predicted correctly.

1989 Loma Prieta Earthquake

⇒ Choose the best model using the cumulative logit procedure at the 95% confidence level. This procedure shows that the variables (permeability, organic content, drainage class, and age) are significant at the $\alpha = 0.05$ for the 1989 quake. The most significant variable is permeability and the least significant variable is texture. Note that texture was also the least significant variable in the 1906 analysis.

The least significant → → → → the most significant
Texture watcont depth clay **ages organic drainage permeability**

⇒ Test the null hypothesis that it is permissible to reduce from the full model to a four-variable (permeability, organic, drainage class, and age) model.

Test statistic = deviance (reduced) – deviance (full)

= 170.662 – 167.604

= 3.058

The critical value is X^2 (0.05, 4) = 9.49

Since T.S. = 3.058 < 9.49, we can not reject the null hypothesis (i.e., it is permissible to drop from the full model to a reduced model).

$\Rightarrow$ Cumulative logit models for 1989 are:

$\ln(p_5 / p_6 + p_7 + p_8) = 5.7161 - 1.129*perm - 0.653*org - 0.597*drain + 1.4743*\text{age}$

$\ln(p_5 + p_6 / p_7 + p_8) = 9.091 - 1.129*perm - 0.653*org - 0.597*drain + 1.4743*\text{age}$

$\ln(p_5 + p_6 + p_7 / p_8) = 11.212 - 1.129*perm - 0.653*org - 0.597*drain + 1.4743*age$

Where the p_5 is the probability of the MMI = 5;

the p_6 is the probability of the MMI = 6;

the p_7 is the probability of the MMI = 7;

the p_8 is the probability of the MMI = 8.

These models indicate that the lower the permeability of water through soil, the greater the amplification of ground shaking; the lower the organic matter in soil, the more amplification of ground shaking; the lower the drainage class, the more amplification of ground shaking; the younger (more unconsolidated) the soil, the more amplification of ground shaking. It is anticipated that the two earthquakes would pick the same significant variables, but only 'age' is common. If the soil is young, it appears that the site is more susceptible to damage.

To show the effects of the combination of permeability, organic content, drainage class, and soil age, the distribution estimates by these combinations are compared to the original (marginal) distribution. The typical distribution (Fig. 33) is similar to the original distribution (Fig. 32) since the typical distribution is from the medians of permeability, organic content, drainage class, and age. Fig. 34 shows the most dangerous respondent and Fig. 35 shows the least dangerous respondent for the 1989 quake.

Table 20 suggests that (13 + 16 + 22 + 0)/ 89 = 57.3% of all sampled sites are predicted correctly.

Multiple Regression Models

Multiple regression fits data to the following equation, where each Xi represents a different X variable:

$Y = ß0 + ß1X1 + ß2X2 + ß3X3 + ß4X4 \ldots + \text{random scatter}$

If there is only a single X variable, then the equation is $Y = ß0 + ß1X1$, and the "multiple regression" analysis is the same as simple linear regression (ß0 is the Y intercept; ß1 is the slope) (Stockburger, 1996).

The multiple regression model gives similar results to the logistical model. The signs of the regression coefficients are reversed from those of the logistical models. This is because the cumulative logit models use the high levels of response variables as the baseline. However, the interpretation is similar.

1906 San Francisco Earthquake

⇒ The multiple regression model is:

Sk06 = 8.806 – 0.042*watcont – 0.92*age + 0.000396*depth

This model includes the same explanatory variables as the logistic model.

⇒ Composite F-test for testing the null hypothesis that it is permissible to reduce from the full model to the three variable (watcont, age, and depth) model.

$$F = \frac{[\ SSE(\text{reduced}) - SSE(\text{full})\ ] / [\ d.f.e.(\text{reduced}) - d.f.e.\ (\text{full})\ ]}{MSE(\text{full})}$$

$$F = \frac{(42.886 - 39.678) / (85 - 80)}{0.49598}$$

≈ 1.294

The critical value is F (0.05,5,80) ≈ 2.30.

Since F ≈ 1.294<2.30, the null hypothesis cannot be rejected (i.e., it is permissible to drop from the full model to the reduced model).

Table 21 suggests that (3 + 14 + 31 + 0) / 89 = 53.9% of all ground shaking at the sampled sites is predicted correctly by the multiple regression model.

1989 Loma Prieta Earthquake

⇒ The multiple regression model for the 1989 quake is:

Sk89 = 5.934 + 0.195*perm – 0.951*age.

This model includes only 2 explanatory variables.

⇒ Composite F-test for testing the null hypothesis that it is permissible to reduce the full model to a 2 variable (permeability and age) model.

$$F = \frac{(42.249 - 38.386) / (86 - 80)}{0.47983}$$

≈ 1.342

The critical value is F (0.05,6,80) ≈ 2.20.

Since F ≈ 1.342 < 2.20, the null hypothesis cannot be rejected (i.e., it is permissible to drop from the full model to the reduced model).

Table 22 suggests that (13 + 15 + 22 + 0) / 89 = 52.6% of all ground shaking at the sampled sites is predicted correctly.

By comparing the rate predicted correctly by the cumulative logistical models with those predicted correctly by the multiple regression model (for 1906, 62.5% > 53.9% and for 1989, 57.3% > 52.6%), the cumulative logistical models are preferred.

The cumulative logistical models assume that the random errors have the multinomial distribution, but the multiple regression models assume normally distributed errors.

Conclusions

- For the data set, distance does not correlate with Modified Mercalli Intensity as predicted by the Joyner-Boore model.
- When the ln(I) in the Joyner-Boore model is replaced by the discrete *MMI*, the cumulative logistical models could be more appropriate than the multiple regression models.
- For 1906 and 1989 earthquakes, only variable ‘age’ is significant in both models.

MODELING

In an earlier study of strong ground motions from the 1989 Loma Prieta earthquake (Hough et al., 1990) it was noted that "the collapsed section of the two-tiered Nimitz Freeway in Oakland was built on San Francisco Bay mud, whereas stiffer alluvial sediments underlie a southern section that was damaged but did not collapse…and ...that soil conditions and resulting ground-motion amplification may have contributed significantly to the failure of the structure." The destruction is almost perfectly correlated to the Quaternary geology and suggests that a drastic change in site amplification occurs at the geologic contact.

Due to the coarse spacing of seismographs that recorded the 1989 earthquake, it is likely that variations in peak ground acceleration were not adequately sampled, therefore correlation with quaternary geology cannot be established. Interpolation of pga between seismic monitoring stations may only reveal general trends in the underlying geology and may not be suitable for a study (like this one) at the 1:24,000 scales. Therefore, more confidence is placed on the results of the Modified Mercalli Intensity analyses. This section is dedicated to modeling the results of the cumulative logit and multiple regression statistical tests for both the 1989 and 1906 earthquakes that occurred in San Francisco.

An ArcGIS subsystem, GRID, performs operations on grids. A grid is defined as "a cellular-based data structure composed of cells or pixels of equal size arranged in columns and rows. The value of each cell, or group of cells, represents the feature

value." (ESRI, 1990). In order to model the results of the cumulative logit and multiple regression models for the 1906 and 1989 earthquakes, several grids have to be created.

The intensity maps provided by ABAG are grids with 100 m grid cells. To model predicted intensity, each grid (representing the different ground characteristics) is produced with 100 m grid cells. All grids are produced from the original datasets that are first re-projected to the Universal Transverse Mercator (UTM) WGS84 coordinate system.

The UTM system divides the earth into 60 zones of 6 degrees of longitude. Each zone is divided into horizontal bands spanning 8 degrees of latitude. A square grid is superimposed on each 6° x 8° section. It's aligned so that vertical grid lines are parallel to the center of the zone, called the central meridian. UTM grid coordinates are expressed as a distance in meters to the east, referred to as the "easting", and a distance in meters to the north, referred to as the "northing". The square grid is ideal for converting data into grids.

Six grids were created before beginning the modeling process. The features represented for these grids reflect age of formation, depth to bedrock, drainage class, organic content, permeability, and available water capacity. The age and depth grids are spatially complete due to the completeness of coverage from the original datasets. The latter four features: drainage class, organic content, permeability, and available water capacity are not spatially complete datasets. That is, the original soil maps do not contain information for every mapped polygon. The no data locations for drainage class, organic

content, permeability, and available water capacity are shown in Figures 8, 10, 11, and 14 respectively.

Geology (Figure 17) was used as a guide for estimating the values of each feature where a "hole" exists. First, soil polygons with unknown values were identified and grouped according to the type of geologic unit on which they are located. Because the database contains information for much of the San Francisco Bay area, the GIS was queried to reveal the most common value (drainage class, organic content, permeability, and available water capacity) associated with that particular geologic unit. Table 23 shows the values used for each geologic unit.

A new spatially complete grid is created for each soil variable and reflects age of formation, depth to bedrock, drainage class, organic content, permeability, and available water capacity and will now be referred to as age, depth, drain, organic, perm, and water respectively.

Cumulative logit models (with same slope)

The best-fit cumulative logit model for 1906 is given by:

$$\ln(p_7 / p_8 + p_9 + p_{10}) = -3.0559 + 0.1126*watcont + 2.5876*age - 0.00119*depth$$

$$\ln(p_7 + p_8 / p_9 + p_{10}) = -1.1035 + 0.1126*watcont + 2.5876*age - 0.00119*depth$$

$$\ln(p_7 + p_8 + p_9 / p_{10}) = 2.4776 + 0.1126*watcont + 2.5876*age - 0.00119*depth$$

Because $p_7 + p_8 + p_9 + p_{10} = 1$,

these formulas can be rearranged to solve for p_7, p_8, p_9, and p_{10} where:

$$p_7 = \frac{e^{-3.0559 + 0.1126*watcont + 2.5876*age \; 0.00119*depth}}{1 + e^{-3.0559 + 0.1126*watcont + 2.5876*age \; 0.00119*depth}},$$

$$p_8 = \frac{e^{-1.1035 + 0.1126*\text{watcont} + 2.5876*\text{age}\ \ 0.00119*\text{depth}} - p_7(e^{-1.1035 + 0.1126*\text{watcont} + 2.5876*\text{age}\ \ 0.00119*\text{depth}} + 1)}{1 + e^{-1.1035 + 0.1126*\text{watcont} + 2.5876*\text{age}\ \ 0.00119*\text{depth}}},$$

$$p_9 = \frac{e^{2.4776 + 0.1126*\text{watcont} + 2.5876*\text{age}\ \ 0.00119*\text{depth}}(1 - p_7 - p_8) - p_7 - p_8}{1 + e^{2.4776 + 0.1126*\text{watcont} + 2.5876*\text{age}\ \ 0.00119*\text{depth}}}, \text{ and}$$

$p_{10} = 1 - (p_9 + p_8 + p_7)$.

The probability (p_7, p_8 ,p_9,and p_{10}) of having ground shaking intensity of magnitudes 7, 8, 9, and 10 respectively can be modeled in GRID using ArcGIS.

Complex mathematical equations can be handled in GRID and multiple grids can be used for each expression. By substituting the grid path name for each variable (watcont, age, and depth) in the above formulas, four new grids are created. These new 100 m grids (Figures 36-39) are called pseven, peight, pnine, and pten, and represent the probabilities of experiencing MMI of seven, eight, nine, or ten respectively for a repeat of the 1906 San Francisco earthquake.

These probability maps are somewhat misleading. For example, a person living along the northern part of San Francisco near the Golden Gate Bridge might pick up the pten map and think to himself or herself that they are safe because they only have an 8% chance of experiencing a MMI of 10 for a repeat of the 1906 San Francisco earthquake. Although the probability of experiencing a MMI of 10 is low in this location, the probability of experiencing a MMI of 8 is 69%. To reduce confusion, two more grids are created. Figure 36 and Figure 37 show the probabilities of experiencing MMI > 7 and MMI > 8 respectively for a repeat of the 1906 event. The grid in Fig. 36 (MMI > 7) is created by simply adding peight + pnine + pten. Similarly, the grid in Fig. 37 (MMI > 8) is created by adding pnine + pten. The probability of experiencing MMI of > 9 is just the pten grid (fig. 38).

The same method is implemented for calculating MMI probabilities for the 1989 Loma Prieta earthquake. The best-fit cumulative logit model for 1989 is given by:

$\ln(p_5 / p_6 + p_7 + p_8) = 5.7161 - 1.129*perm - 0.653*org - 0.597*drain + 1.4743*age$

$\ln(p_5 + p_6 / p_7 + p_8) = 9.091 - 1.129*perm - 0.653*org - 0.597*drain + 1.4743*age$

$\ln(p_5 + p_6 + p_7 / p_8) = 11.212 - 1.129*perm - 0.653*org - 0.597*drain + 1.4743*age$

Because $p_5 + p_6 + p_7 + p_8 = 1$,

these formulas can be rearranged to solve for p_5, p_6, p_7, and p_8 where:

$$p_5 = \frac{e^{5.7161\ 1.129*perm\ \ 0.653*org\ \ 0.597*drain + 1.4743*age}}{1 + e^{5.7161\ 1.129*perm\ \ 0.653*org\ \ 0.597*drain + 1.4743*age}},$$

$$p_6 = \frac{e^{9.091\ 1.129*perm\ \ 0.653*org\ \ 0.597*drain + 1.4743*age} - p_7(e^{9.091\ 1.129*perm\ \ 0.653*org\ \ 0.597*drain + 1.4743*age} + 1)}{1 + e^{9.091\ 1.129*perm\ \ 0.653*org\ \ 0.597*drain + 1.4743*age}},$$

$$p_7 = \frac{e^{11.212\ 1.129*perm\ \ 0.653*org\ \ 0.597*drain + 1.4743*age}(1 - p_7 - p_8) - p_7 - p_8}{1 + e^{11.212\ 1.129*perm\ \ 0.653*org\ \ 0.597*drain + 1.4743*age}}, \text{ and}$$

$p_8 = 1 - (p_7 + p_6 + p_5)$.

The final probability maps (pfive_lp), psix_lp, pseven_lp, and peight_lp) represent the probability of experiencing a MMI of 5, 6, 7, or 8 for a repeat of the 1989 Loma Prieta earthquake. Like the 1906 models, two additional probability grids are created. Figure 39 (MMI > 5) shows the probability of experiencing MMI > 5 and Figure 40 (MMI > 6) shows the probability of experiencing MMI > 6 for a repeat of the 1989 event. Figure 41 shows the probability of experiencing MMI > 7 (MMI = 8) for a repeat of the 1989 Loma Prieta earthquake.

Multiple Regression Models

The multiple regression model for 1906 is given by:

$Sk06 = 8.806 - 0.042*watercont - 0.92*ages + 0.000396*depth$.

This formula can be implemented in GRID of ArcGIS by simply plugging in the locations of the appropriate grids for the variables (e.g. the age grid is plugged into the formula for the *age's* variable). Figure 42 shows the predicted amount of ground shaking in San Francisco for a repeat of the 1906 earthquake.

The multiple regression model for 1989 is given by:

Sk89 = 5.934 + 0.195**permeability* – 0.951**ages*

This formula can also be implemented in GRID of ArcGIS by simply plugging in the locations of the appropriate grids for the variables (e.g. the perm grid is plugged into the formula for the *permeability* variable). Figure 43 shows the predicted amount of ground shaking in San Francisco for a repeat of the 1989 earthquake.

CONCLUSIONS AND DISCUSSION

Are these models good? Is one better than the others? Do they represent reality? Can Modified Mercalli Intensity be used to model ground shaking better than peak ground acceleration? These are all good questions that need to be addressed.

The cumulative logit and multiple regression models are good models and can teach lessons. They demonstrate the importance of sediment and soil characteristics on ground shaking. Both models also demonstrate that there is not a simple relationship between MMI and distance as predicted by the Joyner-Boore model, suggesting that other soil variables play a greater role. As suggested by Tables 19-20 and Tables 21-22, the cumulative logit models correctly predict a higher percentage of actual MMI than the multiple regression models. Age plays the dominant role in both models and suggests that it is the most important variable. This is to be expected due to the assumption that as a soil becomes older, it becomes more consolidated and cemented and begins to act similar to soft rock in an earthquake.

These models reflect reality as closely as the input data represents reality. The soil maps produced by the USDA are the most reliable soil maps currently available. However, some areas are covered by asphalt and buildings and the underlying soil conditions may never be known. Also, humans have impacted the surface of the Earth, which may or may not reflect conditions as they existed in 1906. Depth to bedrock is derived from two different geophysical studies from the1960's. The fact that the depth contours do not exactly coincide is a clue that these maps contain errors. However, these are close approximations and demonstrate relative depths.

MMI is more densely sampled than pga as measured at various seismic monitoring stations in the San Francisco Bay Area. MMI and building destruction patterns give valuable information about the intensity of shaking and the magnitude of an earthquake. These data are very valuable and should be included as important pieces of the puzzle to determine why some areas experience excessive ground motion relative to nearby sites. These data reflect intensity that can be used to model ground motions at large scales (e.g. 1:24000). However, they are not any better or worse than pga. Pga as measured by seismic monitoring stations reflects ground shaking at a specific spot on the ground surface. Due to the low numbers of stations in the San Francisco Bay Area, a spatial study of ground motions may only reveal general statistical trends.

Overall, this study reveals that age, depth to bedrock, permeability and available water content are the most important variables that predict ground shaking. Age is the only variable that is statistically significant for both earthquakes. Since density is directly related to the speed of seismic waves, and age may be an indicator of the amount of compaction or cementation of a deposit, it seems likely that age would be the most important variable. Depth to bedrock is also an important variable, and assuming that ground motions measured on bedrock can represent background shaking, it is intuitive that as the soil/sediment thickness increases, ground shaking should also increase. Permeability, available water capacity, and drainage class are all variables that indicate some degree of compaction within sediments and soils. As permeability increases, the water capacity of the soil increases and the drainage class will go down (low drainage class indicates excessively drained soils). These are all measures of compaction or looseness of the soils. It is likely that as the permeability of the soil increases, the

available water content increases, and as the drainage class becomes more easily drained, the soils become looser. This relationship is shown to be true by the statistics of this study.

The most confidence is placed in the results of the 1906 models. These maps use available water capacity, age, and depth to bedrock as predictors for ground shaking. Also, very little interpolating or addition of data (due to incompleteness of the dataset) was performed on these variables when producing the final results.

Interpolating between strong ground motion sites is probably not a good idea for large-scale studies. More significant trends would probably be revealed at smaller scales (1:100,000). Point analyses of each specific station might be the best way to determine which soil and sediment characteristics are responsible for most of the ground shaking. Future studies of soil with respect to pga should be conducted at very small scales. For instance, an impressive study (yet expensive) could be performed on the entire seismic monitoring network of California. For each station, a thorough geotechnical investigation should consider density as well as the soil variables discussed in this paper. Also, bore holes should be drilled at each site to determine depth to basement rocks. Finally, an intensive statistical analysis could be performed for the entire network using the available historical earthquake records. A study of this magnitude would surely produce reliable results that would act as a model to determine building codes and save seismically active areas around the world an enormous amount of money, reduce structural damage to buildings and lifelines, and above all…save lives!

REFERENCES CITED

ABAG Online. Association of Bay Area Governments. 1995. <http://www.abag.ca.gov>.

Aguirre, Jorge, and Kjioro, I. (1997). Nonlinearity, Liquefaction, and Velocity Variation of Soft Soil Layers in Port Island, Kobe, during the Hyogo-ken Nanbu Earthquake. *Bulletin of the Seismological Society of America.* 87(5):1244-1258.

Aki, K., G. R. Martin, B. H. Chin, N. Abrahamson, A. C. Cornell, and M. Mahdyiar (1995). Probabilistic seismic hazard analysis and the development of earthquake scenario time histories for southern California sites, TASK H-7 of the Southern California Earthquake Center Report on the Characteristics of Earthquake Ground Motions for Seismic Design.

Atwater, B.F., Hedel, C.W., and Helley, E.J., (1977), Late Quaternary depositional history, Holocene sea-level changes, and vertical crustal movement, southern San Francisco Bay, California: *U.S. Geological Survey Professional Paper* 1014, 15p.

Blake, M. C., Jr., R. W. Graymer, and D. L. Jones (2000). Geologic map and map database of parts of Marin, San Francisco, Alameda, Contra Costa, and Sonoma Counties, California. *U. S. Geological Survey miscellaneous field studies MF-2337, Version 1.0* <http://geopubs.wr.usgs.gov/map-mf/mf2337/>.

Bonilla, L. F., J. H. Steidl, G. T. Lindley, A. G. Tumarkin, and R. J. Archuleta (1997). Site amplification in the San Fernando Valley, California: variability of site-effect estimation, *Bulletin of the Seismological Society of America*. 87, 710-730.

Bonilla, M. G. (1964). Bedrock-surface map of the San Francisco South quadrangle, California. *U. S. Geological Survey miscellaneous field studies map MF-334.*

Bonilla, M. G. (1998). Preliminary geologic map of the San Francisco South 7.5' quadrangle and part of the Hunters Point 7.5' quadrangle, San Francisco Bay area, California: a digital database. *U. S. Geological Survey Open file report 98-354* <http://wrgis.wr.usgs.gov/open-file/of98-354/.>

Boore, D.M., and Joyner, W.B. (1991). Estimation of Ground Motion at Deep-soil Sites I in Eastern North America. *Bulletin of the Seismological Society of America.* 81:2167-2185.

Borcherdt, Roger D. (1970). Effects of local geology on ground motion near San Francisco Bay. *Bulletin of the Seismological Society of America.* 60, 29-61.

Borcherdt, Roger D., and GlassMoyer, G. (1992). On the Characteristics of Local Geology and Their Influence on Ground Motions Generated by the Loma Prieta Earthquake in the San Francisco Bay Region, California. *Bulletin of the Seismological Society of America.* 82 (2):603-641.

Borcherdt, R. D., ed. (1994). The Loma Prieta, California, Earthquake of October 17, 1989—Strong ground motion: *U. S. Geological Survey Professional Paper 1551-A*, 272 p.

Brabb, E. E., Graymer, R. W., and Jones, D. L. (1998). Geology of the onshore part of San Mateo County, California: a digital database. *U. S. Geological Survey Open file Report 98-137* < http://wrgis.wr.usgs.gov/open-rile/of98-137/>.

Building Seismic Safety Council (BSSC) (1995). 1994 Edition NEHRP Recommended Provisions for Seismic Regulations for New Buildings, FEMA 222A/223A, developed for the Federal Emergency Management Agency, Washington D. C.

Cassidy, John F., Rogers, Gary C., Weichert, and Dieter, H. (1997). Soil Response on the Fraser Delta to the M = 5.1 Duvall, Washington, Earthquake. *Bulletin of the Seismological Society of America*. 87(5):1354-1361.

Cornell, A. (1968). Engineering seismic risk analysis. *Bulletin of the Seismological Society of America*. 58, 1583-1606.

Drake, D. (1815). *Natural and Statistical View, or Picture of Cincinnati and the Miami County, Illustrated by Maps*, Looker and Wallace, Cincinnati.

Environmental Systems Research Institute, Inc. (ESRI), (1990). Understanding GIS—The ARC/INFO Method. ESRI ARC/INFO Publishing System, p. 30.

Fumal, T. E., and J. C. Tinsley (1985). Mapping shear-wave velocities of near-surface geologic materials, *U. S. Geological Survey Professional Paper. 1360*, 127-150.

GIS Data Depot. 1995. <www.gisdatadepot.com>.

Golden Software, Inc. (1999). Surfer 7.0 User's Guide, 619 pp.

Hartzell, S. (1998). Variability in Nonlinear Sediment Response during the 1994 Northridge, California, Earthquake. *Bulletin of the Seismological Society of America*. 88(6):1426-1437.

Helley, E. J. and K. R. Lajoie (1979). Flatland deposits of the San Francisco Bay region, California: their geology and engineering properties, and their importance to comprehensive planning, *U. S. Geological Survey Professional Paper*. 943, 88 pp.

Holmes, W. T., B. Lizundia, S. Brinkman, J. Conrad, R. Reitherman, W. Dong, J. Burton, and A. Bailey (1990). Preliminary report on damage to unreinforced masonry buildings, The Loma Prieta Earthquake, Rept. Rutherford and Chekene, San Francisco, 34 pp.

Hough, S.E., Fridberg, P.A., Busby, R., Field, E.F., Jacob, K.H., and Borcherdt, R.D. (1990). Sediment-induced Amplification of the Collapse of the Nimitz Freeway. *Nature*. 344(26):853-855.

Joyner, W. B. and D. M. Boore (1981). Peak horizontal acceleration and velocity from strong motion records including records from the 1979 Imperial Valley, California, earthquake, *Bulletin of the Seismological Society of America*. **71**, 2011-2038.

Joyner, W. B., and T. E. Fumal (1985). Predictive mapping of earthquake ground motion, *U. S. Geological Survey Profession Paper. 1360,* 203-220.

Kashiwagi, J., and Hokholt, L. (1991). Soil Survey of San Mateo County, Eastern part, and San Francisco County, California: Provided by the United States Department of Agriculture and the Soil Conservation Service. pp. 120.

Knudsen, K. L., J. S. Noller, J. M. Sowers, and W. R. Lettis, (1997). Quaternary geology and liquefaction susceptibility, San Francisco, California 1:100,000 quadrangle: a digital database. *U. S. Geological Survey Open file Report 97-715* <http://wrgis.wr.usgs.gov/open-file/of97-715>.

Michael, A. J., Ross, S. L., Schwartz, D. P., Hendley, J. W., II, and Stauffer, P. H., (1999). Major quake likely to strike between 2000 and 2930—understanding

earthquake hazards in the San Francisco Bay region. *U. S. Geological Survey Fact Sheet152-99*, 4 p.

Perkins, J. B., and J. Boatwright, (1995). The San Francisco Bay Area-On shaky ground. Association of Bay Area Governments publication number P95001EQK, 35 pp.

Reiter, L. (1990). *Earthquake Hazard Analysis: Issues and Insights*, Columbia University Press, New York, 254 pp.

Rogers, A. M., J. C. Tinsley, and R. D. Borcherdt (1985). Predicting relative ground response, *U. S. Geological Survey Professional Paper 1360*, 221-248.

Rogers, A. M., and S. H. Figures, (1991), Engineering geologic site characterization of the greater Oakland-Alameda area, Alameda and San Francisco Counties, California: Final Report to the National Science Foundation, Grant no. BCS – 9003785.

Schlocker, J. (1961). Bedrock-surface map of the San Francisco North quadrangle, California. *U. S. Geological Survey miscellaneous field studies map MF-334.*

Spudich, P. A., and S. H. Hartzell (1985). Predicting earthquake ground-motion time-histories, *U. S. Geological Survey Professional Paper 1360*, 221-247.

Stockburger, D. W. Introductory Statistics: Concepts, Models, and Applications. Southwest Missouri State University. 19 February 1998 <http://www.psychstat.smsu.edu/introbook/sbk00m.htm>

Strong Motion Database. Institute for Crustal Studies at the University of California, Santa Barbara. 1997 <http://smdb.crustal.ucsb.edu>.

Tinsley, J.C., and T. E. Fumal (1985). Mapping Quaternary sedimentary deposits for areal variations in shaking response, *U. S. Geological Survey Professional Paper 1360*, 101-126.

Wald, D. J., V. Quitoriano, T. H. Heaton, and H. Kanamori., (1999). Relationships between peak ground acceleration, peak ground velocity and modified mercalli intensity in California. *Earthquake Spectra,* Vol. 15, No. 3, pp. 557-564.

Welch, L. E., (1981). Soil survey Alameda County, California, western part: U. S. Department of Agriculture, Soil Conservation Service.

Wills, C. J., M. Peterson, W. A. Bryant, M. Reichle, G. J. Saucedo, S. Tan, G. Taylor, and J. Treiman. (2000). A site-condition map for California based on geology and shear-wave velocity. *Bulletin of the Seismological Society of America*, 90, 6B, pp. S187-S208.

Wood, H. D. 1908). Distribution of apparent intensity in San Francisco, in the California earthquake of April 18, 1906, report of the State Earthquake investigation Commission, Carnegie Institute, Washington, D. C., Publication. 87, 220-245.

Zar, Jerrold H. (1996). Biostatistical Analysis. Prentice Hall: Upper Saddle River, New Jersey, app108-app116.

TABLES

Table 1. Station identification, location and peak ground acceleration for the radial, transverse, and vertical components. Data obtained from Strong Motion Database (1998).

Station	Latitude	Longitude	Radial (cm/s/s)	Transverse (cm/s/s)	Vertical (cm/s/s)
lft	37.946	-122.508	146.76	74.52	59.10
ptb	37.820	-122.520	25.20	96.69	34.10
cfh	37.778	-122.513	119.71	46.75	60.60
vsf	37.783	-122.504	-197.16	-125.66	56.40
sfg	37.806	-122.472	229.40	140.64	57.50
prs	37.792	-122.457	182.23	119.84	56.20
pht	37.790	-122.429	70.20	28.98	30.50
tlh	37.803	-122.408	87.69	55.87	31.90
sft	37.800	-122.400	-134.79	-84.48	47.40
hkb	37.792	-122.400	187.63	76.38	36.20
sob	37.790	-122.400	113.19	-74.40	55.60
rin	37.786	-122.391	109.44	45.09	28.40
tri	37.825	-122.373	156.29	97.12	15.90
ybi	37.807	-122.361	54.10	46.82	27.00
sfu	37.724	-122.475	25.72	173.02	36.70
dmh	37.740	-122.433	25.56	144.62	42.40
saf	37.728	-122.385	125.61	8.77	48.30
rch	37.935	-122.342	-158.96	-22.84	30.50
rbm	37.884	-122.302	85.75	96.33	35.90
gwb	37.870	-122.270	-131.64	-66.69	19.90
bkh	37.870	-122.260	10.66	-81.31	18.50
blb	37.876	-122.249	82.35	92.64	38.00
bks	37.870	-122.240	-8.28	-87.94	22.70
emv	37.844	-122.295	252.98	178.71	58.50
pie	37.823	-122.233	26.96	103.49	25.40
tib	37.806	-122.267	-297.70	-56.97	141.30
osw	37.816	-122.314	76.04	379.33	65.10
ssf	37.674	-122.388	-104.85	53.16	31.20
sfo	37.622	-122.398	373.53	141.04	63.30
a3e	37.657	-122.061	90.33	62.61	44.40
hdm	37.657	-122.082	196.03	88.27	90.50
hwb	37.670	-122.086	-215.37	32.89	81.00
hwc	37.679	-122.082	43.73	53.97	31.90
dfs	37.709	-121.932	78.53	66.48	52.30
snf	37.597	-121.880	-65.14	-81.78	29.80
msj	37.530	-121.919	122.80	94.20	81.30
fms	37.535	-121.929	-155.56	-180.29	68.50
fcy	37.555	-122.248	153.52	38.88	74.70
a01	37.545	-122.231	353.36	126.52	101.00
a02	37.520	-122.250	-127.46	-327.73	84.50
cs1	37.490	-122.310	174.46	-18.64	59.70
a09	37.470	-122.320	-125.69	90.86	49.90
cs2	37.465	-122.343	132.60	3.41	36.40

sfd	37.492	-122.136	166.44	61.63	57.20
vmp	37.468	-122.157	284.23	-122.75	96.50
sla	37.419	-122.205	344.37	12.33	91.80
vpo	37.400	-122.140	106.65	498.28	193.00
svl	37.402	-122.024	267.22	138.32	110.80
agw	37.398	-121.952	183.45	133.37	82.20
sta	37.780	-122.420	-114.35	-28.31	48.50
prh	38.043	-122.797	186.82	-8.49	55.40
cry	37.396	-121.756	56.18	92.49	61.10
crs	37.452	-121.807	-102.64	-83.80	62.40
dvd	37.617	-121.746	107.90	-22.11	27.40
vlr	37.625	-121.762	66.86	29.01	31.60
vmz	37.993	-122.115	76.71	1.67	34.30
stg	37.255	-122.031	585.06	47.03	353.40
sjh	37.340	-121.851	-214.24	-22.55	68.90
lxd	37.202	-121.949	536.48	247.95	131.00
sth	37.210	-121.803	-339.98	-82.74	205.00
hvr	37.338	-121.714	87.05	123.53	55.50
wds	37.429	-122.258	110.84	19.69	48.90

Table 2. Description of Modified Mercalli Intensity that ABAG used to produce intensity maps. Table from ABAG Online (1995).

MMI Value	Description of Shaking Severity	Summary Damage Description	Full Description
I			Not felt. Marginal and long period effects of large earthquakes.
II			Felt by persons at rest, on upper floors, or favorably placed.
III			Felt indoors. Hanging objects swing. Vibration like passing of light trucks. Duration estimated. May not be recognized as an earthquake.
IV			Hanging objects swing. Vibration like passing of heavy trucks; or sensation of a jolt like a heavy ball striking the walls. Standing motor cars rock. Windows, dishes, doors rattle. Glasses clink. Crockery clashes. In the upper range of IV, wooden walls and frame creak.
V	**Light**	**Pictures Move**	Felt outdoors; direction estimated. Sleepers wakened. Liquids disturbed, some spilled. Small unstable objects displaced or upset. Doors swing, close, open. Shutters, pictures move. Pendulum clocks stop, start, change rate.
VI	**Moderate**	**Objects Fall**	Felt by all. Many frightened and run outdoors. Persons walk unsteadily. Windows, dishes, glassware broken. Knickknacks, books, etc., off shelves. Pictures off walls. Furniture moved or overturned. Weak plaster and masonry D cracked. Small bells ring (church, school). Trees, bushes shaken (visibly, or heard to rustle).
VII	**Strong**	**Nonstructural Damage**	Difficult to stand. Noticed by drivers of motor cars. Hanging objects quiver. Furniture broken. Damage to masonry D, including cracks. Weak chimneys broken at roof line. Fall of plaster, loose bricks, stones, tiles, cornices (also unbraced parapets and architectural ornaments). Some cracks in masonry C. Waves on ponds; water turbid with mud. Small slides and caving in along sand or gravel banks. Large bells ring. Concrete irrigation ditches damaged.
VIII	**Very Strong**	**Moderate Damage**	Steering of motor cars affected. Damage to masonry C; partial collapse. Some damage to masonry B; none to masonry A. Fall of stucco and some masonry walls. Twisting, fall of chimneys, factory stacks, monuments, towers, elevated tanks. Frame houses moved on foundations if not bolted down; loose panel walls thrown out. Decayed piling broken off. Branches broken from trees. Changes in flow or temperature of springs and wells. Cracks in wet ground and on steep slopes.
IX	**Violent**	**Heavy Damage**	General panic. Masonry D destroyed; masonry C heavily damaged, sometimes with complete collapse; masonry B seriously damaged. (General damage to foundations.) Frame structures, if not bolted, shifted off foundations. Frames racked. Serious damage to reservoirs. Underground pipes broken. Conspicuous cracks in ground. In alluvial areas sand and mud ejected, earthquake fountains, sand craters.
X	**Very Violent**	**Extreme Damage**	Most masonry and frame structures destroyed with their foundations. Some well-built wooden structures and bridges destroyed. Serious damage to dams, dikes, embankments. Large landslides. Water thrown on banks of canals, rivers, lakes, etc. Sand and mud shifted horizontally on beaches and flat land. Rails bent slightly.
XI			Rails bent greatly. Underground pipelines completely out of service.
XII			Damage nearly total. Large rock masses displaced. Lines of sight and level distorted. Objects thrown into the air.

Table 3. Generalized geologic name and age of each geologic unit to accompany Figures 17 – 18.

Geologic Unit	Description	Age (units of 10,000 years)
af	Artificial fill	0.025
Qhc	Modern stream channel deposits	0.025
Qhbm	Holocene bay mud	1
Qhs	Holocene dune and beach sand	1
Qhb	Holocene basin deposits	1
Qht	Holocene terrace deposits	1
Qhf	Holocene alluvial fan deposits	1
Qhl	Holocene alluvial fan levee deposits	1
Qha	Holocene alluvium, undifferentiated	1
Qf	Late Pleistocene to Holocene alluvial fan deposits	1.8
Qa	Late Pleistocene to Holocene alluvium, undifferentiated	1.8
Qpf	Late Pleistocene alluvial fan deposits	1.8
Qpa	Late Pleistocene alluvium, undifferentiated	1.8
Qps	Late Pleistocene dune and beach sand	1.8
Qmt	Pleistocene marine terrace deposits	164
Qoa	Early to middle Pleistocene alluvium, undifferentiated	520
br	Bedrock	20570
w	Water	NA

Table 4. Description of the type of information in the soils database for this study.

Soil Characteristic	Data Type
Texture	Continuous
Organic Content	Ordinal
Percent Clay	Ordinal
Drainage Class	Ordinal
Plasticity Index	Ordinal
Liquid Limit	Ordinal
Available Water Content	Continuous
Permeability	Ordinal

Tables 5a-c show Spearman's rank correlation coefficient, significance of correlation, and sample number (N) for correlation between three pga components (radial, transverse, and vertical respectively) and depth to bedrock for 10 km distance intervals from the 1989 Loma Prieta epicenter. Two questions are asked concerning Spearman's coefficient for each pga component: (1) Is Spearman's coefficient significant for at least half of the intervals tested, and (2) Are the slopes (+/-) consistent for each interval?

Table 5a. Radial Component.

Distance from epicenter (km)	110	100	90	Significant correlation?	Consistent slope?
Spearman's rho	**+.302**	**-.448**	**+.626**	**Yes**	No
Significance (2-tailed)	**.001**	**.001**	**.001**		
N	**304**	**2334**	**519**		

Table 5b. Transverse Component.

Distance from epicenter (km)	110	100	90	Significant correlation?	Consistent slope?
Spearman's rho	+.030	**+.861**	**+.662**	**Yes**	**Yes**
Significance (2-tailed)	.597	**.001**	**.001**		
N	304	**2867**	**571**		

Table 5c. Vertical Component.

Distance from epicenter (km)	110	100	90	Significant correlation?	Consistent slope?
Spearman's rho	**+.196**	**-.225**	**+.666**	**Yes**	No
Significance (2-tailed)	**.001**	**.001**	**.001**		
N	**309**	**2868**	**574**		

Tables 6a-b show Spearman's rank correlation coefficient, significance of correlation, and sample number (N) for correlation between normalized pga (acceleration due to soil/sediment sites divided by acceleration due to bedrock sites) and depth to the bedrock for 10 km distance intervals from the 1989 Loma Prieta epicenter. Two questions are asked concerning Spearman's coefficient for each pga component: (1) Is Spearman's coefficient significant for at least half of the intervals tested, and (2) Are the slopes (+/-) consistent for each interval?

Table 6a. Radial Acceleration/Bedrock Acceleration.

Distance from epicenter (km)	110	100	90	Significant correlation?	Consistent slope?
Spearman's rho	-.379	+.233	+.492	Yes	No
Significance (2-tailed)	.001	.001	.001		
N	1900	4926	776		

Table 6b. Transverse Acceleration/Bedrock Acceleration.

Distance from epicenter (km)	110	100	90	Significant correlation?	Consistent slope?
Spearman's rho	-.379	+.233	+.492	Yes	No
Significance (2-tailed)	.001	.001	.001		
N	1900	4926	776		

Tables 7a-b show Spearman's rank correlation coefficient, significance of correlation, and sample number (N) for correlation between Modified Mercalli Intensity and depth to bedrock for 10 km distance intervals from the 1906 San Francisco epicenter (Table 7a) and the 1989 Loma Prieta epicenter (Table 7b). Two questions are asked concerning Spearman's coefficient for each earthquake: (1) Is Spearman's coefficient significant for at least half of the intervals tested, and (2) Are the slopes (+/-) consistent for each interval?

Table 7a. Depth to bedrock vs. MMI (1906).

Distance from epicenter (km)	110	100	90	Significant correlation?	Consistent slope?
Spearman's rho	+.317	+.667	+.604	Yes	Yes
Significance (2-tailed)	.001	.001	.001		
N	284	1781	477		

Table 7b. Depth to bedrock vs. MMI (1989).

Distance from epicenter (km)	110	100	90	Significant correlation?	Consistent slope?
Spearman's rho	+.317	+.630	+.502	Yes	Yes
Significance (2-tailed)	.001	.001	.001		
N	284	1781	477		

Tables 8a-c show Spearman's rank correlation coefficient, significance of correlation, and sample number (N) for correlation between three pga components (radial, transverse, and vertical respectively) and soil variables for 10 km distance intervals from the 1989 Loma Prieta epicenter. Two questions are asked concerning Spearman's coefficient for each pga component: (1) Is Spearman's coefficient significant for at least half of the intervals tested, and (2) Are the slopes (+/-) consistent for each interval?

Table 8a. Radial Component

Distance from epicenter (km)	110	100	90	80	70	60	Signif. Correl?	Consist. Slope?
Liquid Limit Spearman's rho	-.273	**+.391**	+.722	**-.264**	**+.213**	**-.410**	**Yes**	No
Significance (2-tailed)	.306	**.015**	.067	**.012**	**.030**	**.001**		
N	16	**38**	7	**90**	**105**	**64**		
Plasticity Spearman's rho	-.273	**+.348**	+.501	-.093	**+.247**	**-.340**	**Yes**	No
Significance (2-tailed)	.306	**.032**	.252	.386	**.012**	**.006**		
N	16	**38**	7	89	**104**	**63**		
Clay % Spearman's rho	**-.259**	-.060	+.160	**-.192**	+.087	-.234	No	No
Significance (2-tailed)	**.002**	.338	.312	**.012**	.255	.063		
N	**146**	254	42	**172**	175	64		
Permeability Spearman's rho	+.080	-.015	+.013	+.119	+.142	-.117	No	No
Significance (2-tailed)	.331	.805	.932	.117	.058	.357		
N	151	281	45	176	178	64		
Drainage Spearman's rho	-.033	+.079	**-.408**		**+.473**	**-.412**	**Yes**	No
Significance (2-tailed)	.743	.286	**.017**		**.001**	**.001**		
N	101	182	**34**		**187**	**75**		
Organic % Spearman's rho	+.038	+.014	-.107	+.029	**+.263**	-.130	No	No
Significance (2-tailed)	.649	.827	.499	.707	**.001**	.306		
N	146	254	42	172	**175**	64		
Water Content Spearman's rho	**+.466**	-.026	-.104	+.061	-.013	+.145	No	No
Significance (2-tailed)	**.001**	.669	.507	.430	.868	.251		
N	**150**	267	43	172	175	64		
Texture Spearman's rho	-.005	-.011	+.249	+.046	+.010	-.152	No	No
Significance (2-tailed	.948	.848	.112	.537	.895	.157		
N	153	285	42	183	184	88		

Table 8b.Transverse Component

Distance from epicenter (km)	110	100	90	80	70	60	Signif. Correl?	Consist. Slope?
Liquid Limit Spearman's rho	-.022	+.134	+.577	-.183	**+.346**	+.143	No	No
Significance (2-tailed)	.935	.414	.175	.081	**.000**	.252		
N	16	39	7	92	**107**	66		
Plasticity Spearman's rho	-.022	+.189	+.309	-.076	**+.346**	**+.382**	No	No
Significance (2-tailed)	.935	.250	.501	.473	**.001**	**.002**		
N	16	39	7	91	**106**	**66**		
Clay % Spearman's rho	+.081	-.036	+.108	**-.168**	**-.149**	**+.554**	**Yes**	No
Significance (2-tailed)	.328	.568	.485	**.027**	**.047**	**.000**		
N	146	256	44	**174**	**178**	**66**		
Permeability Spearman's rho	**-.180**	+.078	+.060	+.097	+.136	-.138	No	No
Significance (2-tailed)	**.027**	.189	.686	.200	.068	.269		
N	**151**	283	47	178	181	66		
Drainage Spearman's rho	**+.246**	-.054	**-.511**		**+.475**	+.223	**Yes**	No
Significance (2-tailed)	**.014**	.470	**.002**		**.001**	.052		
N	**100**	184	**35**		**190**	77		
Organic % Spearman's rho	-.064	+.120	-.144	+.039	+.075	**+.393**	No	No
Significance (2-tailed)	.443	.056	.351	.608	.319	**.001**		
N	146	256	44	174	178	**66**		
Water Content Spearman's rho	**-.443**	**-.206**	-.170	+.046	-.029	-.026	No	No
Significance (2-tailed)	**.000**	**.001**	.263	.549	.700	.833		
N	**150**	**269**	45	174	178	66		
Texture Spearman's rho	+.138	**+.132**	+.220	-.003	-.040	**-.209**	No	No
Significance (2-tailed	.089	**.025**	.151	.963	.586	**.048**		
N	153	**287**	44	184	190	**90**		

Table 8c. Vertical Component.

Distance from epicenter (km)	110	100	90	80	70	60	Signif. Correl?	Consist. Slope?
Liquid Limit Spearman's rho	**-.806**	**+.427**	+.144	**-.238**	**+.356**	**-.413**	**Yes**	No
Significance (2-tailed)	**.001**	**.007**	.758	**.022**	**.001**	**.001**		
N	**16**	**39**	7	**92**	**104**	**66**		
Plasticity Spearman's rho	**-.806**	**+.413**	+.270	-.042	**+.377**	**-.250**	**Yes**	No
Significance (2-tailed)	**.001**	**.009**	.558	.691	**.001**	**.045**		
N	**16**	**39**	7	91	**103**	**65**		
Clay % Spearman's rho	**-.237**	**-.128**	+.258	**-.296**	+.023	-.094	**Yes**	**Yes**
Significance (2-tailed)	**.004**	**.041**	.090	**.001**	.762	.452		
N	**146**	**256**	44	**175**	174	66		
Permeability Spearman's rho	-.040	+.026	-.033	**+.270**	**+.147**	-.181	No	No
Significance (2-tailed)	.627	.658	.825	**.001**	**.05**	.147		
N	151	283	47	**179**	**177**	66		
Drainage Spearman's rho	+.019	+.017	**+.596**	**+.240**	**+.560**	**-.417**	**Yes**	No
Significance (2-tailed)	.854	.814	**.001**	**.001**	**.001**	**.001**		
N	100	184	**35**	**204**	**185**	**77**		
Organic % Spearman's rho	+.026	+.002	+.039	-.011	**+.259**	-.068	No	No
Significance (2-tailed)	.758	.971	.802	.881	**.001**	.586		
N	146	256	44	175	**174**	66		
Water Content Spearman's rho	**+.356**	**-.139**	+.077	+.070	-.084	**+.257**	**Yes**	No
Significance (2-tailed)	**.001**	**.023**	.615	.360	.268	**.037**		
N	**150**	**269**	45	175	174	**66**		
Texture Spearman's rho	-.086	+.020	**+.356**	-.057	+.007	**-.213**	No	No
Significance (2-tailed	.289	.741	**.018**	.437	.919	**.043**		
N	153	287	**44**	190	185	**91**		

Tables 9a-b show Spearman's rank correlation coefficient, significance, and sample number (N) for correlation between normalized pga (soil/sediment acceleration divided by bedrock acceleration) and soil variables for 10 km intervals from the 1989 Loma Prieta epicenter. Two questions are asked concerning Spearman's coefficient: (1) Is the coefficient significant for at least half of the intervals tested, and (2) Are the slopes (+/-) consistent for?

Table 9a.Radial Component

Distance from epicenter (km)	110	100	90	80	70	Signif. Correl?	Consist. Slope?
Liquid Limit Spearman's rho	-.109	**+.609**	-.016			No	No
Significance (2-tailed)	.629	**.001**	.903				
N	22	**67**	57				
Plasticity Spearman's rho	-.109	**+.579**	-.019	-.051	**-.429**	No	No
Significance (2-tailed)	.629	**.001**	.887	.408	**.001**		
N	22	**67**	57	269	**232**		
Clay % Spearman's rho	**-.188**	**-.137**	+.230	**+.134**	**+.323**	**Yes**	No
Significance (2-tailed)	**.009**	**.01**	.086	**.027**	**.001**		
N	**191**	**348**	57	**271**	**236**		
Permeability Spearman's rho	+.053	+.005	-.037	+.085	-.041	No	No
Significance (2-tailed)	.453	.926	.785	.161	.535		
N	201	398	57	271	236		
Drainage Spearman's rho	+.045	+.016	**-.362**	-.072	+.123	No	No
Significance (2-tailed)	.598	.799	**.006**	.240	.060		
N	137	246	**57**	271	236		
Organic % Spearman's rho	-.009	-.036	-.086	-.084	**-.139**	No	No
Significance (2-tailed)	.897	.506	.527	.168	**.032**		
N	191	348	57	271	**236**		
Water Content Spearman's rho	**+.456**	-.002	-.051			No	No
Significance (2-tailed)	**.001**	.962	.709				
N	**199**	375	57				
Texture Spearman's rho	+.022	+.087	.162	**+.162**	**+.413**	No	No
Significance (2-tailed)	.750	.081	.256	**.011**	**.001**		
N	206	407	51	**248**	**229**		

Table 9b.Transverse Component

Distance from epicenter (km)	110	100	90	80	70	Signif. Correl?	Consist. Slope?
Liquid Limit Spearman's rho	-.008	+.222	-.099			No	No
Significance (2-tailed)	.972	.062	.450				
N	23	71	60				
Plasticity Spearman's rho	-.008	**+.248**	-.101	-.041	**-.415**	No	No
Significance (2-tailed)	.972	**.037**	.444	.503	**.001**		
N	23	**71**	60	276	**241**		
Clay % Spearman's rho	-.024	-.060	+.150	**+.193**	**+.489**	No	No
Significance (2-tailed)	.741	.258	.253	**.001**	**.001**		
N	195	361	60	**278**	**245**		
Permeability Spearman's rho	**-.168**	+.049	-.056	+.045	-.115	No	No
Significance (2-tailed)	**.016**	.317	.672	.456	.071		
N	**206**	413	60	278	245		
Drainage Spearman's rho	**+.189**	-.093	-.192	**+.194**	**+.333**	**Yes**	**Yes**
Significance (2-tailed)	**.026**	.138	.141	**.001**	**.001**		
N	**140**	257	60	**278**	**245**		
Organic % Spearman's rho	+.001	**+.131**	-.212	+.002	-.025	No	No
Significance (2-tailed)	.992	**.013**	.104	.974	.694		
N	195	**361**	60	278	245		
Water Content Spearman's rho	**-.294**	**-.209**	-.015			No	No
Significance (2-tailed)	**.001**	**.001**	.909				
N	**204**	**389**	60				
Texture Spearman's rho	+.117	**+.168**	+.212	**+.257**	**+.575**	**Yes**	**Yes**
Significance (2-tailed	.090	**.001**	.123	**.001**	**.001**		
N	211	**423**	54	**255**	**237**		

Tables 10a-b show Spearman's rank correlation coefficient, significance correlation, and number of samples (N) for correlation between Modified Mercalli Intensity and soil variables for 10 km distance intervals from the 1906 San Francisco epicenter (Table 10a) and the 1989 Loma Prieta epicenter (Table 10b). Two questions are asked for each soil variable (1) Is Spearman's coefficient significant for at least half of the intervals tested, and (2) Are the slopes (+/-) consistent for each interval?

Table 10a. Soils vs. MMI (1906)

Distance from epicenter (km)	50	40	30	20	10	Signif. Correl?	Consist. Slope?
Liquid Limit Spearman's rho	+.080	**-.481**	+.180	+.448	+.101	No	No
Significance (2-tailed)	.5	**.001**	.2	.1	.5		
N	25	**18**	23	18	31		
Plasticity Spearman's rho	-.141	-.102	+.207	+.437	-.106	No	No
Significance (2-tailed)	.2	.5	.1	.2	.5		
N	25	18	23	18	31		
Clay % Spearman's rho	-.191	**+.268**	**+.261**	+.359	+.035	**Yes**	**Yes**
Significance (2-tailed)	.1	**.001**	**.005**	.001	.5		
N	146	**125**	**98**	**118**	175		
Permeability Spearman's rho	**+.313**	**-.714**	-.010	-.082	**+.121**	**Yes**	No
Significance (2-tailed)	**.005**	**.001**	.3	.5	**.05**		
N	**151**	**125**	102	168	**178**		
Drainage Spearman's rho	**+.328**	**+.711**	+.003	**+.361**	**+.300**	**Yes**	**Yes**
Significance (2-tailed)	**.001**	**.001**	.4	**.001**	**.001**		
N	**152**	**129**	110	**168**	**178**		
Organic % Spearman's rho	-.182	**+.328**	+.133	-.053	-.005	No	No
Significance (2-tailed)	.1	**.001**	.2	.5	.7		
N	146	**132**	102	156	175		
Water Content Spearman's rho	+.104	+.052	+.001	**-.251**	-.090	No	No
Significance (2-tailed)	.5	.5	.7	**.001**	.2		
N	150	145	102	**156**	175		
Texture Spearman's rho	**+.199**	-.095	+.006	**+.190**	**+.161**	**Yes**	**Yes**
Significance (2-tailed)	**.05**	.2	.5	**.01**	**.01**		
N	**150**	142	102	**154**	**175**		

Table 10b. Soils vs. MMI from the Loma Prieta Earthquake 1906; M = 7.1

Distance from epicenter (km)	110	100	90	80	70	80	Signif. Correl?	Consist. Slope?
Liquid Limit Spearman's rho	-.044	**+.689**	+.450	**+.307**	**+.381**	**-.006**	**Yes**	**Yes**
Significance (2-tailed)	.5	**.001**	.5	**.05**	**.001**	**.5**		
N	25	**31**	23	**34**	**42**	**12**		
Plasticity Spearman's rho	-.252	**+.721**	+.450	**+.368**	**+.228**	**-.258**	**Yes**	No
Significance (2-tailed)	.5	**.001**	.5	**.01**	**.05**	**.05**		
N	25	**31**	23	**35**	**41**	**13**		
Clay % Spearman's rho	**+.289**	**+.017**	**+.355**	+.004	**+.300**	-.010	**Yes**	**Yes**
Significance (2-tailed)	**.001**	**.02**	**.05**	.7	**.001**	.5		
N	**146**	**125**	**98**	172	**175**	69		
Permeability Spearman's rho	-.044	+.103	+.101	+.139	+.108	+.217	**Yes**	**Yes**
Significance (2-tailed)	.6	.1	.03	.2	.2	.1		
N	151	125	102	168	178	64		
Drainage Spearman's rho	**+.226**	**+.303**	**+.425**	+.075	**+.212**	**+.545**	**Yes**	**Yes**
Significance (2-tailed)	**.05**	**.001**	**.05**	.5	**.005**	**.001**		
N	**152**	**129**	**110**	168	**178**	**75**		
Organic % Spearman's rho	**+.251**	-.061	-.071	**+.183**	**+.207**	**+.234**	**Yes**	**Yes**
Significance (2-tailed)	**.005**	.5	.45	**.05**	**.01**	**.05**		
N	**146**	132	102	**156**	**175**	**64**		
Water Content Spearman's rho	+.080	-.002	+.133	-.051	+.003	-.019	No	No
Significance (2-tailed)	.5	.8	.5	.5	.7	.2		
N	150	145	102	156	175	64		
Texture Spearman's rho	-.024	**+.169**	**+.480**	-.081	-.091	**+.193**	**Yes**	**Yes**
Significance (2-tailed)	.2	**.01**	**.005**	.5	.2	.05		
N	150	**142**	**102**	154	175	62		

Tables 11a-c show Spearman's rank correlation coefficient, significance of correlation, and sample number (N) for correlation between three pga components (radial, transverse, and vertical respectively) and age of formation for 10 km distance intervals from the 1989 Loma Prieta epicenter. Two questions are asked concerning Spearman's coefficient for each pga component: (1) Is Spearman's coefficient significant for at least half of the intervals tested, and (2) Are the slopes (+/-) consistent for each interval?

Table 11a. Radial Component.

Distance from epicenter (km)	110	100	90	80	70	60	Signif. correl?	Consist slope?
Spearman's rho	+.136	**-.176**	**-.353**	**-.187**	**-.414**	-.163	Yes	Yes
Significance (2-tailed)	.016	**.01**	**.01**	**.05**	**.01**	.613		
N	310	**276**	**200**	**132**	**64**	12		

Table 11b. Transverse Component

Distance from epicenter (km)	110	100	90	80	70	60	Signif. correl?	Consist slope?
Spearman's rho	**-.213**	**-.330**	**-.340**	-.070	-.248	+.413	Yes	Yes
Significance (2-tailed)	**.01**	**.01**	**.01**	.42	.05	.182		
N	**327**	**284**	**208**	136	67	12		

Table 11c. Vertical Component

Distance from epicenter (km)	110	100	90	80	70	60	Signif. correl?	Consist slope?
Spearman's rho	+.061	+.061	**-.170**	**-.247**	**-.315**	+.288	Yes	Yes
Significance (2-tailed)	.267	.306	**.05**	**.01**	**.01**	.364		
N	330	284	**209**	**137**	**68**	12		

Tables 12a-b show Spearman's rank correlation coefficient, significance, and sample number (N) for correlation between normalized pga (soil/sediment acceleration divided by bedrock acceleration) and age of formation for 10 km intervals from the 1989 Loma Prieta epicenter. Two questions are asked concerning Spearman's coefficient: (1) Is the coefficient significant for at least half of the intervals tested, and (2) Are the slopes (+/-) consistent for?

Table 12a. Radial Component

Distance from epicenter (km)	110	100	90	80	70	Signif. correl?	Consist. slope?
Spearman's rho	+.116	-.091	-.274	-.237	-.496	Yes	Yes
Significance (2-tailed)	.05	.08	.01	.01	.01		
N	412	386	280	195	92		

Table 12b. Transverse Component.

Distance from epicenter (km)	110	100	90	80	70	Signif. correl?	Consist. slope?
Spearman's rho	-.138	-.291	-.349	-.128	-.307	Yes	Yes
Significance (2-tailed)	.01	.01	.01	.07	.01		
N	431	402	293	207	96		

Tables 13a-b show Spearman's rank correlation coefficient, significance correlation, and number of samples (N) for correlation between Modified Mercalli Intensity and soil variables for 10 km distance intervals from the 1906 San Francisco epicenter (Table 10a) and the 1989 Loma Prieta epicenter (Table 10b). Two questions are asked for each soil variable (1) Is Spearman's coefficient significant for at least half of the intervals tested, and (2) Are the slopes (+/-) consistent for each interval?

Table 13a. Age vs. MMI (1906).

Distance from epicenter (km)	50	40	30	20	10	Signif. correl?	Consist. slope?
Spearman's rho	**-.159**	**-.332**	**-.490**	+.075	-.272	**Yes**	**Yes**
Significance (2-tailed)	**.3**	**.05**	**.06**	.8	.4		
N	**43**	**54**	**15**	15	12		

Table 13b. Age vs. MMI (1989).

Distance from epicenter (km)	110	100	90	80	70	Signif. correl?	Consist. slope?
Spearman's rho	**-.275**	**-.567**	**-.389**	-.111	-.186	**Yes**	**Yes**
Significance (2-tailed)	**.01**	**.01**	**.01**	.5	.5		
N	**114**	**118**	**44**	34	15		

Table 14. Summary of statistics from Tables 5-13. The most influential variables on ground motion are (in order of importance) age, depth, drainage class, clay content, and texture with the latter two tied for fourth place.

Variable	Number of Yes's	Number of No's
Depth	**10**	**4**
Liquid Limit	3	9
Plasticity Index	2	10
Clay Content	**6**	**6**
Permeability	1	11
Drainage Class	**8**	**4**
Organic Content	2	10
Available Water Capacity	0	12
Texture	**6**	**6**
Age	**12**	**0**

Table 15. Dataset used for multivariate statistical analysis. Units of each variable are discussed on pp. 23-4 of text.

Station	Sk06	Sk89	Texture	WaterCont	Perm	Organic	Drainage	Clay	Age	Depth	Dist06	Dist89
2	8	7	8	0.135	5	3	3	4	1	35	12373	111962.9
4	7	5	4.6	0.135	2	3	3	4	20570	670	7450	97740.26
5	9	6	6.5	0.175	4	2	6	4	0.025	74	11889	92477.92
6	9	5	7.5	0.175	6	1	2	1	20570	911	6299	97669.85
8	7	6	1.5	0.175	6	1	2	1	20570	239	12355	104867.7
10	9	7	2	0.065	5	5	2	1	1	162	16484	109716.8
12	10	6	6.5	0.175	4	2	6	4	0.025	505	13008	90864.75
13	8	5	4.6	0.11	2	3	3	4	20570	93	7489	96965.65
15	8	6	-0.375	0.135	1	4	3	5	20570	0	8463	107695.9
16	7	6	8	0.135	5	3	3	4	20570	8	13689	109714.7
17	9	8	6.5	0.175	4	2	6	4	0.025	237	15718	108282.3
18	9	8	6.5	0.175	4	2	6	4	0.025	119	13164	103361
22	8	6	6.5	0.175	4	2	6	4	0.025	111	10082	98714.78
24	9	7	8	0.135	5	3	3	4	1	2489	933	104395.5
26	8	5	4.6	0.11	2	3	3	4	20570	156	8765	95682.7
27	9	5	-0.375	0.135	1	4	3	5	20570	30	10923	92717.84
29	9	6	6.5	0.175	4	2	6	4	0.025	93	14037	90029.76
30	9	6	6.5	0.175	4	2	6	4	0.025	238	14829	89493.66
32	7	5	-0.375	0.135	1	4	3	5	20570	330	6284	99446.48
33	7	5	4.6	0.11	2	3	3	4	20570	477	5099	100088.4
35	8	6	-8	0.175	6	1	2	1	20570	153	4346	103685.7
37	9	8	6.5	0.175	4	2	6	4	0.025	88	13551	105590.4
40	7	6	6	0.165	4	5	3	7	20570	69	12585	111289.9
41	8	7	2	0.065	5	5	2	1	20570	92	11750	108565
42	9	7	2	0.065	5	5	2	1	1	119	7575	109045.8
46	9	7	6.5	0.175	4	2	6	4	0.025	159	11638	99067.56
47	9	6	6.5	0.175	4	2	6	4	0.025	134	11590	94704.78
48	9	6	8	0.135	5	3	3	4	164	514	5720	98444.72
49	9	6	8	0.135	5	3	3	4	164	1783	1983	102072.9
50	10	5	8	0.175	5	3	3	4	20570	218	9585	94208.42
51	8	5	4.6	0.11	2	3	3	4	20570	110	8873	95413.89
52	10	6	-8	0.175	6	1	2	1	20570	58	8679	95319.65
54	7	6	4.5	0.055	1	2	3	1	20570	102	14185	114061.4
55	9	8	6.5	0.175	4	2	6	4	1	36	14279	111712.7
56	9	8	6.5	0.175	4	2	6	4	0.025	129	15083	106565.9
57	9	7	6.5	0.175	4	2	6	4	0.025	164	12722	102436.3
61	7	6	-8	0.175	6	1	2	1	20570	0	9736	107438.8
63	9	8	6.5	0.175	4	2	6	4	0.025	105	16130	110815
64	9	8	8	0.03	5	3	3	4	1	56	13793	112753
65	9	7	2	0.065	5	5	2	1	1	249	4982	107901.8
68	7	6	-8	0.175	6	1	2	1	20570	21	8098	104499.9
69	7	6	2	0.175	5	5	2	1	20570	41	12906	110603.3
71	9	8	6.5	0.03	4	2	6	4	0.025	56	15806	110796.7
72	9	8	6.5	0.175	4	2	6	4	0.025	207	14461	105819
74	9	7	1.5	0.065	5	5	2	1	1	91	9417	110514.7

75	8	7	1.5	0.065	5	52	1	1	88	9957	109665.3
78	7	6	1.5	0.175	6	12	1	20570	208	12315	103984.6
83	9	7	6.5	0.175	4	26	4	0.025	177	11392	102701.6
85	8	7	1.5	0.065	5	52	1	1	56	13553	107177.5
88	10	5	3.75	0.135	4	33	1	20570	727	7556	96307.11
89	8	5	4.6	0.11	2	33	4	20570	284	7860	96424.78
90	10	7	6	0.15	3	33	6	20570	0	9918	94003.83
91	7	5	4.6	0.11	2	33	4	20570	548	6361	98671.66
93	8	6	6.5	0.175	4	26	4	0.025	211	10517	96841.84
95	7	6	1.5	0.175	6	13	1	20570	0	8935	107256.4
96	7	6	4.5	0.175	6	12	1	20570	47	15184	110322.9
98	8	6	8	0.135	5	33	4	20570	0	12213	111593.6
101	9	7	2	0.065	5	52	1	1	152	10250	112028
102	8	7	2	0.065	5	52	1	1	101	10568	110843.6
103	8	7	1.5	0.175	6	12	1	20570	24	11836	109822.1
104	7	7	1.5	0.065	5	52	1	20570	0	10416	109129.1
105	8	7	2	0.065	5	52	1	1	0	10727	108147.5
107	9	8	6.5	0.175	4	26	4	0.025	147	14006	105910
110	8	6	6	0.165	4	53	7	20570	0	13172	113280.9
111	9	7	2	0.065	5	52	1	1	258	4567	107194.2
112	10	7	1.5	0.065	5	52	1	20570	2082	1558	105032.6
117	9	6	8	0.135	5	33	4	164	1638	3640	100106.8
119	9	6	8	0.135	5	33	4	164	304	5416	99122.65
120	8	5	4.6	0.11	2	33	4	20570	62	6353	98272.12
121	7	5	4.6	0.11	2	33	4	20570	296	8251	96839.92
125	7	5	-0.375	0.135	1	43	5	20570	276	10441	95622.4
126	9	6	-6	0.175	4	26	4	0.025	137	11000	95455.2
128	9	6	6.5	0.175	4	26	4	0.025	135	11374	94753
131	9	6	6.5	0.175	4	26	4	0.025	151	11920	92643.64
132	8	5	6.5	0.175	4	26	4	164	15	10878	93515.1
135	9	6	3.75	0.135	4	33	1	20570	838	8473	95167.9
138	9	6	8	0.135	5	33	4	164	596	10498	93198.79
139	9	6	6.5	0.175	4	26	4	0.025	300	11263	92828.88
140	9	6	8	0.05	3	77	11	0.025	148	12638	91384.38
141	9	6	6.5	0.175	4	26	4	0.025	118	13417	90784.59
142	8	5	-0.375	0.135	1	43	5	20570	141	8921	95553.77
146	8	6	6.5	0.175	4	26	4	0.025	144	10199	97317.83
147	8	6	3.75	0.135	4	33	1	20570	170	10717	99633.63
149	9	7	6.5	0.175	4	26	4	0.025	111	12729	101867.6
155	8	7	2	0.065	5	52	1	1	152	10711	110894.8
156	9	7	2	0.065	5	52	1	1	116	8405	109632.5
157	9	7	1.5	0.065	5	52	1	1	323	9175	111244.2
158	9	7	2	0.065	5	52	1	1	266	6286	109004.4
159	9	7	8	0.135	5	33	4	164	320	3256	105365.4
160	9	7	2	0.065	5	52	1	1	0	6932	107666.9

Table 16. 1906 San Francisco Earthquake (x = 0).

Model	Procedure	Parameter	Estimate	Standard Error	P-value	Comment
Model (*)	Genmod (with $b_2 = -1$)	Intercept	9.42	0.2786		b_3 is significant but not negative.
		b_3	0.12	0.0260	<0.0001	
Model (**)	reg	Intercept	9.52	0.5384		B_2 and b_3 are positive. B_2 is significant, but b_3 not at $\alpha = 0.05$.
		b_2	1.12	0.5209	0.034	
		b_3	0.14	0.0741	0.0659	
Model (***)	reg	Intercept	8.54	0.2892		b_3 is negative, but not significant.
		b_3	-.01	0.0270	0.6837	

Table 17. 1989 Loma Prieta Earthquake (x = 0).

Model	Procedure	Parameter	Estimate	Standard Error	P-value	Comment
Model (*)	Genmod (with $b_2 = -1$)	Intercept	1.70	1.1529		b_3 is significant but not negative.
		b_3	0.09	0.0112	<0.0001	
Model (**)	glm	Intercept	53.96	152.65		b_2 and b_3 are neither negative nor significant.
		b_2	15.43	42.150	0.7152	
		b_3	0.23	0.4138	0.5768	
Model (***)	glm	Intercept	-1.92	1.1661		b_3 is significant, but not negative.
		b_3	0.08	0.0113	<0.001	

Table 18. Pearson Correlation Coefficients, N = 89.

	sk06	sk89	ds06	ds89
sk06	1.00000	0.37011 0.0004	-0.04378 0.6837	-0.24152 0.0226
sk89	0.37011 0.0004	1.00000	0.35876 0.0006	0.60555 <.0001
ds06	-0.04378 0.6837	0.35876 0.0006	1.00000	0.16076 0.1323
ds89	-0.24152 0.0226	0.60555 <.0001	0.16076 0.1323	1.00000

Table 19. Results of the cumulative logit model. Predicted MMI vs. actual MMI for 1906. These results suggest that 62.5% of all sampled sites were predicted correctly.

1906		Predicted MMI			
		7	*8*	*9*	*10*
Actual MMI	*7*	**8**	9	0	0
	8	4	**10**	9	0
	9	0	5	**37**	0
	10	0	4	2	**0**

Table 20. Results of the cumulative logit model. Predicted MMI vs. actual MMI for 1989. These results suggest that 57.3% of all sampled sites were predicted correctly.

1989		Predicted MMI			
		5	*6*	*7*	*8*
Actual MMI	*5*	**13**	3	1	0
	6	2	**16**	17	0
	7	1	4	**22**	0
	8	0	0	10	**0**

Table 21. Results of the multiple regression model. Predicted MMI vs. actual MMI for 1906. These results suggest that 53.9% of all sampled sites were predicted correctly.

1906		Predicted MMI			
		7	*8*	*9*	*10*
Actual MMI	*7*	**3**	14	0	0
	8	0	**14**	13	0
	9	0	6	**31**	2
	10	0	4	2	**0**

Table 22. Results of the multiple regression model. Predicted MMI vs. actual MMI for 1989. These results suggest that 52.6% of all sampled sites were predicted correctly.

1989		Predicted MMI			
		5	*6*	*7*	*8*
Actual MMI	*5*	**13**	3	1	6
	6	2	**15**	18	0
	7	0	5	**22**	0
	8	0	0	10	**0**

Table 23. Values of permeability, organic content, available water capacity, and drainage class inferred from the respective geologic units to fill in missing data for San Francisco.

Geologic Unit	Permeability	Organic Content	Avail. Water	Drain Class
Qhs	NA	2	.05	2
Af	NA	NA	NA	3
Qoa	NA	NA	NA	3
Br	1	1	.05	NA

FIGURES

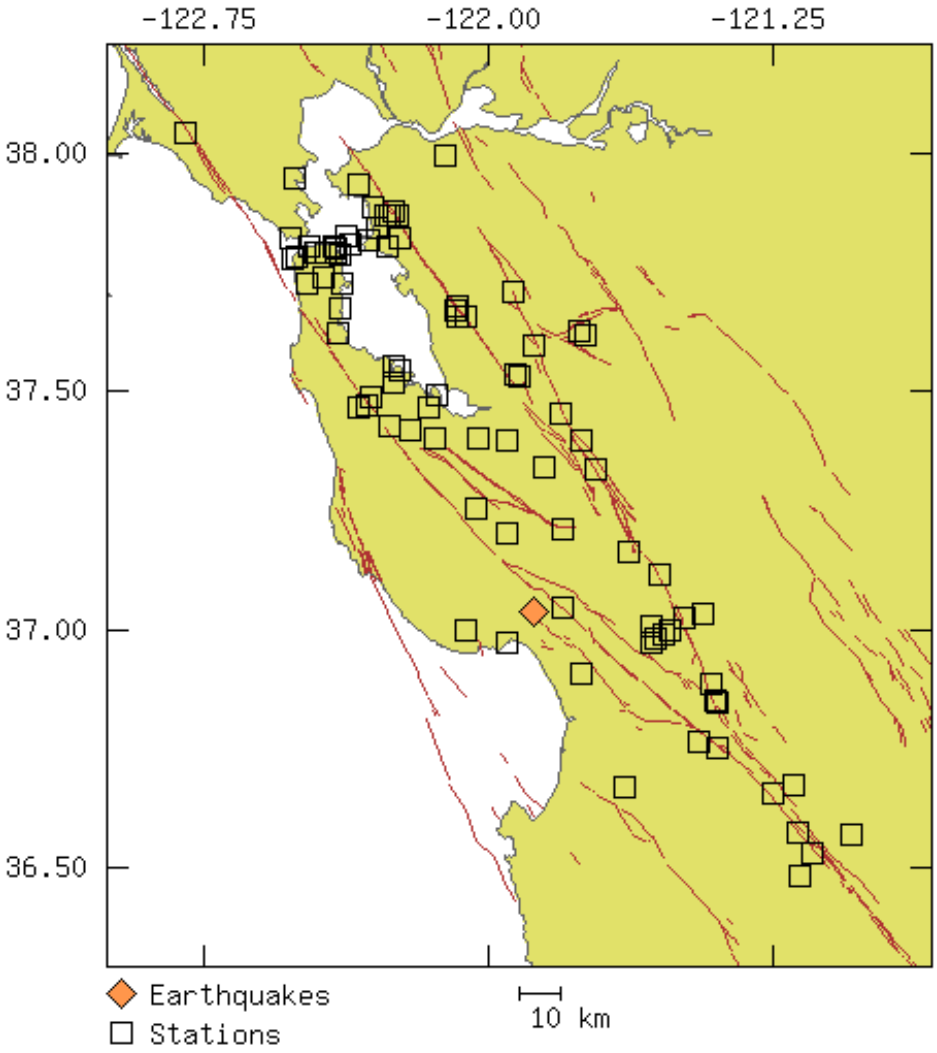

Figure 1. Location of stations that recorded the Loma Prieta earthquake (M 7.1) on October 18, 1989. Source (Strong Motion Database (1997).

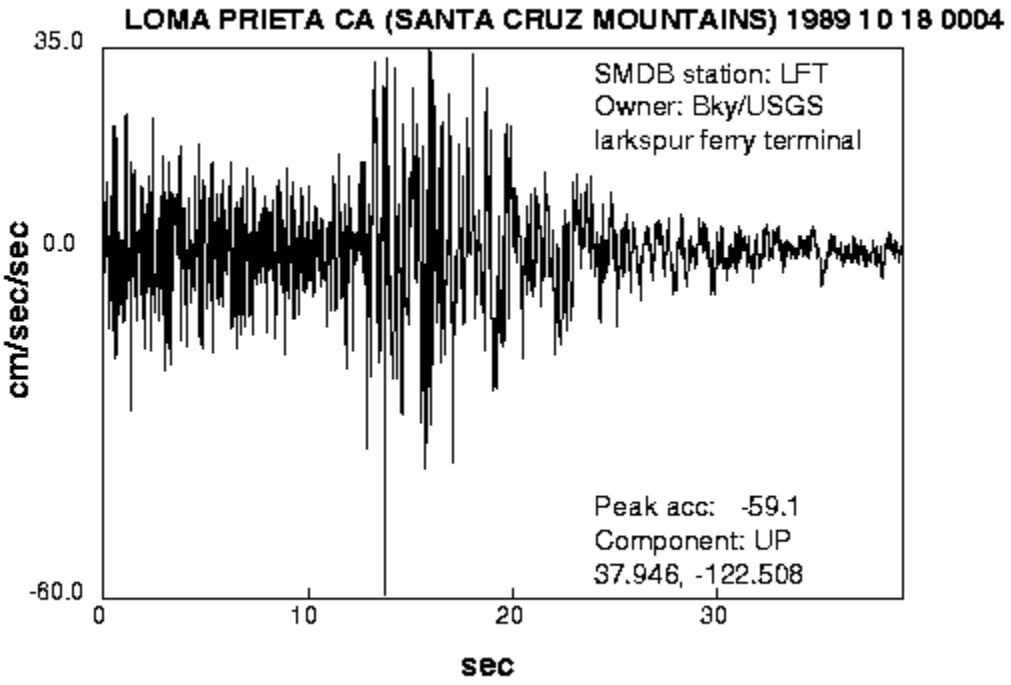

Figure 2. Example of data recorded by a strong ground motion sensor from the Loma Prieta earthquake. Source (Strong Motion Database (1997).

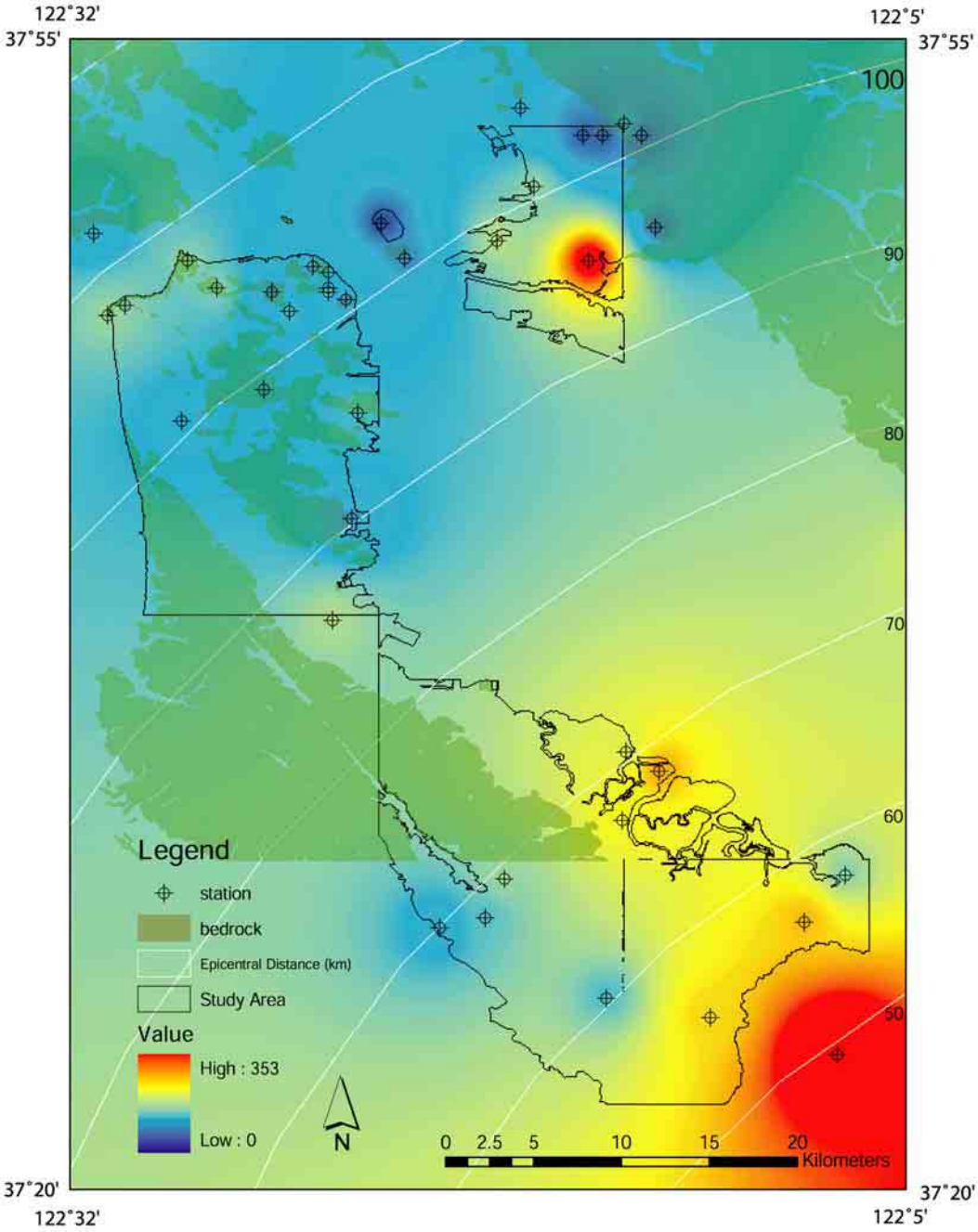

Figure 3. Extrapolated vertical acceleration (cm/s/s) in color with the locations of the stations (Strong Motion Database (1997) that recorded the 1989 Loma Prieta earthquake. Generalized bedrock (Knudsen et al., 1997) in green. Contours of distance (km) from the epicenter of the earthquake in white. The study area is outlined in black.

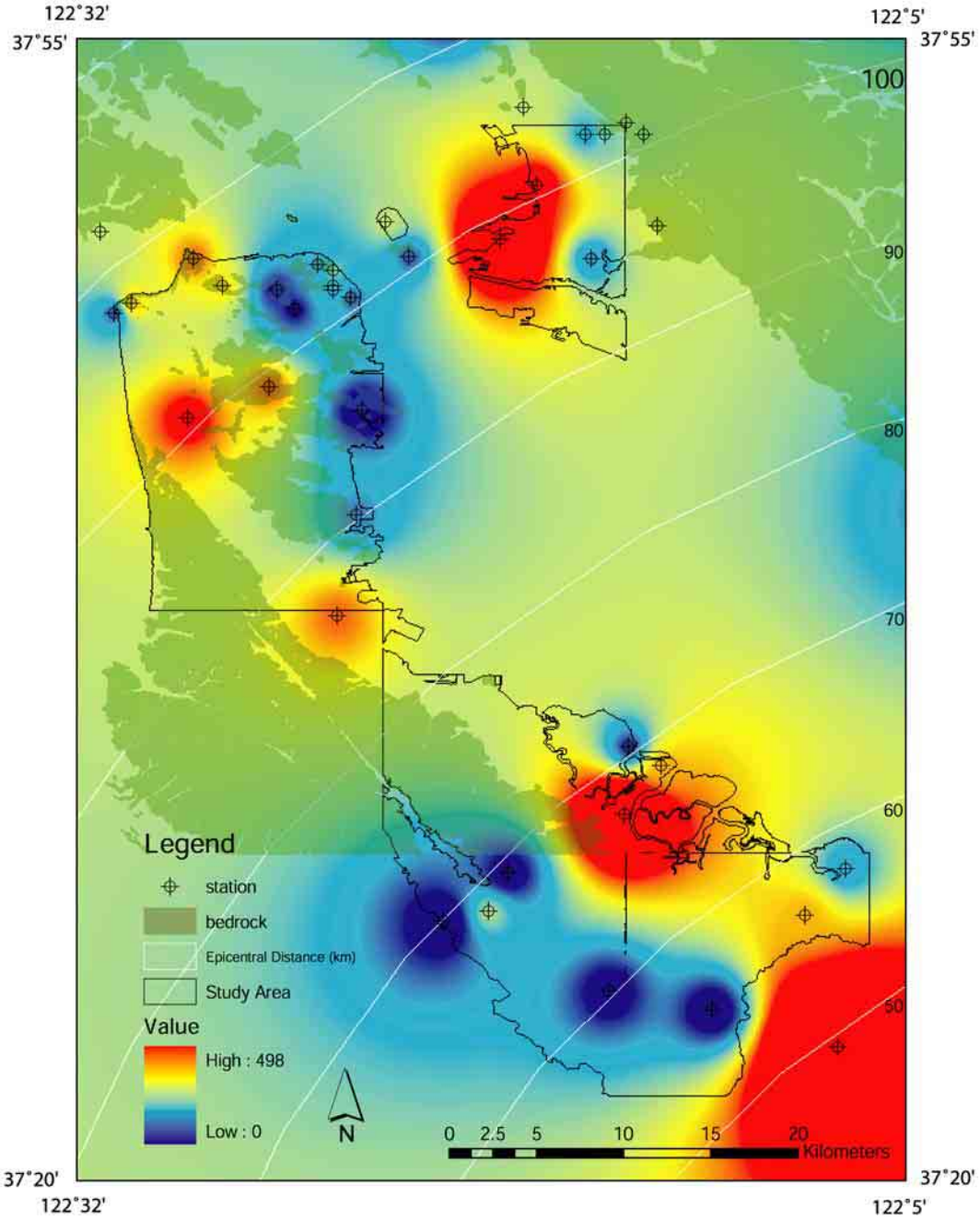

Figure 4. Extrapolated transverse acceleration (cm/s/s) in color with the locations of the stations (Strong Motion Database (1997) that recorded the 1989 Loma Prieta earthquake. Generalized bedrock (Knudsen et al., 1997) in green. Contours of distance (km) from the epicenter of the earthquake in white. The study area is outlined in black.

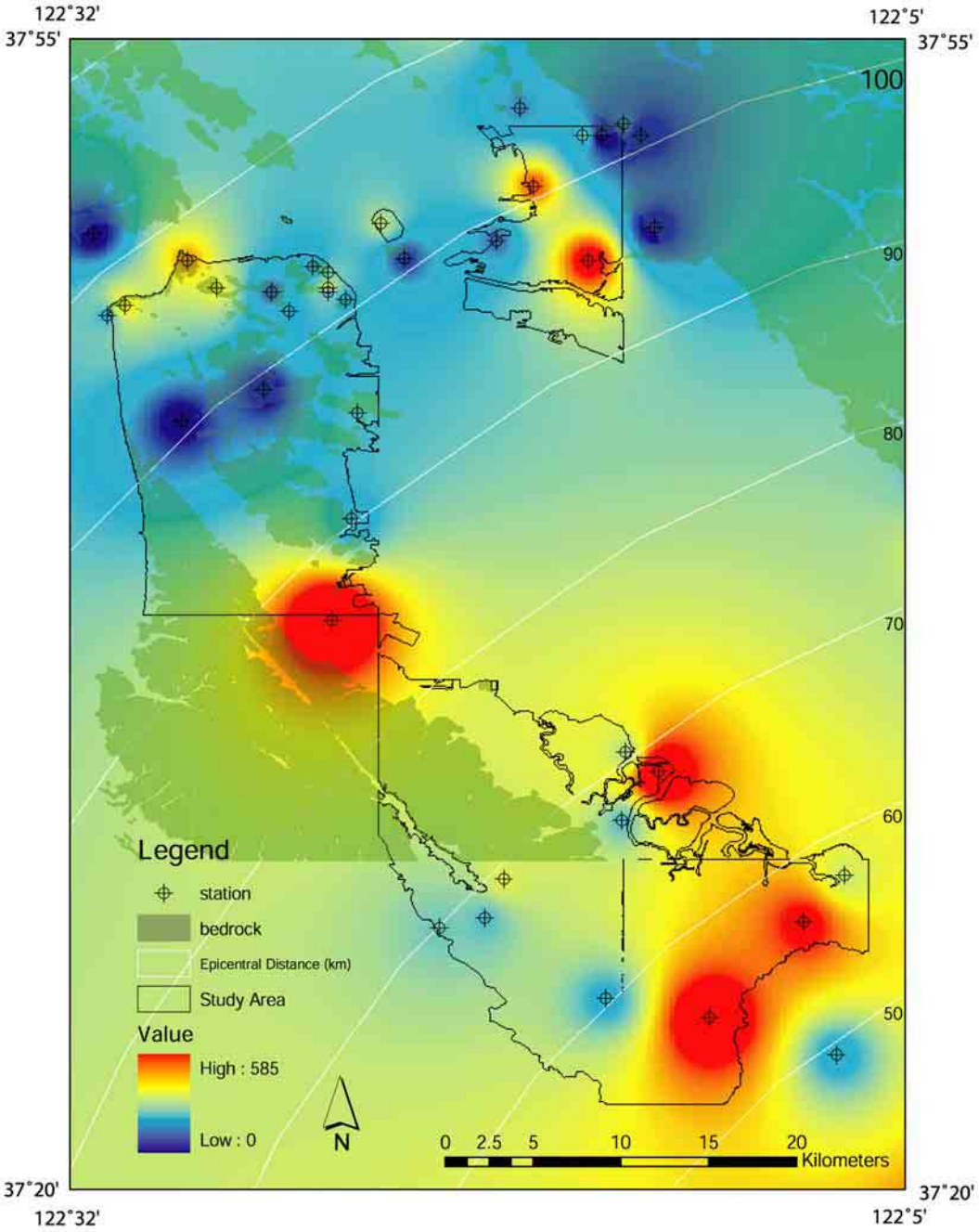

Figure 5. Extrapolated radial acceleration (cm/s/s) in color with the locations of the stations (Strong Motion Database (1997) that recorded the 1989 Loma Prieta earthquake. Generalized bedrock (Knudsen et al., 1997) in green. Contours of distance (km) from the epicenter of the earthquake in white. The study area is outlined in black.

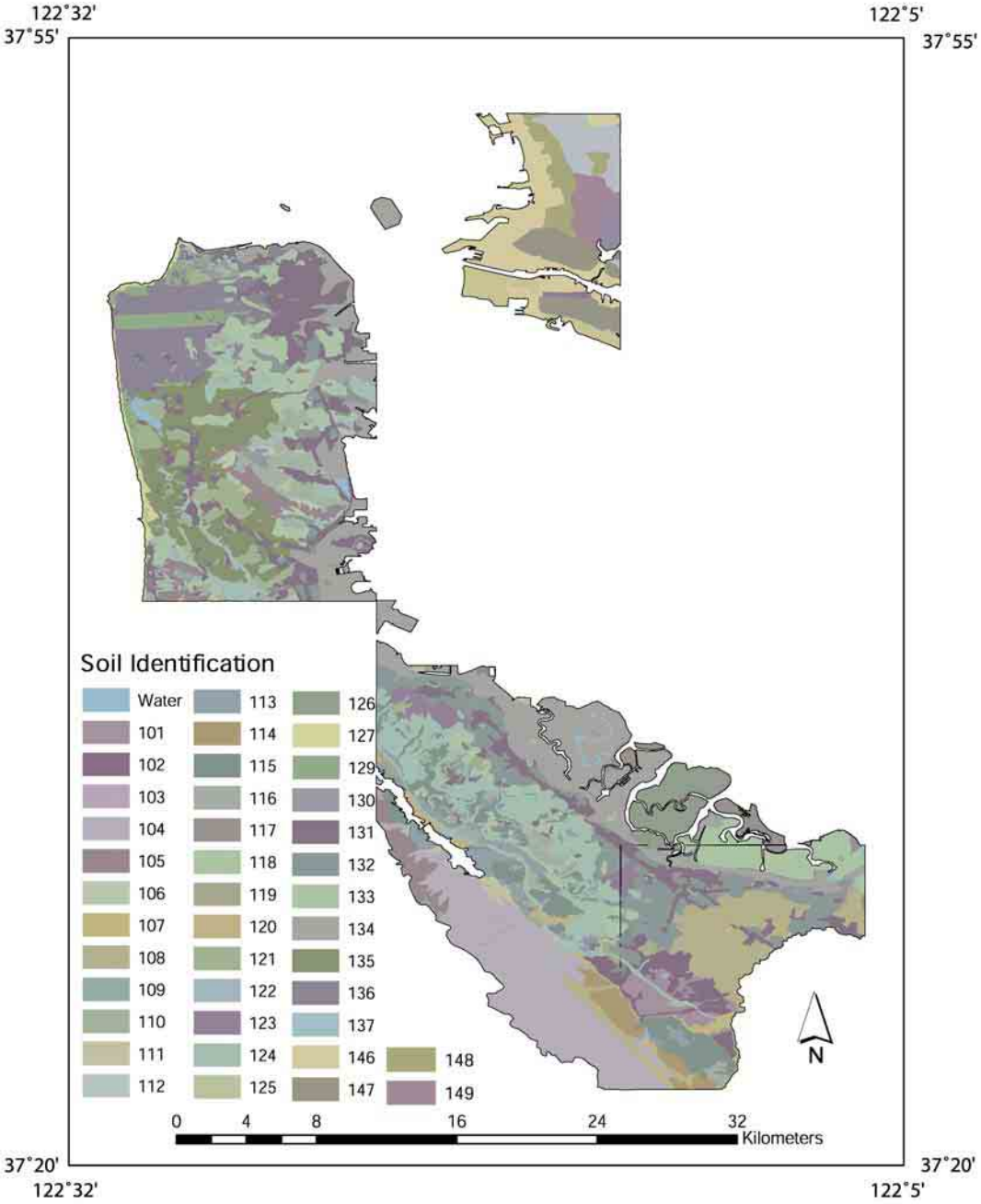

Figure 6. Identification numbers of the different types of soils as described by the United States Department of Agriculture (Kashiwagi and Hokholt, 1991; Welch, 1981). Appendix A contains a description of each soil type by soil identification number.

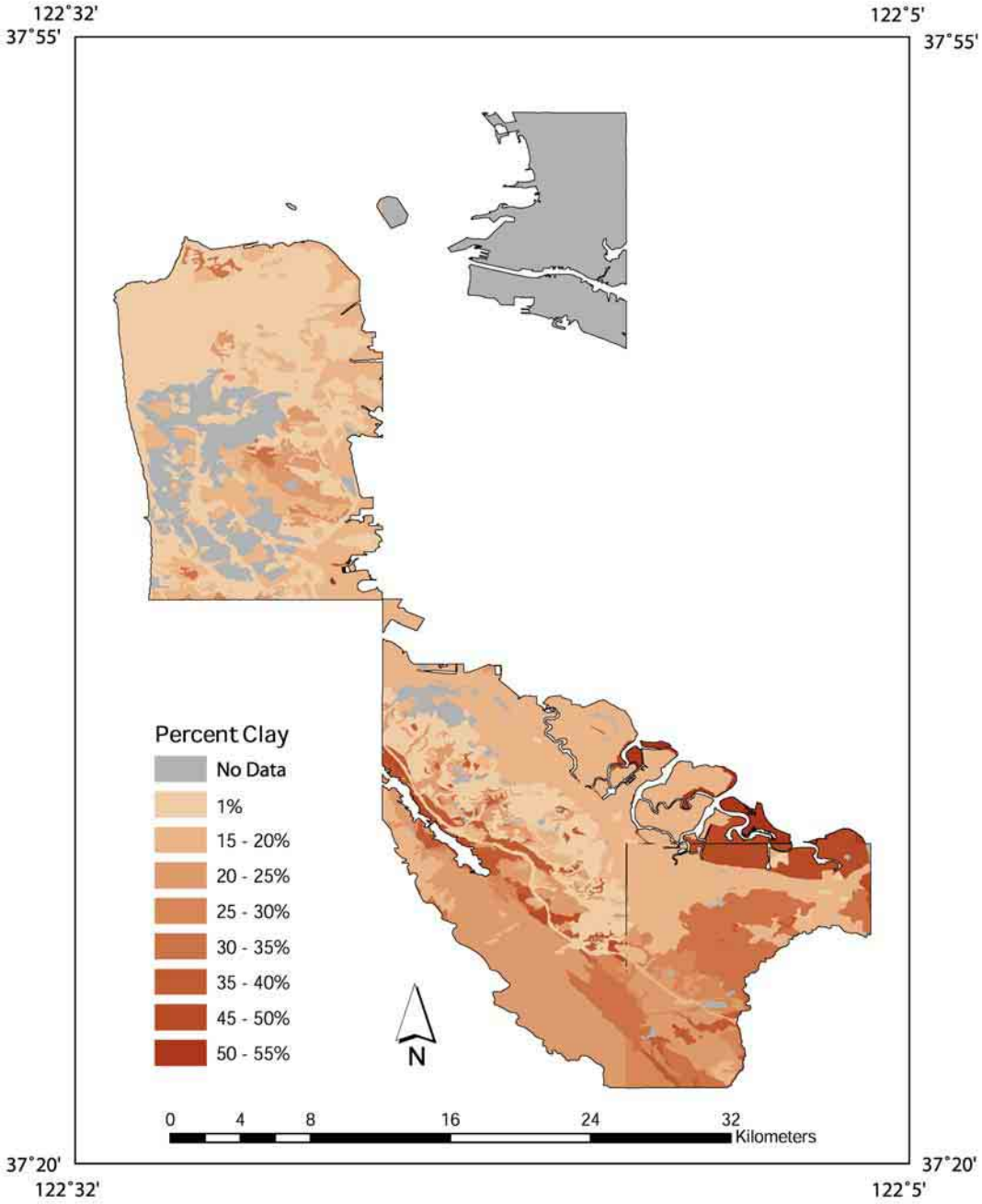

Figure 7. Distribution of clay as a percentage of the soil (Kashiwagi and Hokholt, 1991; Welch, 1981).

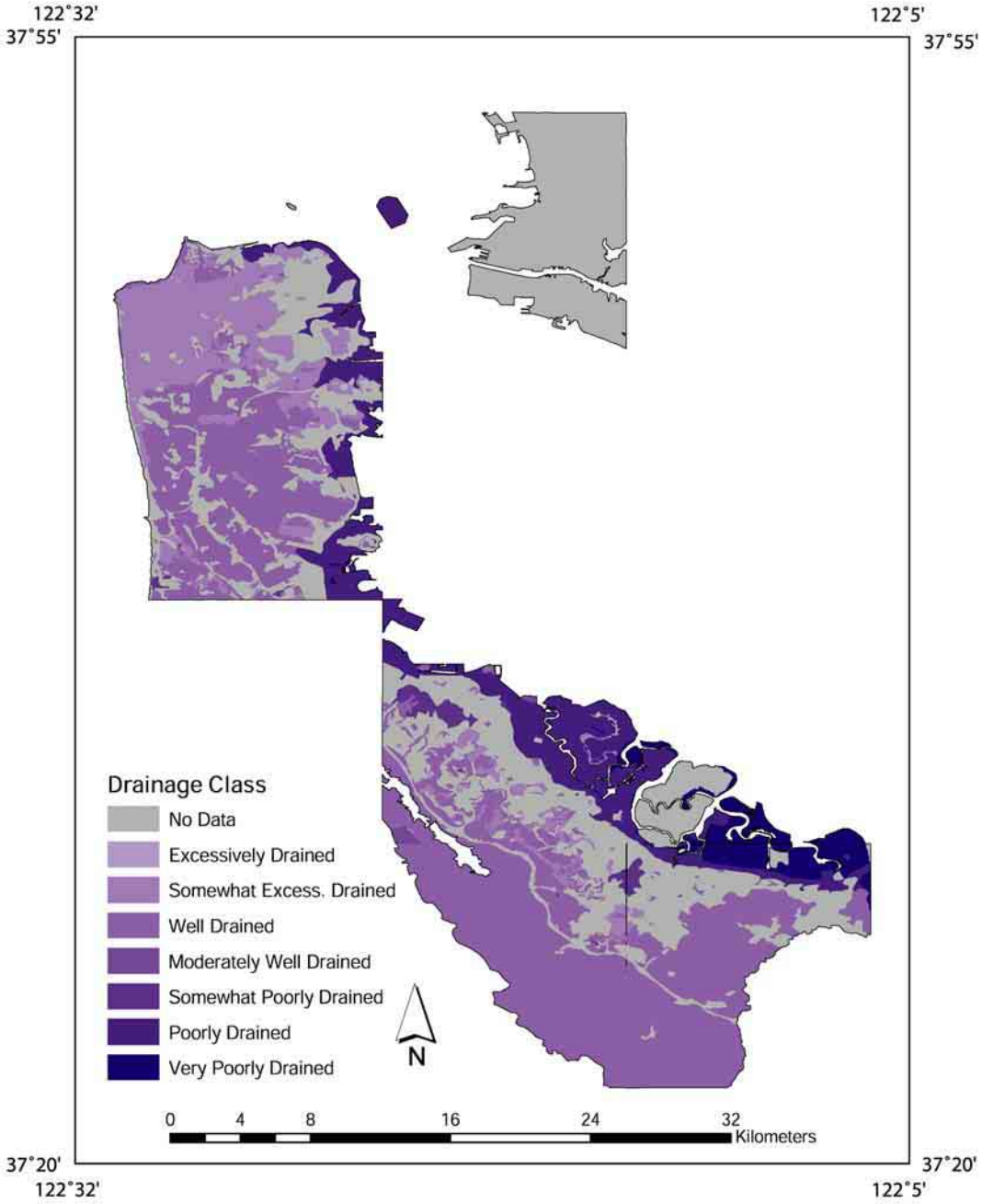

Figure 8. Distribution of drainage classes of soils/unconsolidated sediments in the San Francisco Bay area (Kashiwagi and Hokholt, 1991; Welch, 1981).

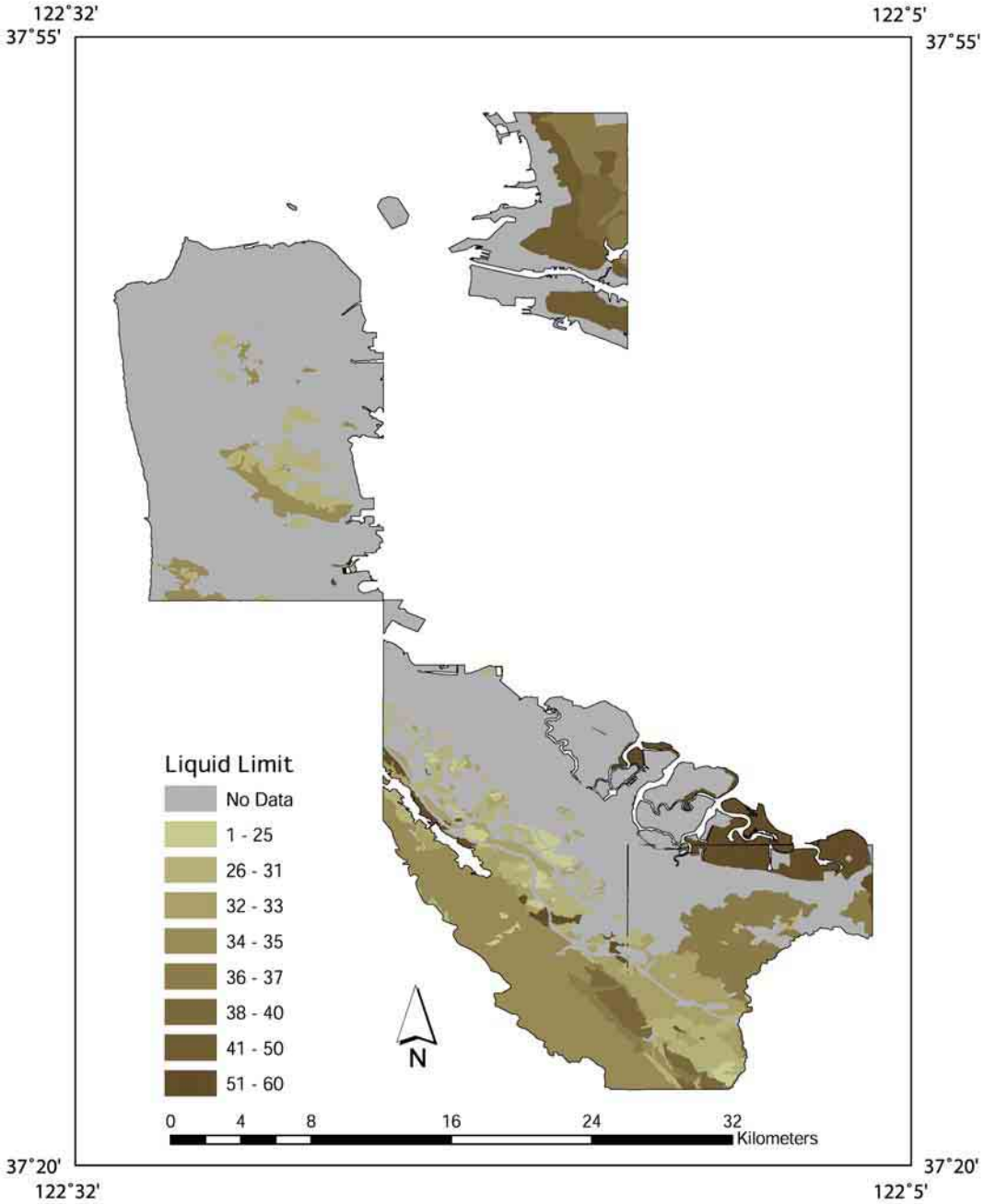

Figure 9. Liquid limit distribution showing the water content as a percentage of soil at the arbitrarily defined boundary between the liquid and plastic states (Kashiwagi and Hokholt, 1991; Welch, 1981).

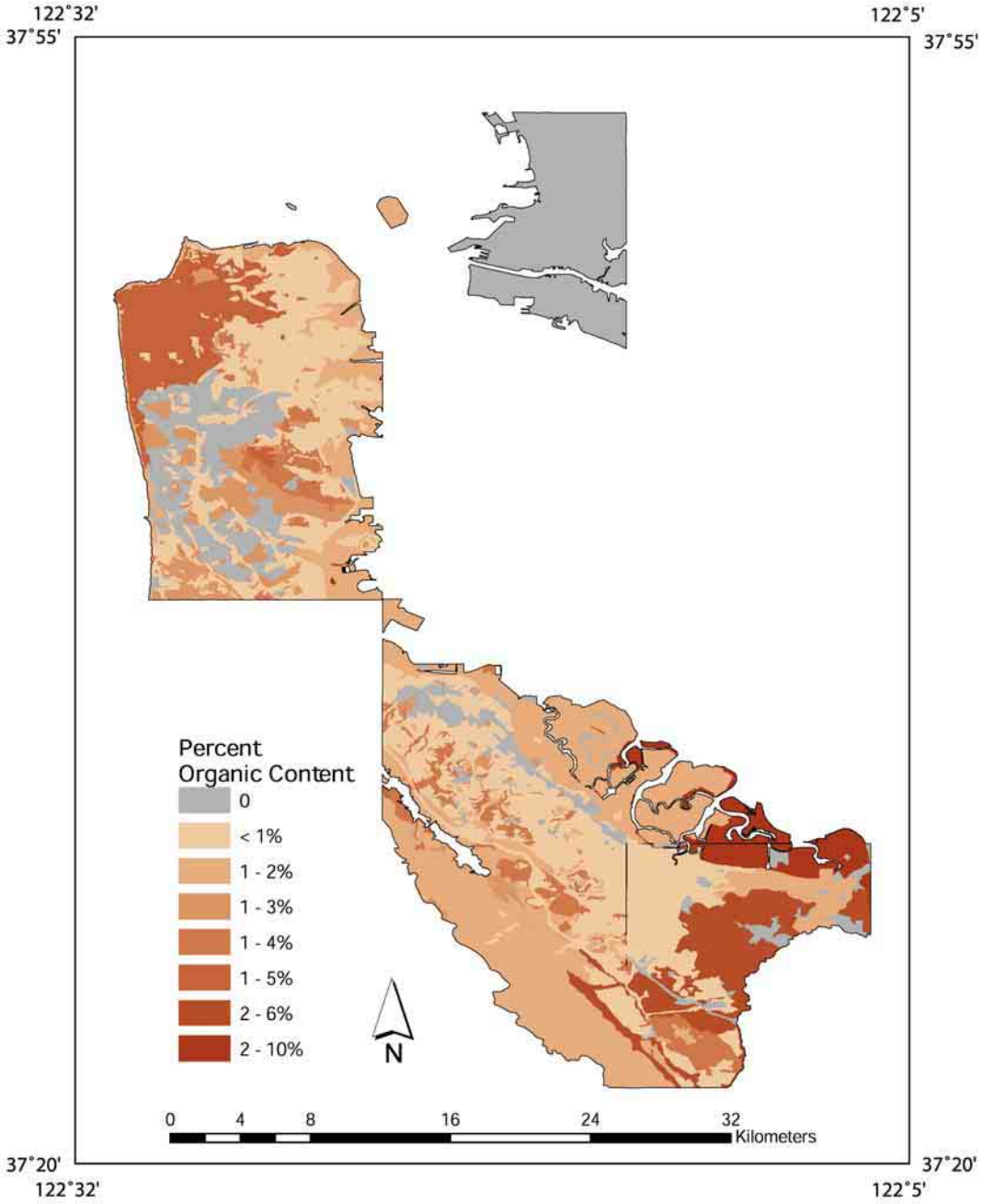

Figure 10. Organic content as a percentage of the soil (Kashiwagi and Hokholt, 1991; Welch, 1981).

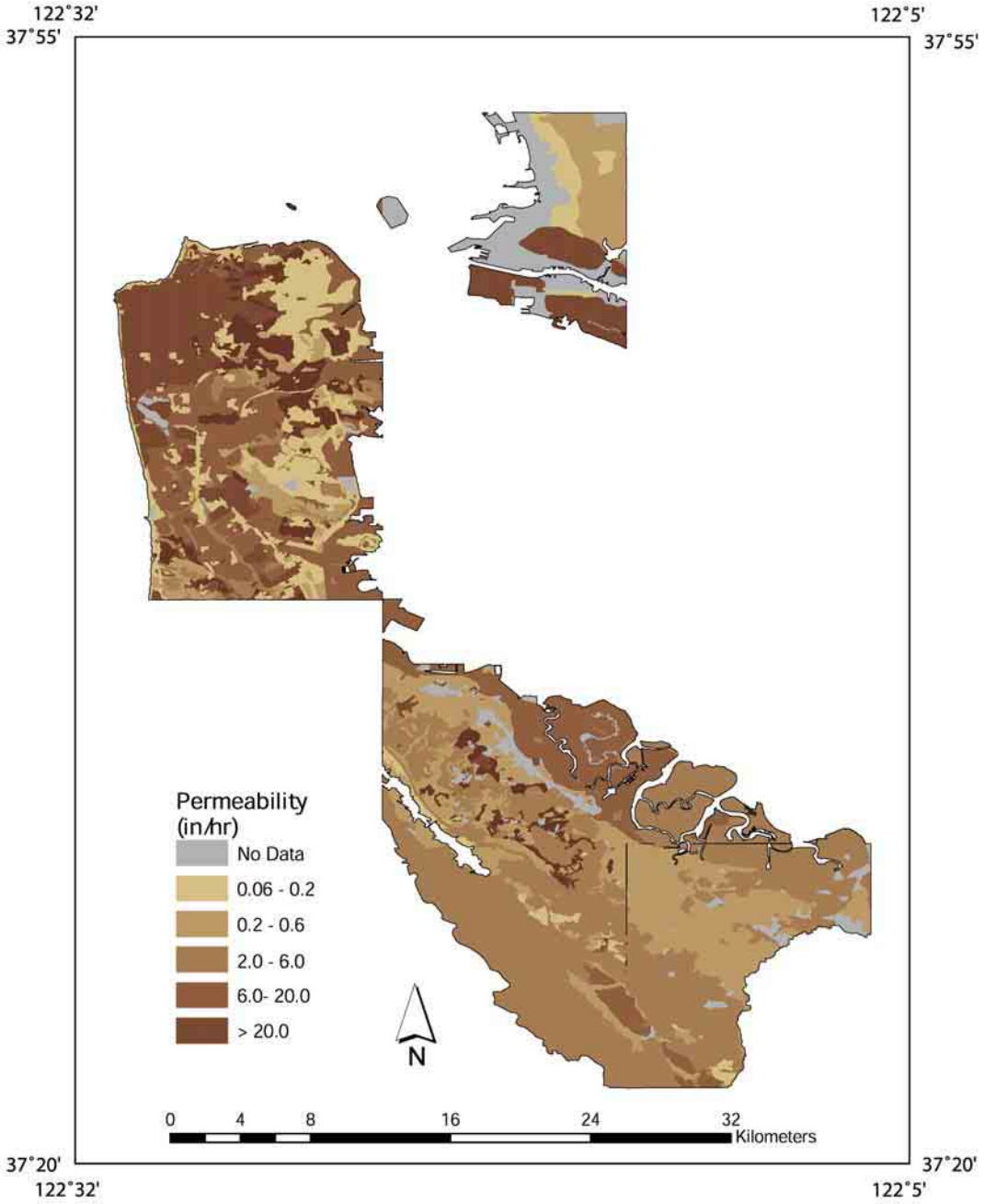

Figure 11. Permeability of water through soil, measured in inches/hour (Kashiwagi and Hokholt, 1991; Welch, 1981).

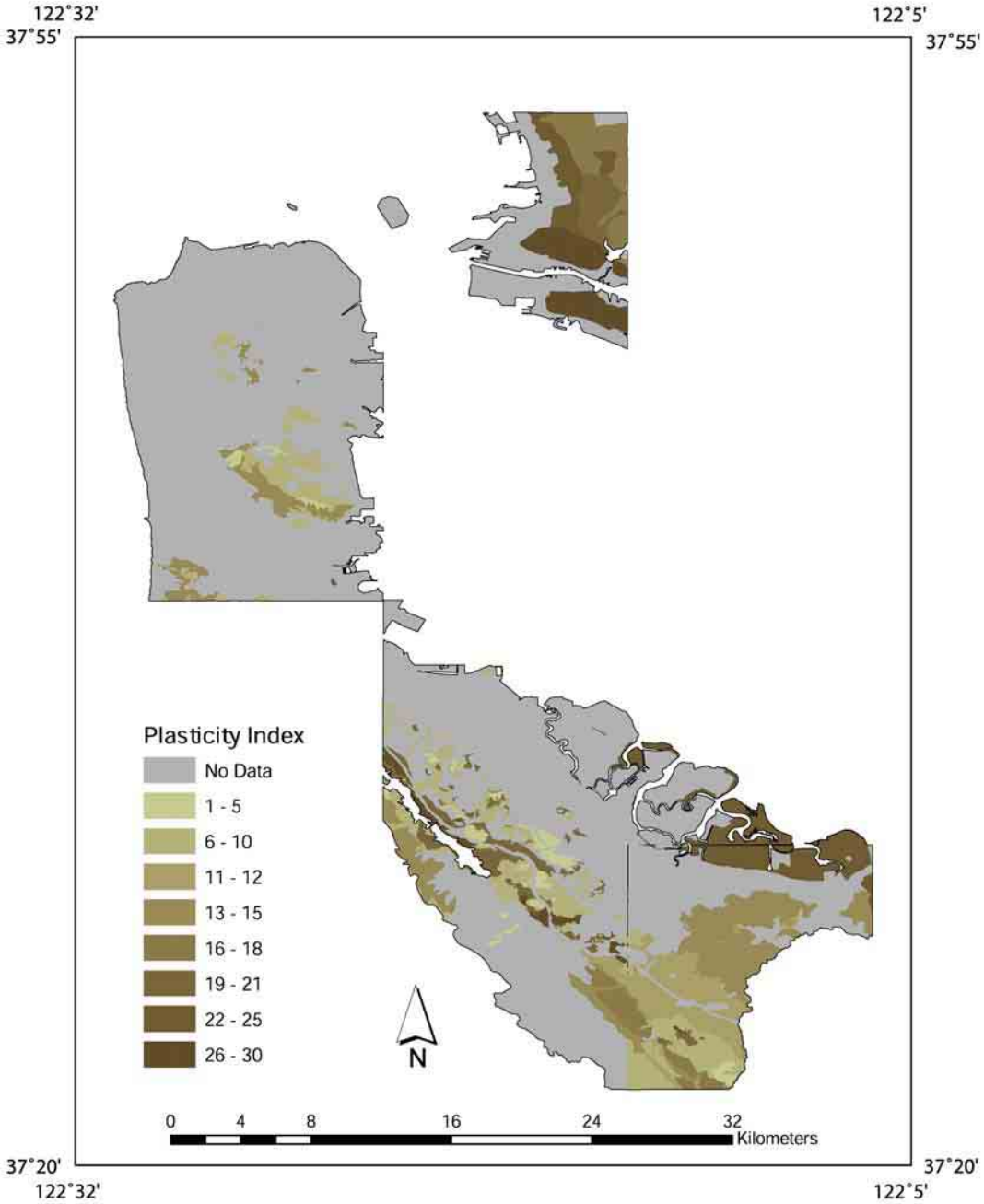

Figure 12. Plasticity index distribution as a percentage of water content of soil at the boundary between the plastic and brittle states (Kashiwagi and Hokholt, 1991; Welch, 1981).

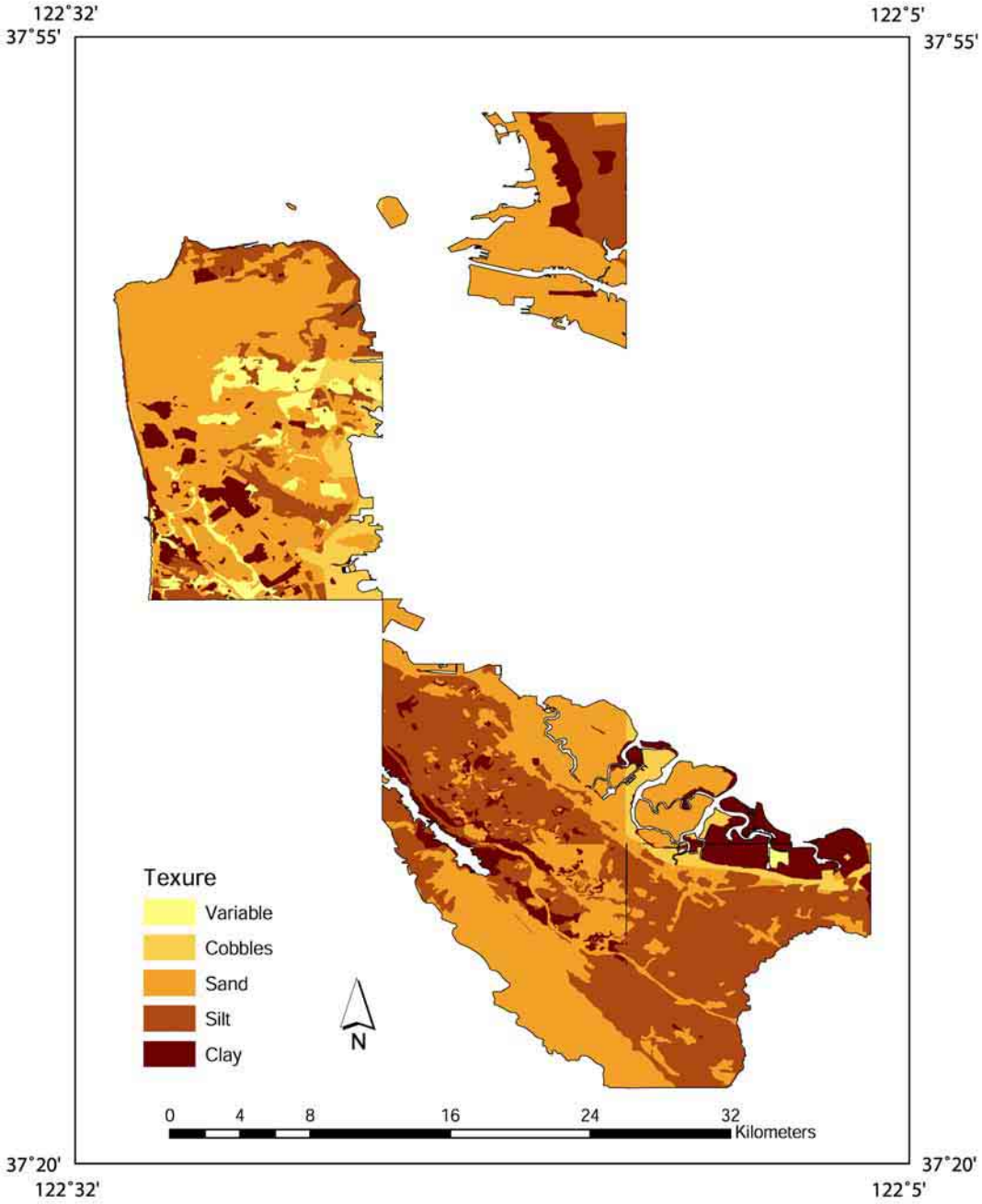

Figure 13. Generalized texture of the soil (Kashiwagi and Hokholt, 1991; Welch, 1981).

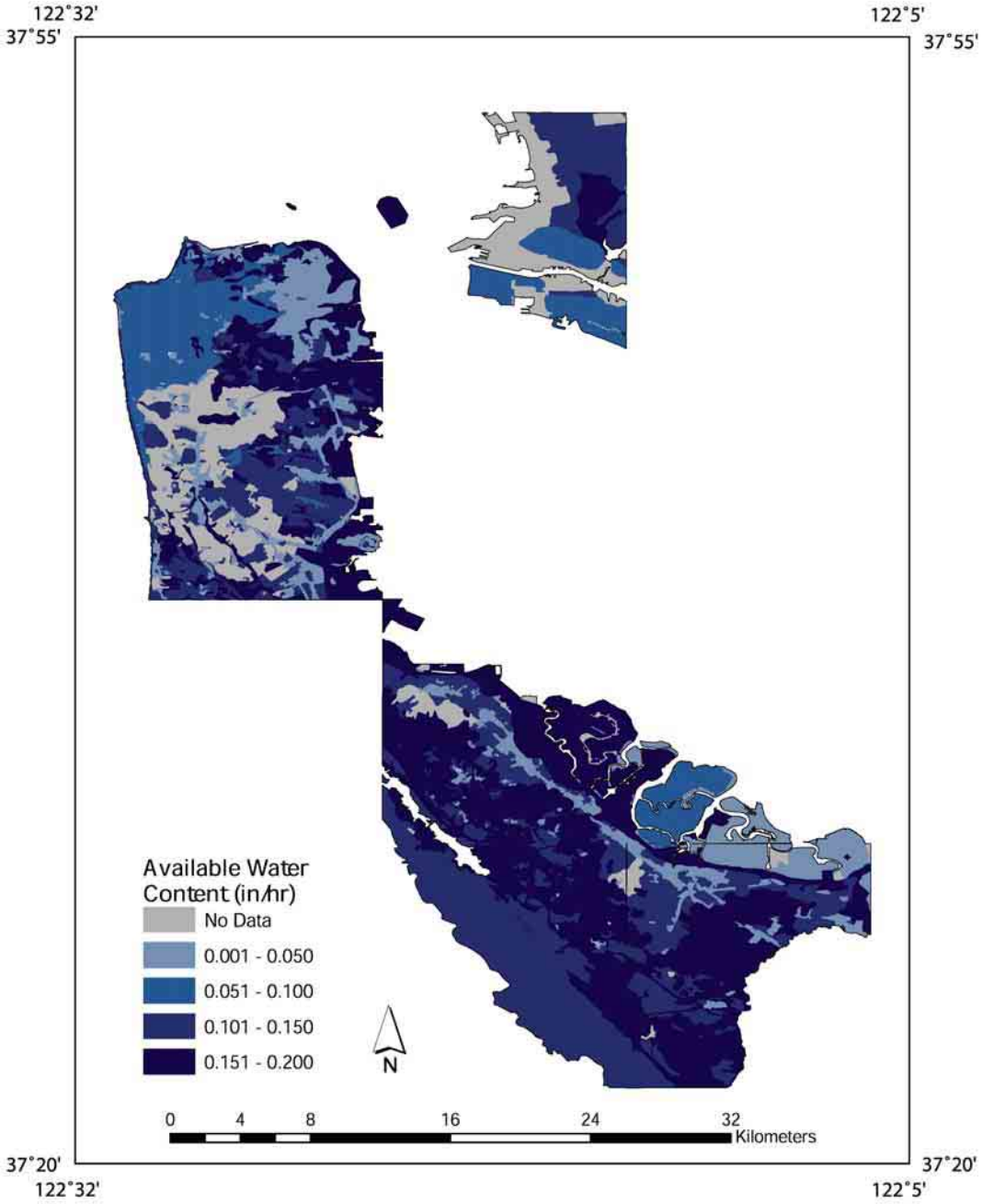

Figure 14. Water capacity of the soil measured in inches/hour (Kashiwagi and Hokholt, 1991; Welch, 1981).

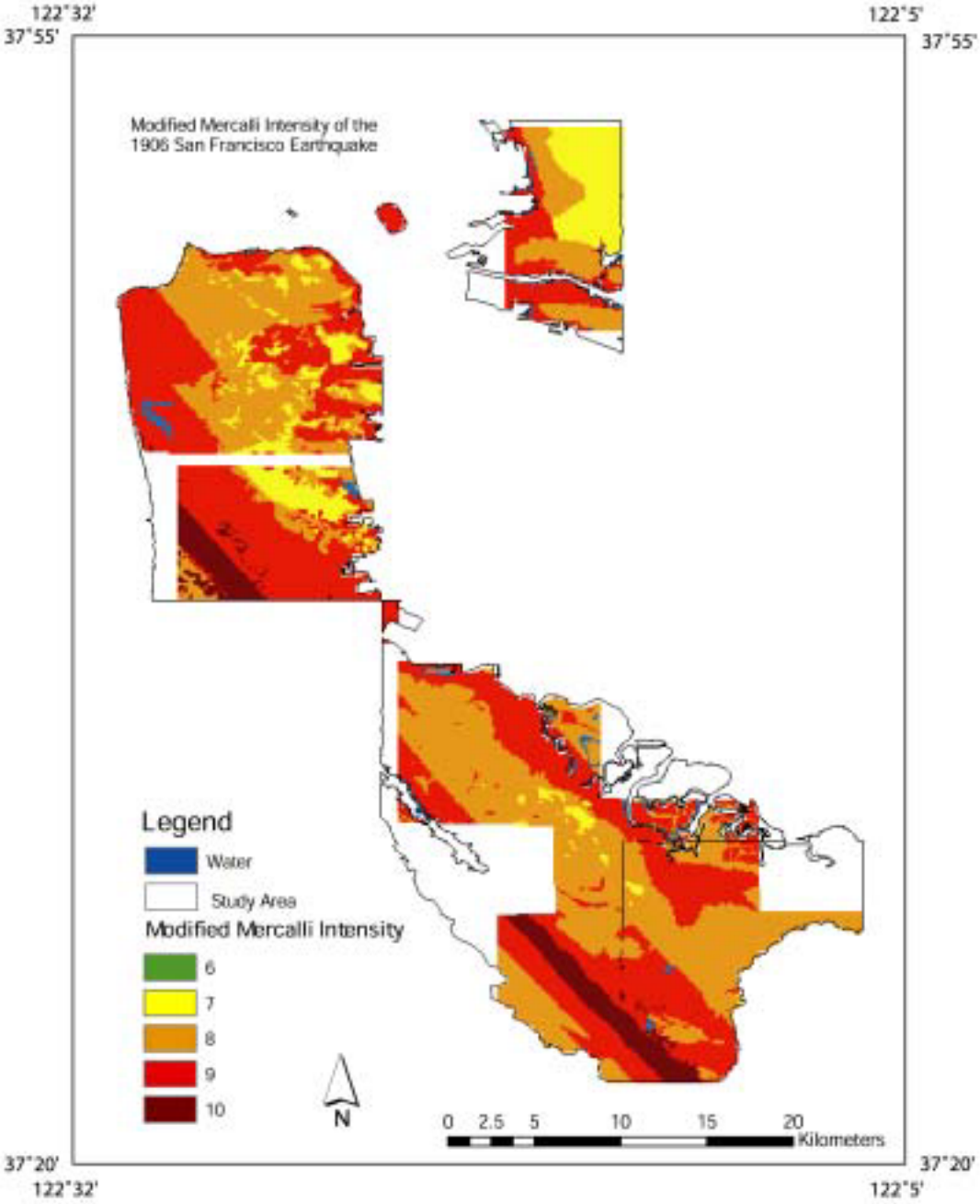

Figure 15. Modified Mercalli Intensity (MMI) from the 1906 San Francisco earthquake. Original data was collected by the Association of Bay Area Governments (ABAG Online, 1995). Maps are only available for different cities within the San Francisco Bay area and is the reason for gaps in the data.

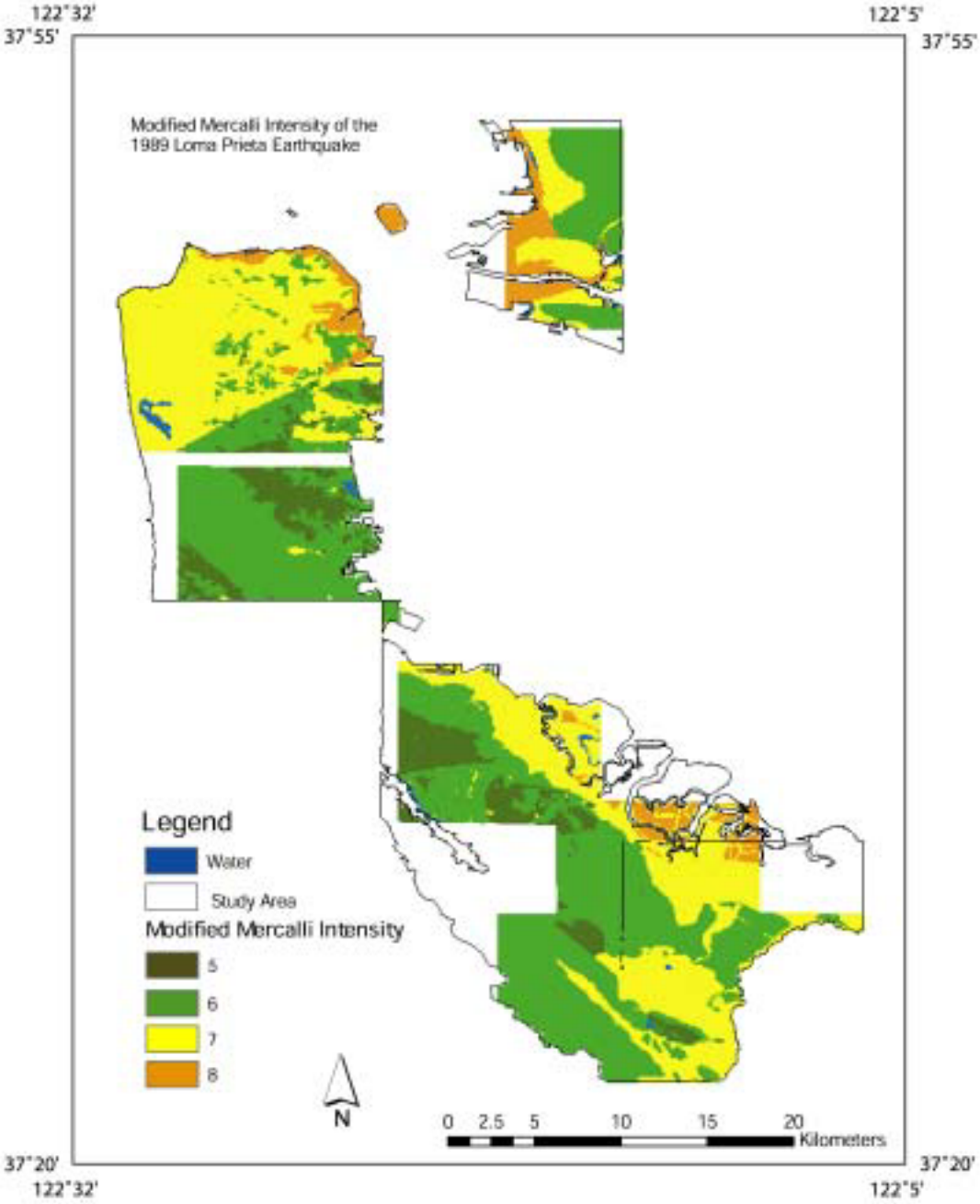

Figure 16. Modified Mercalli Intensity (MMI) from the 1989 Loma Prieta earthquake. Original data was collected by the Association of Bay Area Governments (ABAG Online, 1995). Maps are only available for different cities within the San Francisco Bay area and is the reason for gaps in the data.

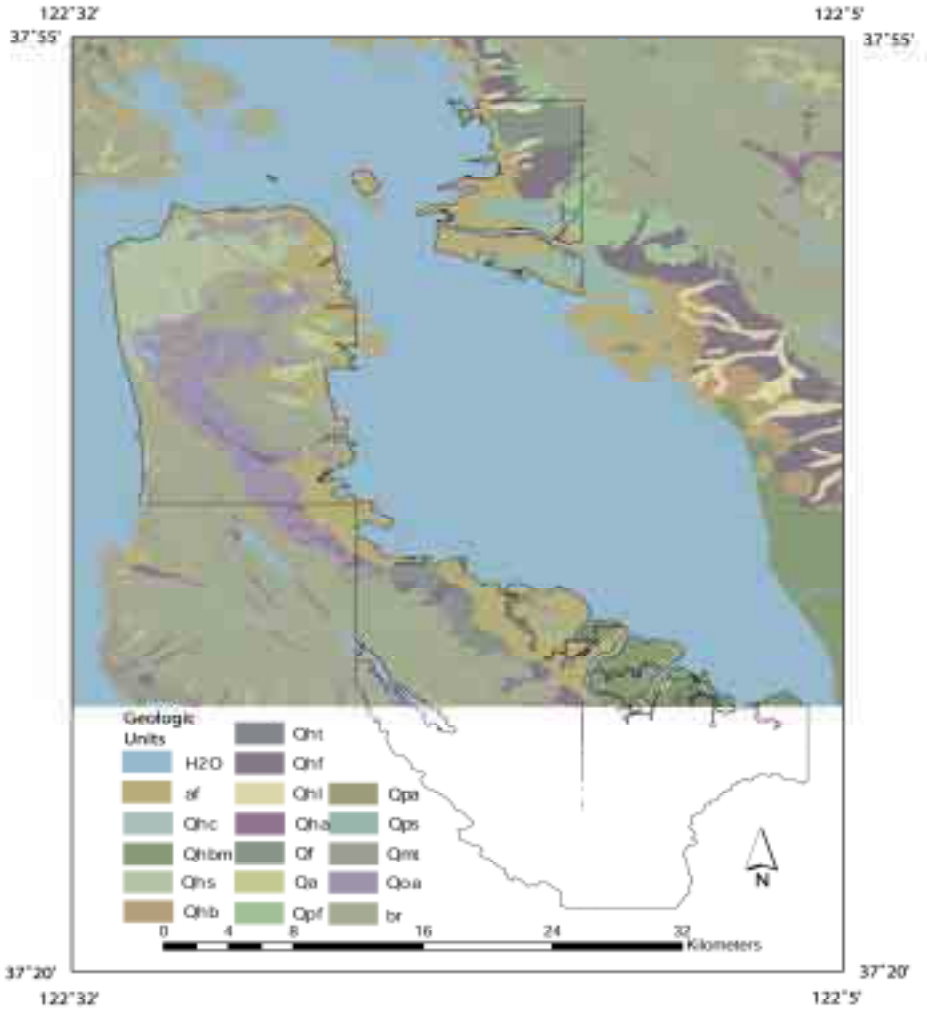

Figure 17. Geologic units of the San Francisco Bay area. Table 3 contains a brief description of the geologic units. For a complete description, see Knudsen et al., 1997.

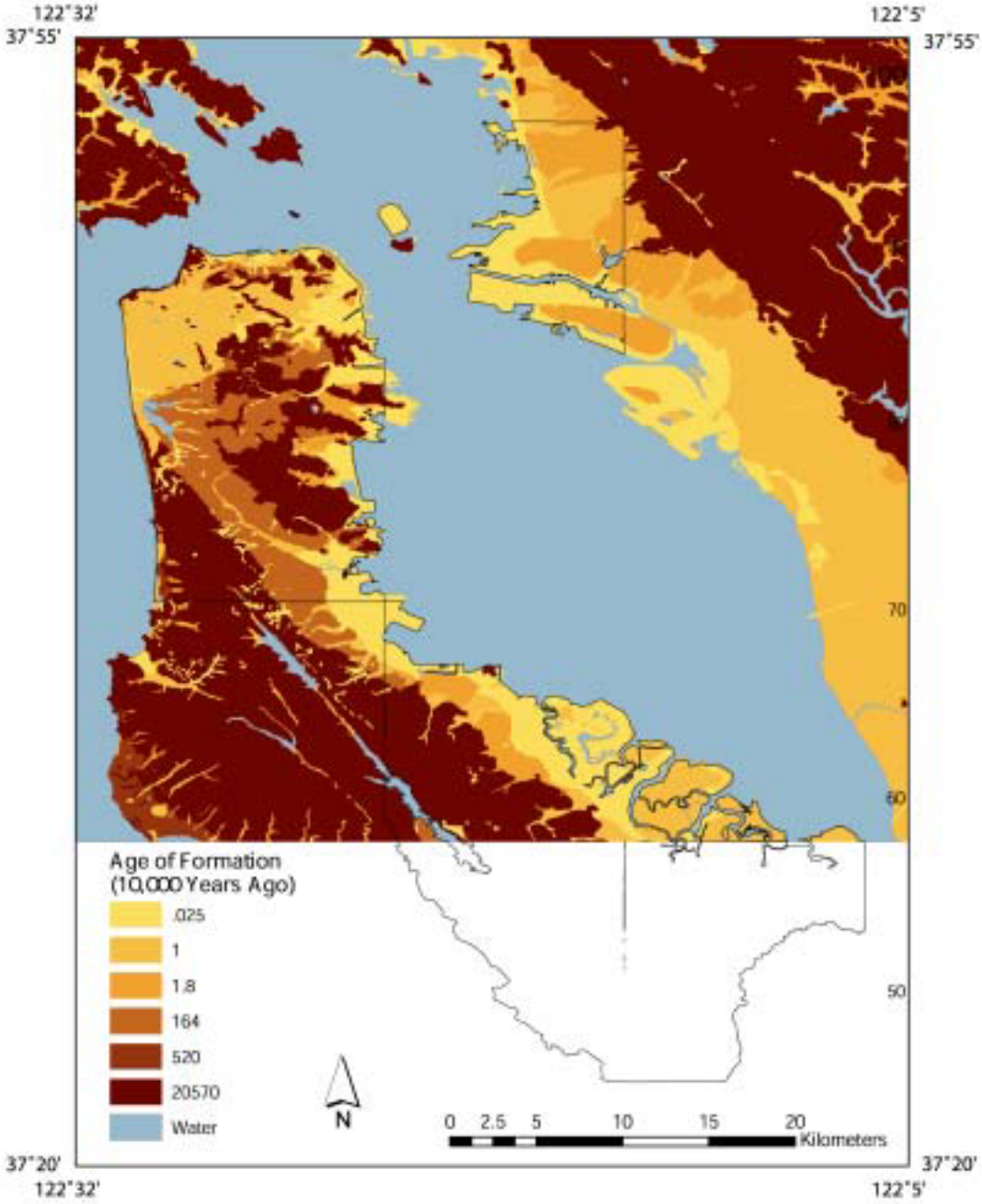

Figure 18. Relative ages of each Quaternary geologic unit. Table 24 shows the geologic units from which these ages were derived. For more information, see Knudsen et al/. 1997.

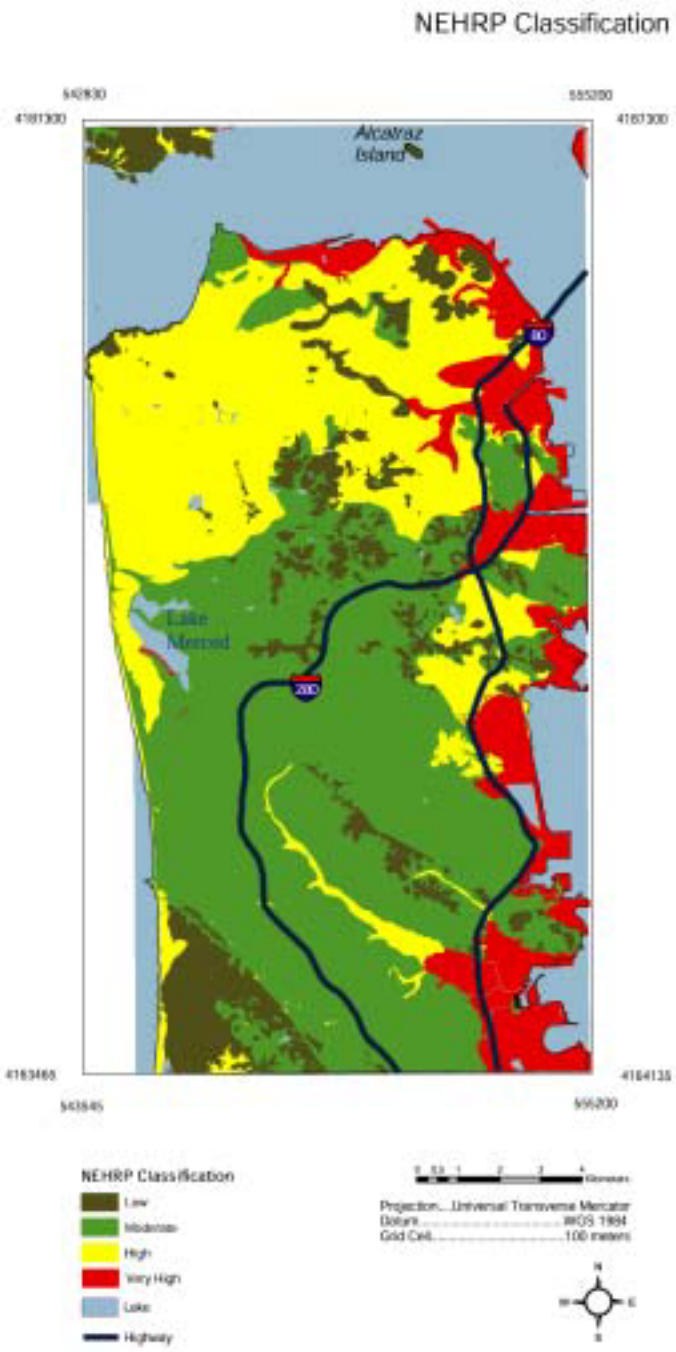

Figure 19. Current building codes in San Francisco as determined by the National Earthquake Hazards Reduction Program (NEHRP).

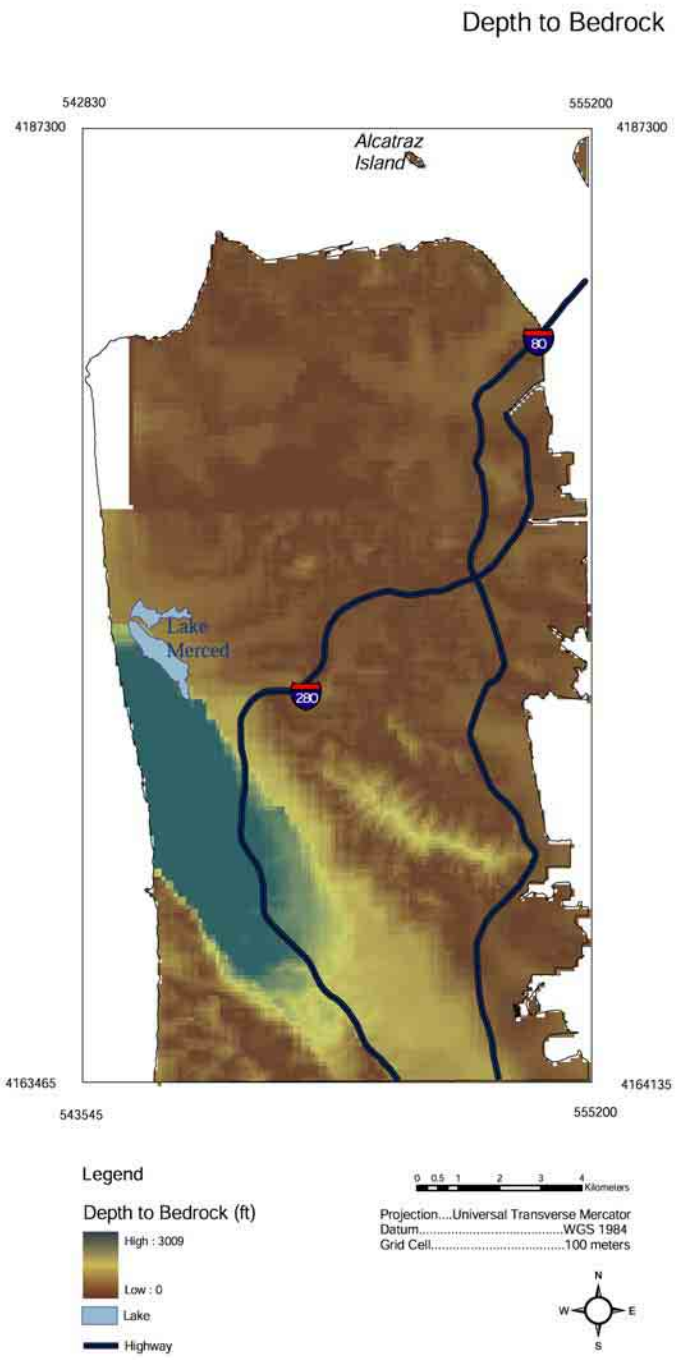

Figure 20. Depth (feet) to the bedrock (Bonilla 1964; Schlocker, 1961).

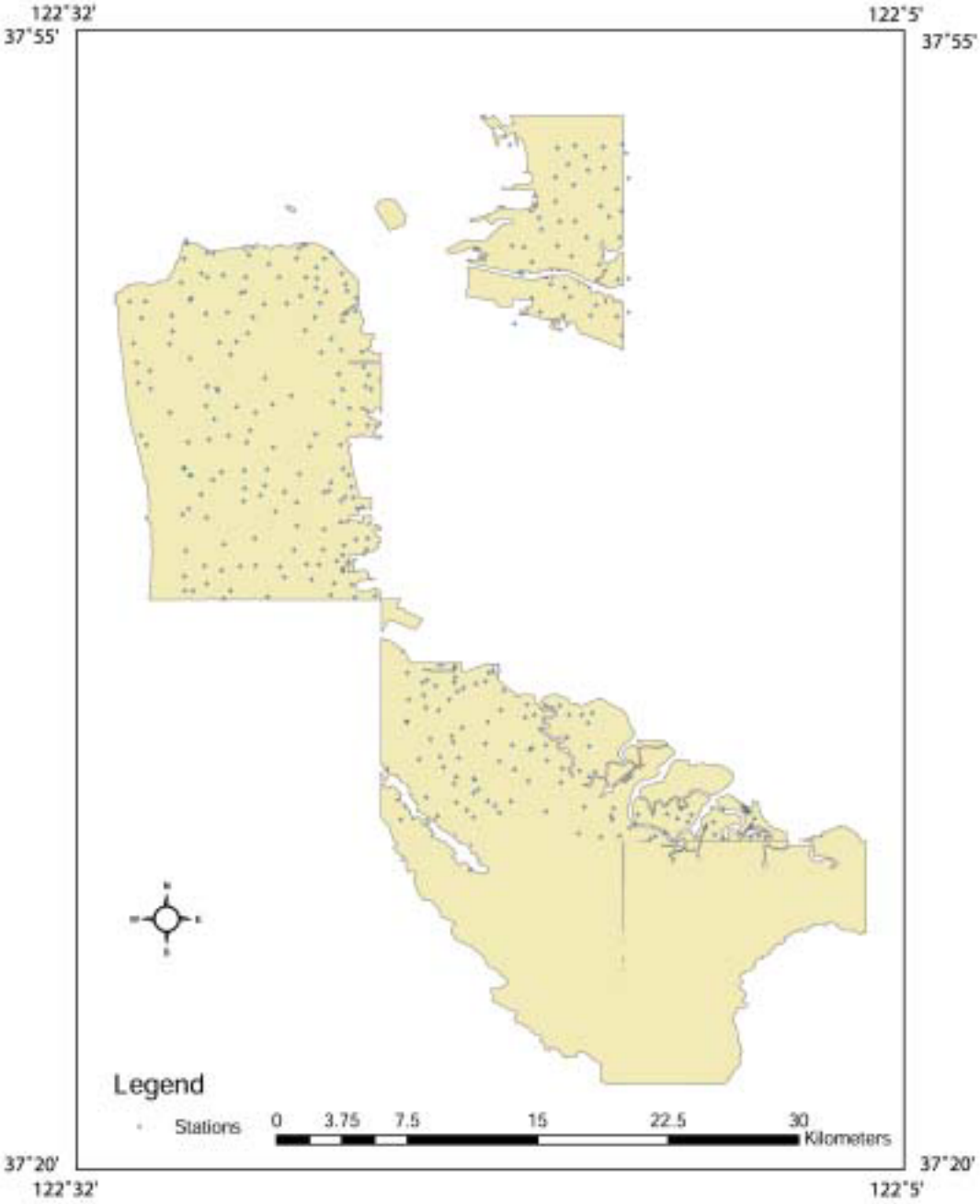

Figure 21. Sampling stations for multivariate statistical analysis.

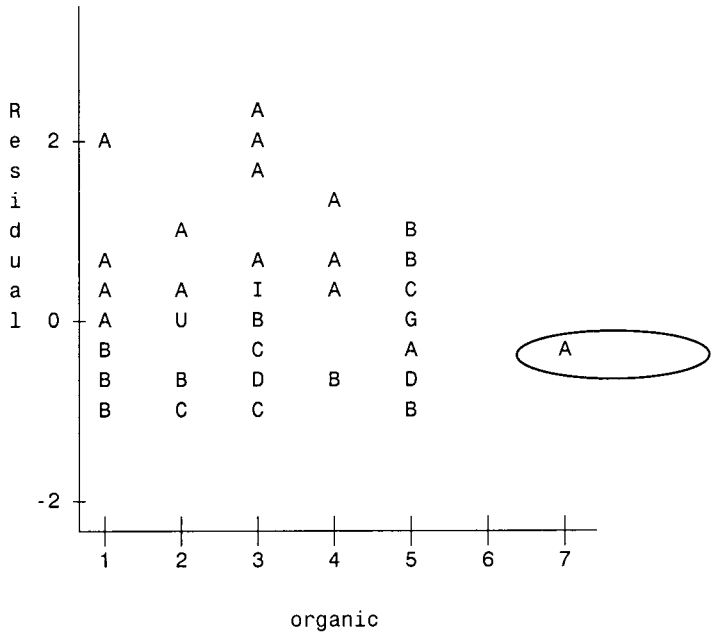

Figure 22. Plot of residual vs. organic content for 1906. "A" represents a site in the database that occurred one time, "B" represents a site that occurred two times…"U" represents a site that occurred 21 times.

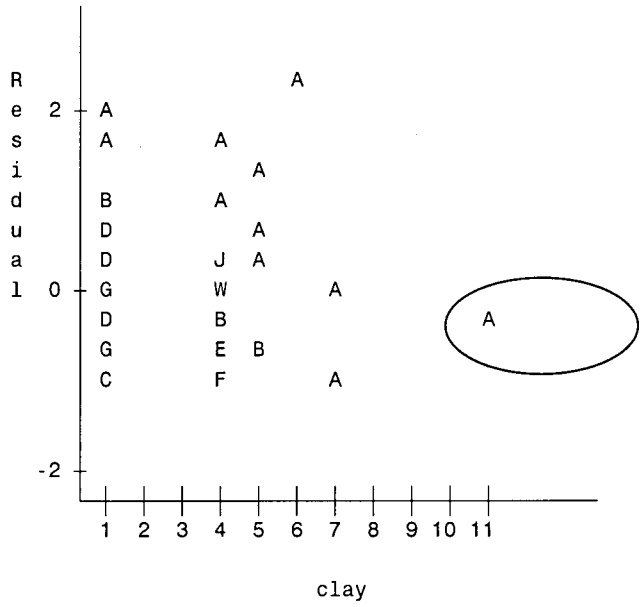

Figure 23. Plot of resudual vs. clay content for 1906. "A" represents a site in the database that occurred one time, "B" represents a site that occurred two times…"W" represents a site that occurred 23 times.

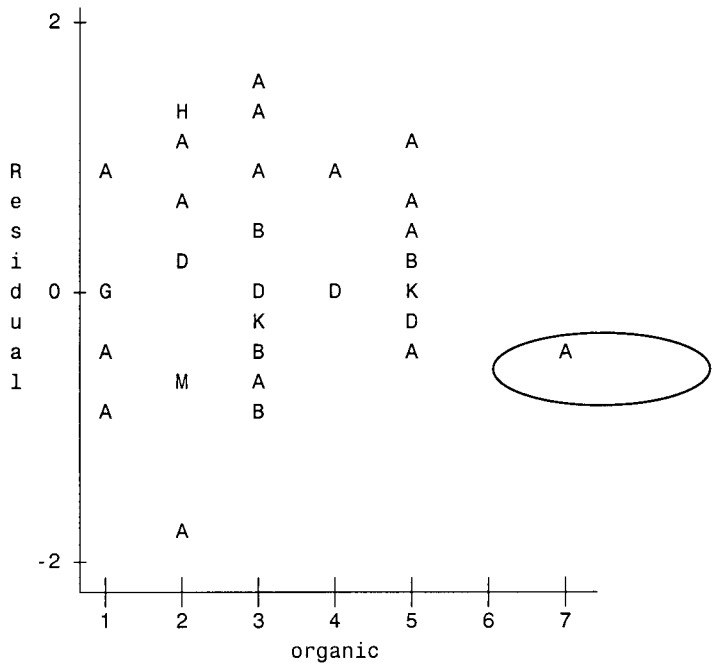

Figure 24. Plot of residual vs. organic content for 1989. "A" represents a site in the database that occurred one time, "B" represents a site that occurred two times…"M" represents a site that occurred 13 times.

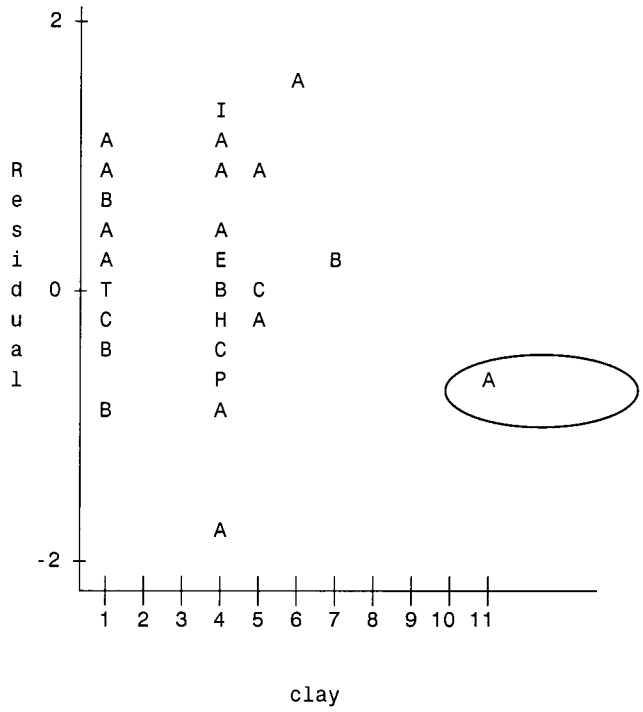

Figure 25. Plot of residual vs. clay content for 1989. "A" represents a site in the database that occurred one time, "B" represents a site that occurred two times…"T" represents a site that occurred 20 times.

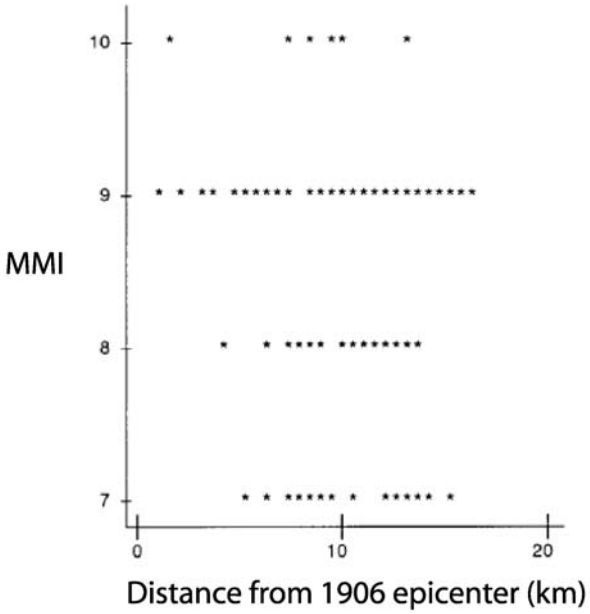

Figure 26. Plot of shaking vs. distance from the epicenter for the 1906 San Francisco quake.

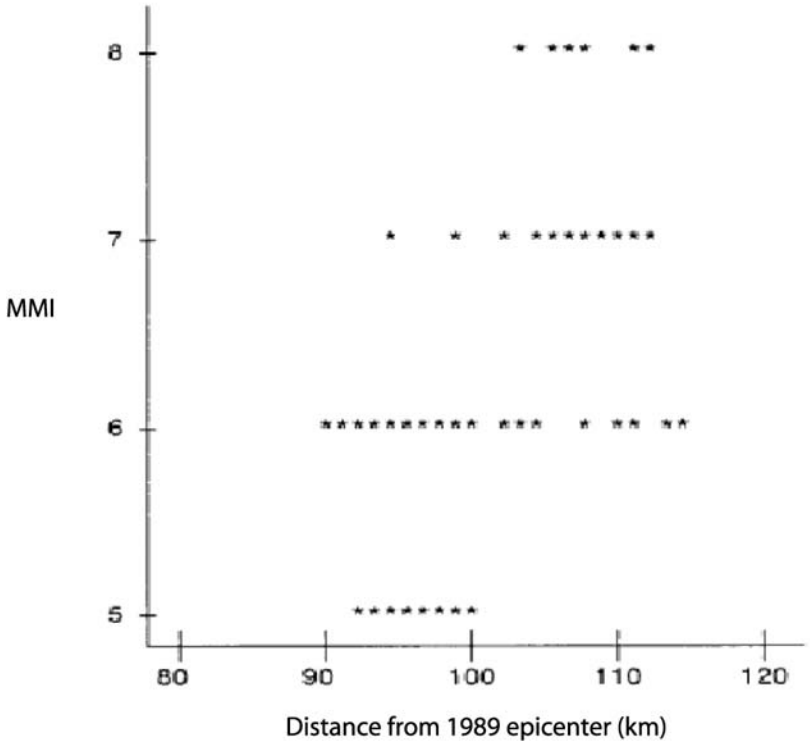

Figure 27. Plot of shaking vs. distance from the epicenter for the 1989 quake.

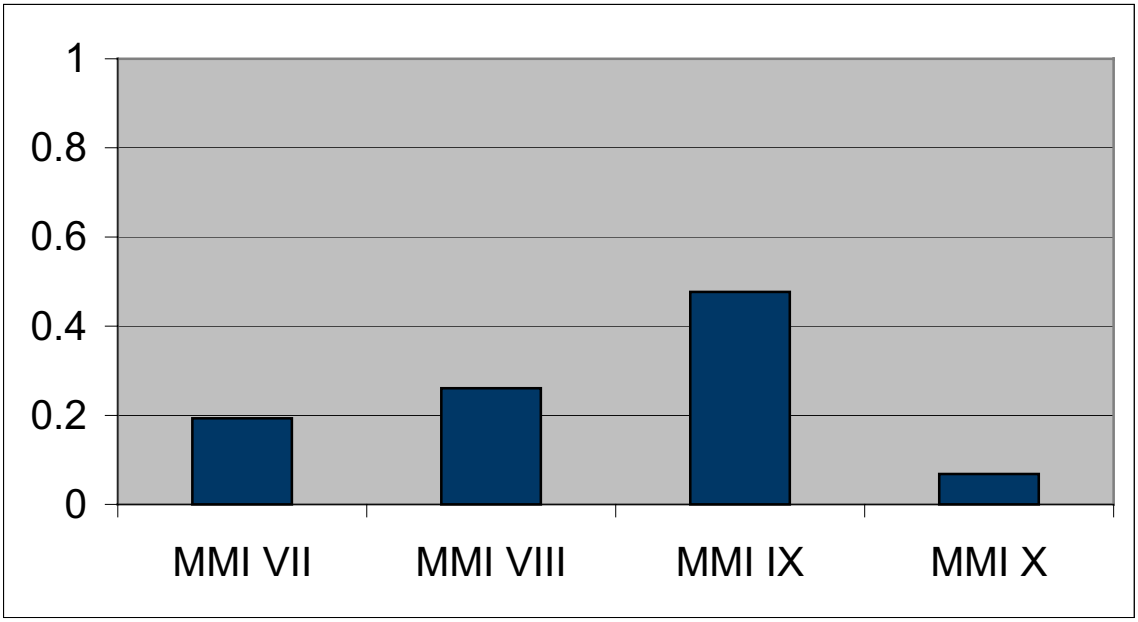

Figure 28. Probability vs. Modified Mercalli Intensity showing the original distribution of points for the 1906 San Francisco earthquake.

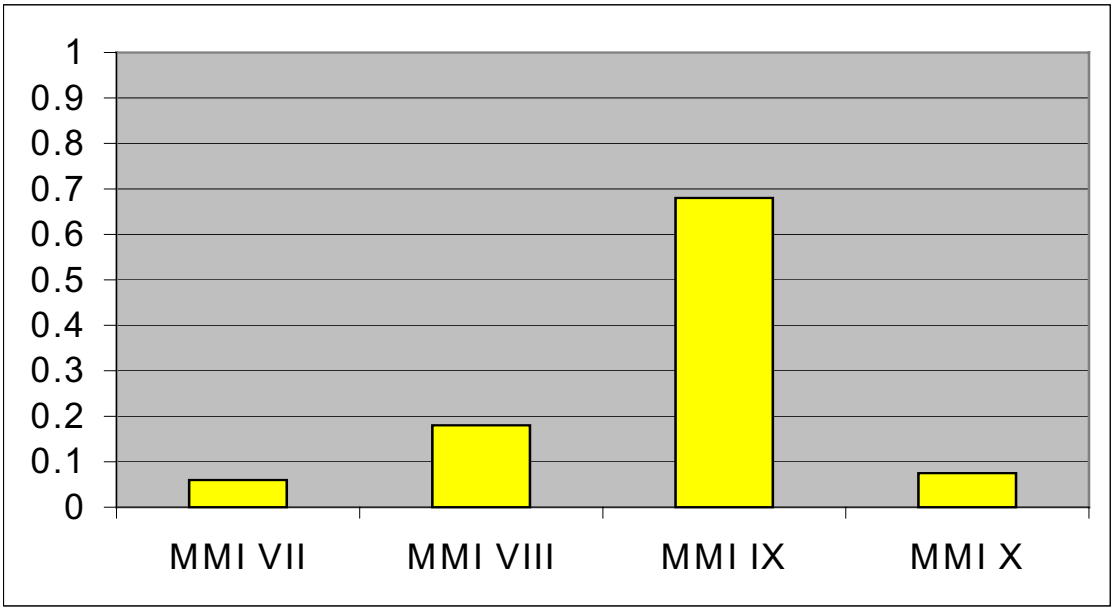

Figure 29. Probability vs. Modified Mercalli Intensity showing a "typical" distribution of points for the 1906 San Francisco earthquake. The median values of water content, age, and depth were used to estimate this distribution.

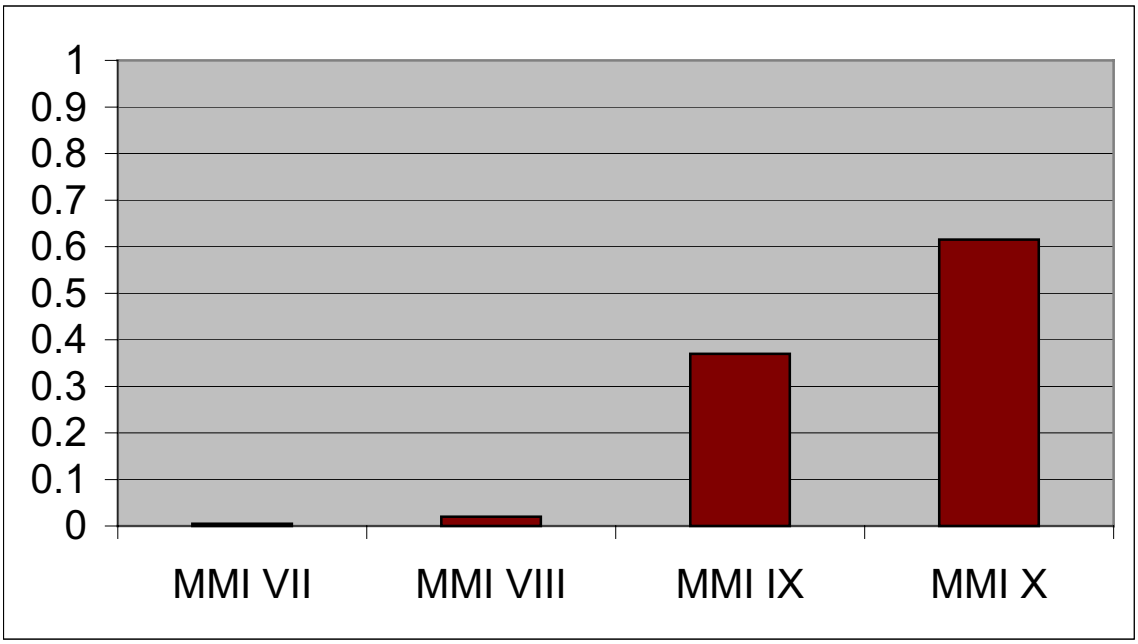

Figure 30. Most Dangerous Distribution for 1906. The maximum values of water content, age, and depth were used to estimate this distribution.

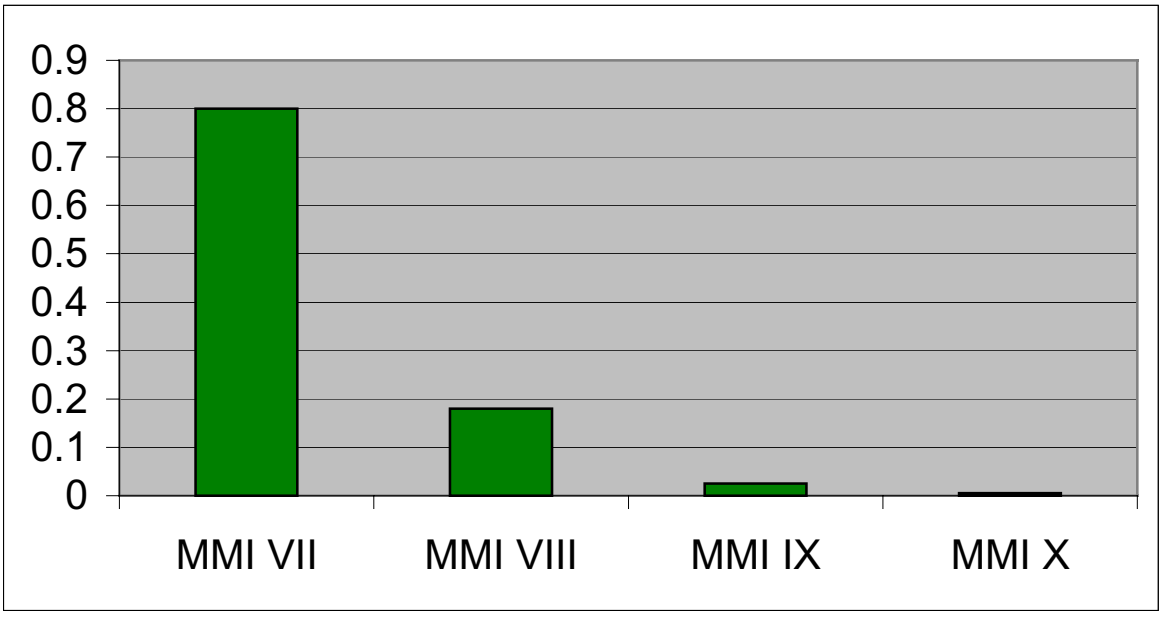

Figure 31. Least Dangerous Distribution for 1906. The minimum values of water content, age, and depth were used to estimate this distribution.

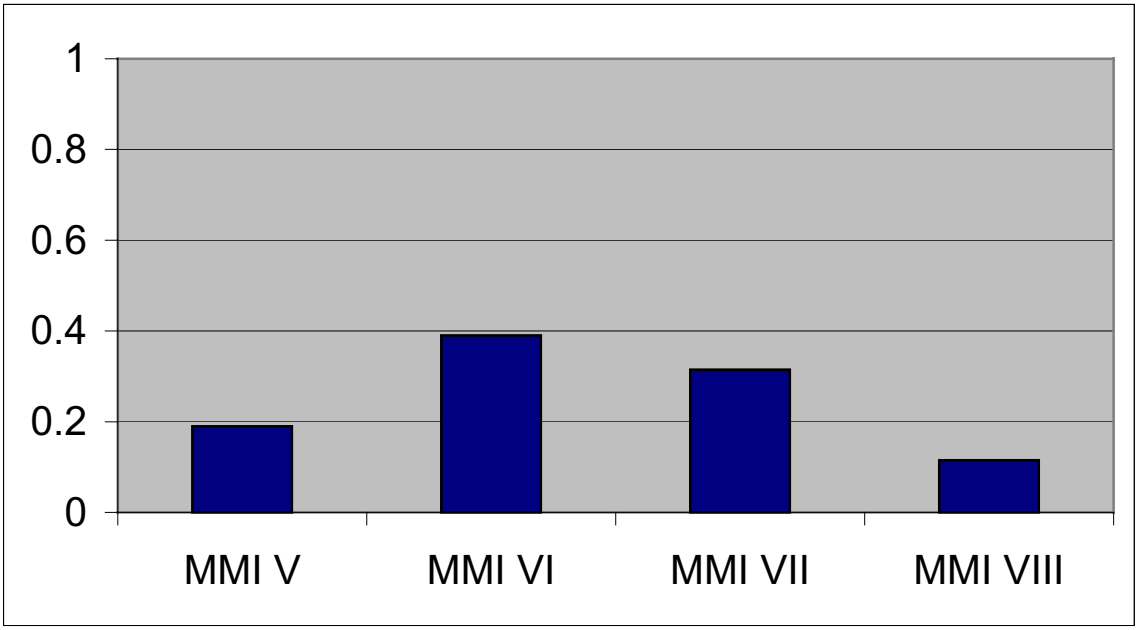

Figure 32. Probability vs. Modified Mercalli Intensity showing the original distribution of points for the 1989 Loma Prieta earthquake.

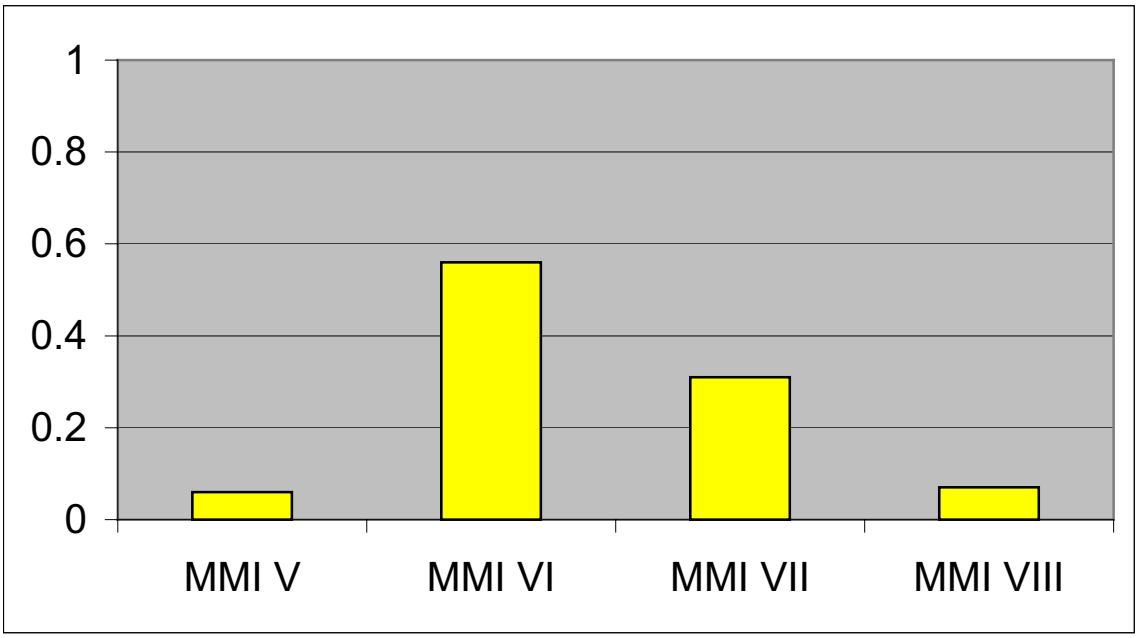

Figure 33. Probability vs. Modified Mercalli Intensity showing a "typical" distribution of points for the 1989 Loma Prieta earthquake. The median values of permeability, organic content, drainage class, and age were used to estimate this distribution.

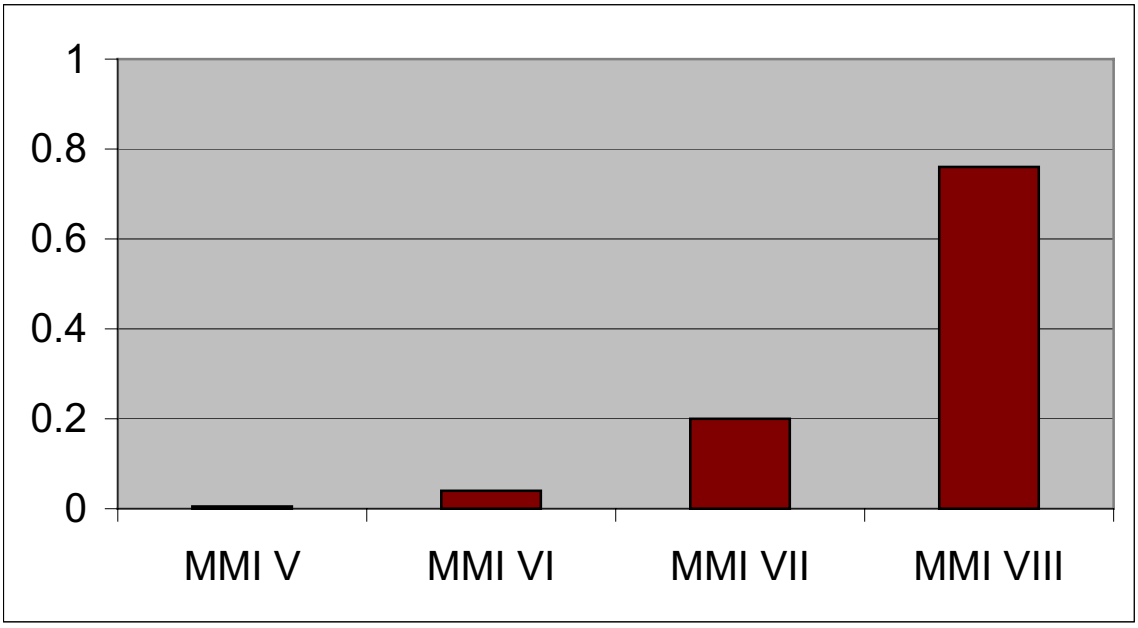

Figure 34. Most Dangerous Distribution for 1989. The maximum values of permeability, organic content, drainage class, and age were used to estimate this distribution.

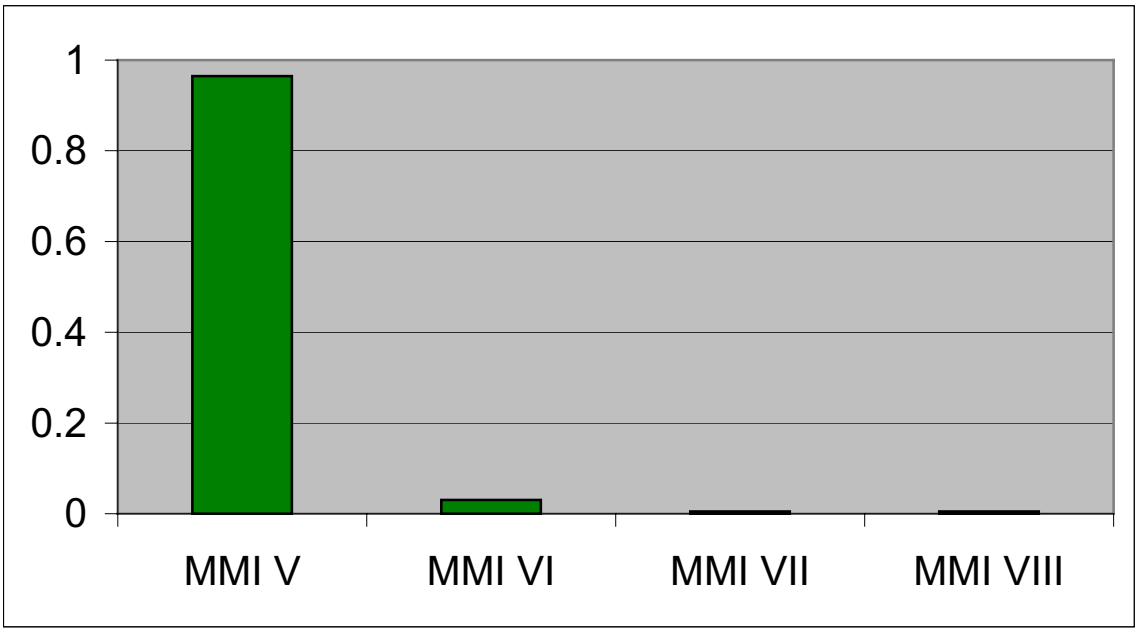

Figure 35. Least Dangerous Distribution for 1989. The minimum values of permeability, organic content, drainage class, and age were used to estimate this distribution.

Figure 36. Probability of experiencing Modified Mercalli > 7 for a repeat of the 1906 San Francisco earthquake.

Figure 37. Probability of experiencing Modified Mercalli Intensity > 8 for a repeat of the 1906 San Francisco earthquake.

Figure 38. Probability of experiencing Modified Mercalli Intensity > 9 (MMI = 10) for a repeat of the 1906 San Francisco earthquake.

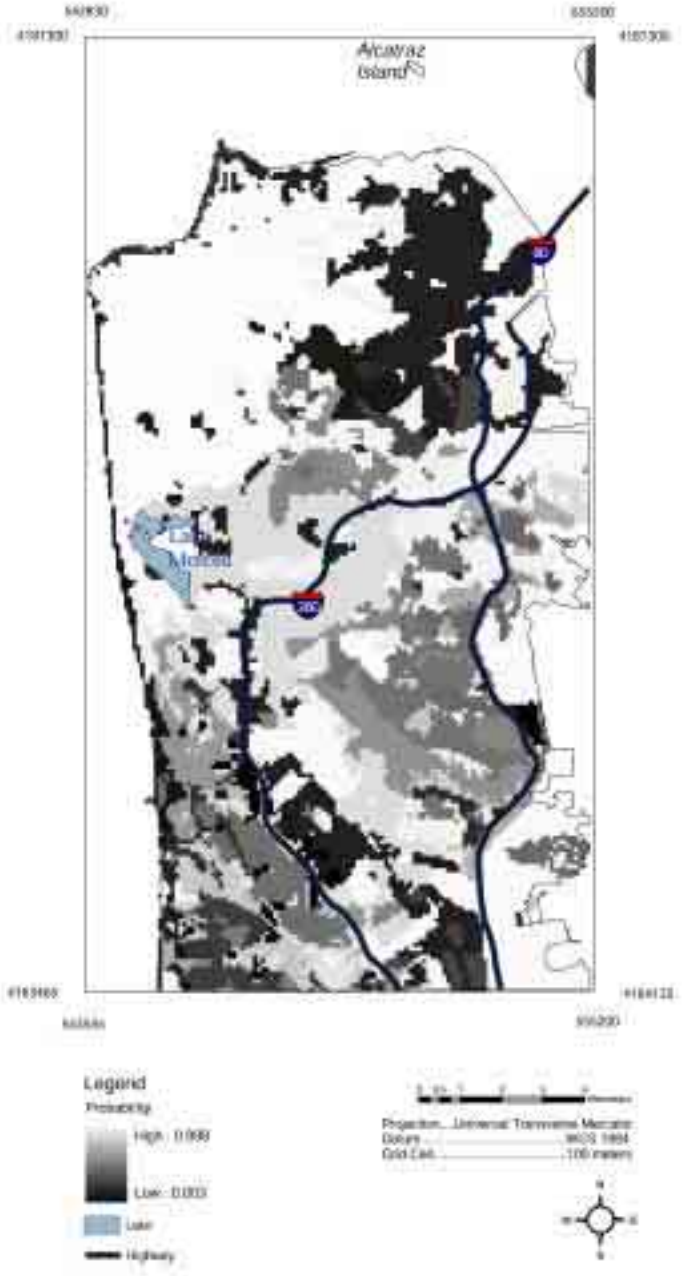

Figure 39. Probability of experiencing Modified Mercalli Intensity > 5 for a repeat of the 1989 Loma Prieta earthquake.

Figure 40. Probability of experiencing Modified Mercalli Intensity > 6 for a repeat of the 1989 Loma Prieta earthquake.

Figure 41. Probability of experiencing Modified Mercalli Intensity > 7 (MMI = 8) for a repeat of the 1989 Loma Prieta earthquake.

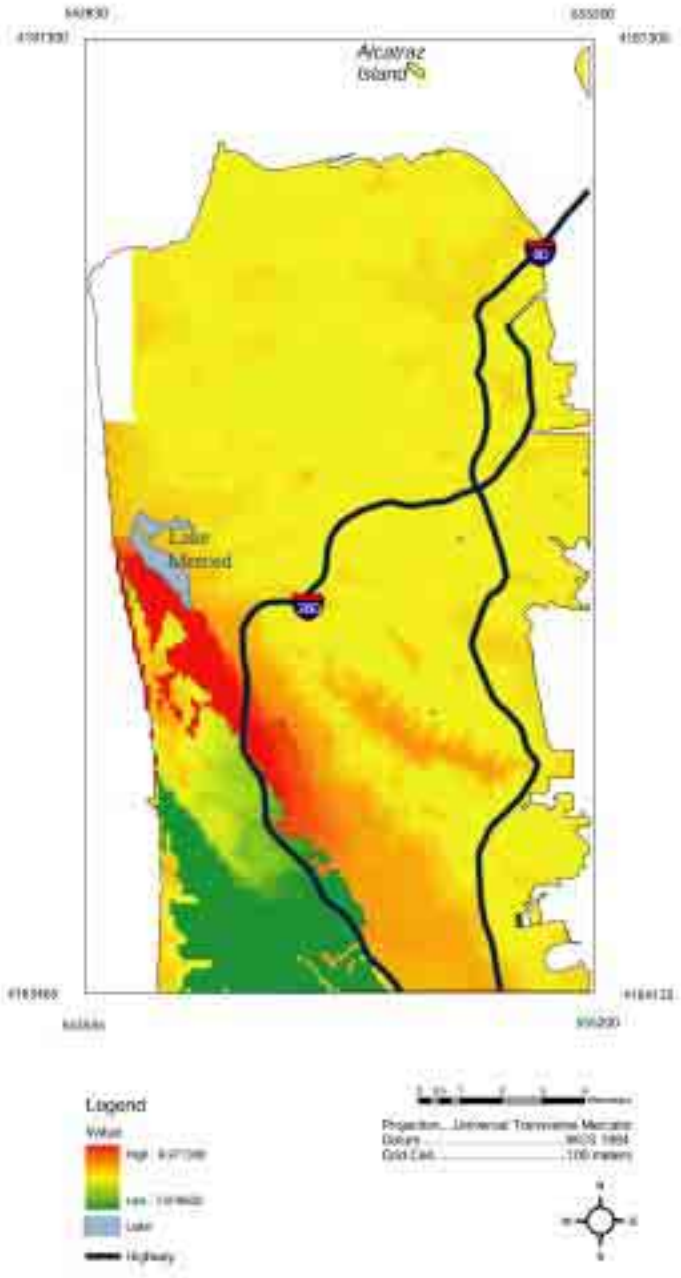

Figure 42. Strong ground motion susceptibility map for a repeat of the 1906 San Francisco earthquake.

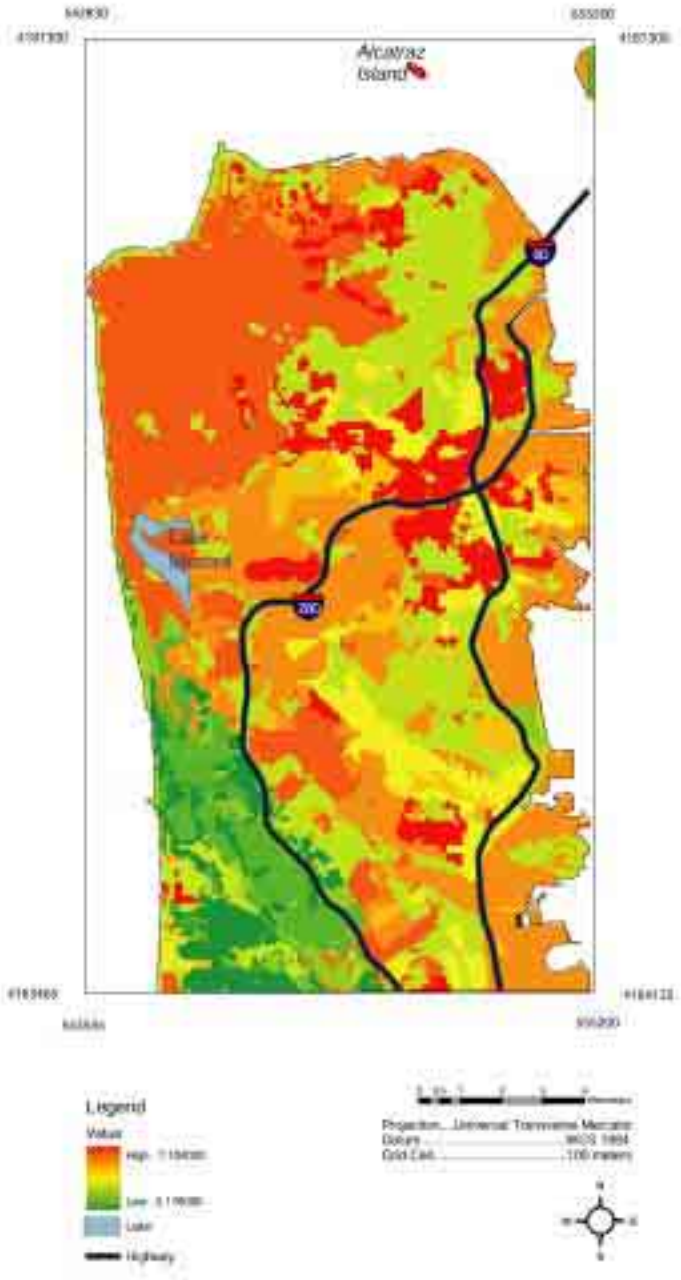

Figure 43. Strong ground motion susceptibility map for a repeat of the 1989 Loma Prieta earthquake.

APPENDIX A

101 – Accelerator-Fagan association – This unit is 45 percent Accelerator loam and 30 percent Fagan loam.

Accelerator – This deep, well-drained soil weathered from soft sandstone and siltstone. Permeability is moderately slow, available water capacity is moderate or high, and runoff is medium. The surface layer is light gray and light brownish gray loam (23 inches thick). The upper six inches of the subsoil is light gray clay loam and the lower 12 inches is yellow gravelly clay loam. Depth to bedrock is about 40 to 60 inches.

Fagan – This deep, well-drained soil weathered from soft sandstone and shale. Depth to bedrock is about 40 to 60 inches. Permeability is slow, available water capacity is moderate or high and runoff is medium. The surface layer is brown loam over grayish brown clay loam (19 inches thick). The upper 7 inches of the subsoil is yellowish brown clay loam and the lower 17 inches is yellowish brown clay. 102 – Accelerator-Fagan-Urban land – This unit is 35 percent Accelerator loam, 25 percent Fagan loam, and 25 percent Urban land.

Accelerator – This deep, well-drained soil weathered from soft sandstone and siltstone. Depth to bedrock is about 40 to 60 inches. Permeability is moderately slow, available water capacity is moderate or high, and runoff is medium. The surface layer is light gray and light brownish gray loam (23 inches thick). The upper six inches of the subsoil is light gray clay loam and the lower 12 inches is yellow gravelly clay loam.

Fagan – This deep, well-drained soil weathered from soft sandstone and shale. Depth to bedrock is about 40 to 60 inches. Permeability is slow, available water capacity

is moderate or high and runoff is medium. The surface layer is brown loam over grayish brown clay loam (19 inches thick). The upper 7 inches of the subsoil is yellowish brown clay loam and the lower 17 inches is yellowish brown clay.

Urban land – Consists of areas covered by asphalt, concrete, buildings, and other structures. The material covered by these structures is similar to the Acclerator and Fagan soils.

103 – Alambique sandy loam – This moderately deep, well-drained soil weathered from hard sandstone. Permeability is moderate, available water capacity is low or moderate, and runoff is rapid or very rapid. The surface layer is brown sandy loam (6 inches) and the underlying material (to 30 inches) is brown and grayish brown loam. Depth to bedrock ranges from 20 to 40 inches.

104 – Alambique-McGarvey complex – This unit is 45 percent Alambique gravelly loam and 35 percent McGarvey loam. Included in this unit are small areas of soils that are similar to the Alambique and McGarvey soils but are more than 40 inches deep to bedrock. Also included are small areas of Rock outcrop, soils similar to the Alambique but depth to bedrock is less than 20 inches, and Maymen soils that are similar to the McGarvey soil bur are loamy throughout.

Alambique – This moderately deep, well drained soil weathered from hard sandstone. Permeability is moderate, available water capacity is low or moderate, and runoff is rapid or very rapid. The surface layer is brown and yellowish red gravelly loam (12 inches) and the underlying material (to 30 inches) is reddish yellow gravelly loam. Depth to bedrock ranges from 20 to 40 inches.

McGarvey – This moderately deep, well-drained soil weathered from soft sandstone. Depth to bedrock ranges from 20 to 40 inches. Permeability is slow, available water capacity is low or moderate, and runoff is rapid or very rapid. The surface layer is pinkish gray and light brown loam about 7 inches thick. The upper 20 inches of the subsoil is light reddish brown clay loam, and the lower 10 inches is reddish brown clay.

105 – Barnabe-Candlestick complex – This unit is 45 percent Barnabe very gravelly sandy loam and 35 percent Candlestick fine sandy loam. These two soil types intermingle in a complex fashion and were therefore mapped as one unit. Included in this unit are small areas of Kron and Buriburi soils, Rock outcrop, and Candlestick Variant soils.

Barnabe – This very shallow, well-drained soil weathered from hard, fractured sandstone. Depth to bedrock ranges from 8 to 20 inches, permeability is moderate, available water capacity is low, and runoff is rapid or very rapid. The soil is dark grayish brown very gravelly sandy loam (12 inches).

Candlestick – This moderately deep, well-drained soil weathered from hard, fractured sandstone. Depth to bedrock ranges from 20 to 40 inches, permeability is moderately slow, available water capacity is low to moderate, and runoff is rapid or very rapid. The surface layer is 14 inches thick. The upper part is brown fine sandy loam and the lower part is brown loam. The subsoil is pale brown sandy clay loam about 10 inches thick.

106 – Barnabe-Rock outcrop complex – This unit is 40 percent Barnabe very gravelly sandy loam and 40 percent Rock outcrop. Included in this unit are small areas of Kron, Buriburi, and Candlestick soils.

Barnabe – This very shallow and shallow, well drained soil weathered from hard, fractured sandstone. Depth to bedrock ranges from 8 to 20 inches, permeability is moderate, and available water capacity is very low, and runoff is rapid or very rapid. The soil is dark grayish brown very gravelly sandy loam (12 inches).

Rock outcrop – Consists mainly of exposures of hard, fractured sandstone.

107 – Botella loam – This very deep, well-drained soil formed in alluvium derived from various rocks. Permeability is moderate, available water capacity is very high, and runoff is slow. The surface layer is dark grayish brown loam about 36 inches thick. The upper 13 inches of the subsoil is dark grayish brown clay loam, and the lower part to a depth of 60 inches or more is brown clay loam.

108 – Botella-Urban land complex – This unit is 45 percent Botella clay loam and 30 percent Urban land. Included in this unit are small areas of Orthents, and cut and fill.

Botella – This very deep, well-drained soil formed in alluvium derived from various kinds of rock. Permeability is moderate, available water capacity is very high, and runoff is slow. The surface layer is dark grayish brown clay loam about 6 inches thick. The upper 11 inches of the subsoil is dark grayish brown clay loam, and the lower part to a depth of 60 inches or more is brown clay loam.

Urban land – Consists of areas covered by asphalt, concrete, buildings, and other structures. The material covered by these structures is similar to the Botella loam.

109 – Candlestick-Barnabe complex – This unit is 45 percent Candlestick fine sandy loam and 25 percent Barnabe very gravelly sandy loam. Included in this unit are areas of Kron and Buriburi soils; Rock outcrop; and Orthents, cut and fill.

Candlestick – This moderately deep, well-drained soil weathered from hard, fractured sandstone. Depth to bedrock ranges from 20 to 40 inches, permeability is moderately slow and available water capacity is low to moderate. The surface layer is 14 inches thick. The upper part is brown fine sandy loam and the lower part is brown loam. The subsoil is pale brown sandy clay loam about 10 inches thick.

Barnabe – This very shallow and shallow, well drained soil weathered from hard, fractured sandstone. Depth to bedrock ranges from 8 to 20 inches, permeability is moderate, available water capacity is very low, and runoff is rapid. The soil is dark grayish brown very gravelly sandy loam (12 inches).

110 – Candlestick-Kron-Buriburi complex – This unit is 40 percent Candlestick fine sandy loam, 25 percent Kron sandy loam, and 20 percent Buriburi gravelly loam. These intricately mingled soils were mapped together.

Candlestick – This moderately deep, well-drained soil is weathered from hard, fractured sandstone. Depth to bedrock ranges from 20 to 40 inches, permeability is moderately slow and available water capacity is low to moderate. The surface layer is 14 inches thick. The upper part is brown fine sandy loam and the lower part is brown loam. The subsoil is pale brown sandy clay loam about 10 inches thick.

Kron – This shallow, well-drained soil weathered from hard, fractured sandstone. Depth to bedrock ranges from 10-20 inches, permeability is moderate, available water capacity is very low, and runoff is rapid to very rapid. Typically, the surface layer is dark

brown and brown loam about 21 inches thick. The subsoil is yellowish brown clay loam to a depth of 60 inches or more.

Buriburi – This moderately deep, well-drained soil weathered from hard, fractured sandstone. Depth to bedrock ranges from 20-40 inches, permeability is moderately slow, available water capacity is low, and runoff is rapid to very rapid. The surface layer is dark grayish brown gravelly loam. The depth to bedrock ranges from 20 to 40 inches.

111 – Candlestick Variant loam – This very deep, well-drained soil formed from various kinds of rock. Permeability is moderately slow, available water capacity is very high, and runoff is slow or medium. Typically, the surface layer is dark brown and brown loam about 21 inches thick. The subsoil is yellowish brown clay loam to a depth of 60 inches or more.

112 – Candlestick Variant loam – This very deep, well-drained soil formed from various kinds of rock. Permeability is moderately slow, available water capacity is very high, and runoff is rapid. Typically, the surface layer is dark brown and brown loam about 21 inches thick. The subsoil is yellowish brown clay loam to a depth of 60 inches or more.

113 – Fagan loam – This deep, well-drained soil weathered from soft sandstone and shale. Permeability is slow, available water capacity is moderate or high and runoff is rapid or very rapid. Depth to bedrock is about 40 to 60 inches. The surface layer is brown loam over grayish brown clay loam (19 inches thick). The upper 7 inches of the subsoil is yellowish brown clay loam and the lower 17 inches is yellowish brown clay.

114 – Francisquito-Urban land complex – This unit is 45 percent Francisquito loam and 35 percent Urban land. Included in this unit are small areas of Botella, Fagan, and Los Gatos soils and Orthents, cut and fill.

Francisquito – This very deep, well-drained soil formed in alluvium derived from various kinds of rock. Permeability is slow, available water capacity is very high and runoff is medium. The surface layer is light yellowish brown loam (16 inches). The upper 10 inches of the subsoil is a combination of yellowish brown, light yellowish brown, brown, and strong brown clay loam. The lower portion to a depth of 60 inches or more is light yellowish brown, yellowish brown, and brown clay.

Urban land – Consists of areas covered by asphalt, concrete, buildings, and other structures. The material covered by these structures is similar to the Francisquito soil.

115 – Los Gatos loam – This moderately deep, well-drained soil weathered from hard, fractured sandstone. Depth to bedrock ranges from 20 to 40 inches, permeability is moderately slow, available water capacity is low or moderate, and runoff is rapid or very rapid. The surface layer is dark grayish brown and light yellowish brown loam (22 inches). The subsoil is reddish yellow sandy clay loam (14 inches).

116 – Maymen gravelly loam – This shallow, well drained soil weathered from sandstone. Depth to bedrock ranges from 10 to 20 inches, permeability is moderate, available water capacity is very low, and runoff is rapid. The surface layer is pale brown gravelly loam (4 inches). The subsoil to a depth of 12 inches is reddish yellow gravelly loam.

117 – Novato clay – This very deep, very poorly drained soil formed in alluvium derived from various kinds of rocks. Permeability is slow, available water capacity is low, and runoff is very slow. The surface layer is gray clay (6 inches). The upper 10 inches of subsoil is light olive gray clay, and the lower part to a depth of 60 inches or more is gray and dark gray clay.

118 – Novato clay -- This very deep, very poorly drained soil formed in alluvium derived from various kinds of rocks. Permeability is slow, available water capacity is low, and runoff is very slow. The surface layer is gray and light olive gray clay (16 inches). The upper 14 inches of subsoil is gray clay, the next 15 inches is dark gray clay, and the lower part to a depth of 60 inches or more is gray clay.

119 – Obisbo clay – This shallow, well-drained soil weathered from hard, serpentinitic rock. Depth to bedrock ranges from 10 to 20 inches, permeability is slow, available water capacity is very low, and runoff is medium. The soil is dark gray and very dark gray clay (12 inches).

120 – Obisbo clay – This shallow, well-drained soil weathered from hard, serpentinitic rock. Depth to bedrock ranges from 10 to 20 inches, permeability is slow, available water capacity is very low, and runoff is rapid. The soil is dark gray and very dark gray clay (12 inches).

121 – Orthents, cut and fill – This very shallow to very deep, well drained soil formed in alluvium and residium derived dominantly from hard or soft sandstone. This soil varies greatly in thickness and texture. Runoff is moderate. Included in this unit are deep, dark alluvial soils that are loam or fine sandy loam throughout.

122 – Orthents, cut and fill – These very shallow to very deep, well-drained soils are on uplands. The soils formed in residium derived dominantly from sandstone. This unit consists of soils that have been cut and filled for urban development. They vary greatly in thickness and texture because of the difference in kind and type of fill; runoff is rapid or very rapid.

123 – Orthents, cut and fill-Urban land complex – This unit is 70 percent Orthents, cut and cut and fill, and 35 percent Urban land.

Orthents -- These deep and very deep, poorly drained to well drained soils consist of areas that have been cut and filled for urban development. They vary greatly in thickness and texture because of the difference in kinds and type of fill. Runoff is slow.

Urban land – This land consists of areas that are covered by asphalt, concrete, buildings, and other structures. The material covered by these structures consists of soils similar to the Orthents.

124 – Orthents, cut and fill-Urban land complex – This unit is 50 percent Orthents, cut and fill, and 35 percent urban land. Included in this unit are small areas of Fagan and Obisbo, Maymen, and Los Gatos soils.

Orthents – This soil has been cut and filled for urban development, varies greatly in thickness and texture of the surface layer. Areas in the steeper areas contain outcropping rock. This unit contains highly variable properties and characteristics and runoff is medium to very rapid.

Urban land – This land consists of areas covered by asphalt, concrete buildings, and other structures. The material covered by these structures is similar to the Orthents.

125 – Pits and Dumps – This unit consists of gravel pits, refuse dumps, and rock quarries.

126 – Reyes clay – This very deep, somewhat poorly drained soil formed in alluvium from various kinds of rocks. Permeability is slow, available water capacity is very high, and runoff is very slow. The soil is gray clay to a depth of 60 inches or more.

127 – Rock outcrop-Orthents complex – This unit consists of long and narrow, generally rocky areas that rise abruptly along the coastline. The unit is 45 percent Rock outcrop and 45 percent Orthents. Rock outcrop consists of sandstone, shale, and igneous rock.

Orthents – This unit consists of mixed alluvium of varying depths, areas of loamy soils that are less than 10 inches thick, and pockets of windblown sand. Small areas of Miramar, Scarper, and Sirdak soils and Typic Argiustolls are found in this unit.

129 – Sirdak sand – This very deep, somewhat excessively drained soil is on coastal dunes and formed in eolian sand. The depth to bedrock is 60 inches or more. Included in this unit are small areas of Dune land, beaches, Typic Argiustolls, and soils that are similar to the Sirdak soil but have sandstone, chert, a cemented layer, and clayey subsoil.

130 – Typic Argiustolls, loamy-Urban land association – This unit is 50 percent Typic Argiustolls, loamy, and 30 percent Urban land.

Typic Argiustolls – This soil is loamy, deep, and well drained. They formed in alluvium derived from coastal sediment. The texture consists of sandy loam or sandy clay loam 10 to 20 inches thick. The subsoil to a depth of 60 inches or more is clay loam, sandy clay loam, clay, or sandy clay that is 25-45 percent clay. Permeability is moderately slow or slow, available water capacity is high and runoff is medium.

Urban land – This land consists of areas covered by asphalt, concrete or other structures overlying soils similar to Typic Argiustolls. Included in this unit are small areas of Candlestick, Candlestick Variant, Miramar, Obisbo, Sirdak, and Scarper soils.

131 – Urban land – This unit consists of areas where more than 85 percent of the surface is covered by asphalt, concrete, buildings and other structures overlying soil similar to Orthents.

132 – Urban land-Orthents, cut and fill complex – This unit is on coastal terraces and alluvial fans. This unit is 50 percent Urban land and 45 percent Orthents cut and fill. The material covered by urban land is similar to Orthents. The Orthents are deep and are loam or clay loam. In most areas the texture varies greatly, because it has been graded and moved and fill material has been added. Included in this unit are areas of Botella soils; Orthents reclaimed; Sirdak soils; and deep alluvial soils that are loam or fine sandy loam throughout. Included soils make up about 5 percent.

133 – Urban land-Orthents, cut and fill complex – This unit is 50 percent Urban land and 40 percent Orthents, cut and fill. The material covered by the Urban land is similar to the Orthents.

134 – Urban land-Orthents, reclaimed complex – This unit is in areas that were once part of San Francisco Bay and adjacent tidal flats. It is about 65 percent Urban land and 30 percent Orthents.

135 – Urban land-Orthents – This unit is on coastal terraces, hills, and ridge tops. It consists of 65 percent Urban land and 25 percent Orthents, smoothed. Included in this unit are small areas of loamy sand or silty loam that have characteristics similar to the Orthents.

Orthents – This well drained soil has been cut and filled for home site and urbad development. The fill material in these soils formed in soft sandstone and is generally fine sandy loam or loam. Runoff is medium to rapid.

Urban land – This unit consists of areas where more than 85 percent of the surface is covered by asphalt, concrete, buildings and other structures overlying soil similar to the Orthents.

136 – Urban land-Sirdak complex – This unit is on stabilized dunes. It consists of 45 percent Urban land and 35 percent Sirdak sand. Included in this unit are small areas of soil that similar to the Sirdak soil but are underlain by sandstone, shale, or chert at depths less than 40 inches.

Sirdak – This very deep and somewhat excessively drained soil formed in eolian material derived dominantly from beach sand. The depth to bedrock is > 60 inches, permeability is rapid, available water capacity is low, and runoff is slow. The surface layer is dark brown and dark yellowish brown sand (17 inches). The underlying material to a depth of 60 inches or more is yellowish brown sand.

137 – Zeni-Zeni Variant gravelly loams – This unit is 40 percent Zeni gravelly loam and 35 percent Zeni Variant gravelly loam. Included in this unit are small areas of Alambique and Maymen soils that are similar to the Zeni soil but have more clay in the subsoil.

Zeni – This moderately deep, well-drained soil weathered from sandstone. Depth to bedrock ranges from 20 to 40 inches. Permeability is moderate, available water capacity is low or moderate, and runoff is rapid or very rapid. The surface layer is pale brown gravelly loam (9 inches). The upper 9 inches of the subsoil is reddish yellow gravelly clay loam, and the lower 8 inches is very pale brown gravelly clay loam.

Zeni Variant – This moderately deep, well-drained soil weathered from metasedimentary rock. Depth to bedrock ranges from 20 to 40 inches, permeability is moderately slow, available water capacity is low or moderate, and runoff is rapid or very rapid. The surface layer is very dark grayish brown and dark grayish brown gravelly loam (13 inches). The upper 18 inches of the subsoil is pale brown and very pale brown

very gravelly clay loam, and the lower 8 inches is light yellowish brown gravelly clay loam.

146 – Urban land – This area consists of land that is covered by buildings, roads, parking lots, and other urban structures. The soil is mainly heterogeneous fill.

147 – Urban land-Baywood complex – This complex is 60 percent Urban land, 35 percent Baywood loam, and 5 percent other soils including laugenour loam, and Omni silty clay loam.

Urban land – This area is covered by buildings and other structures. The soil material has been altered or mixed but it closely resembles the Baywood complex.

Baywood complex – This very deep, somewhat excessively drained soil formed in eolian sediment that derived from old beach deposits. Permeability is rapid, available water capacity is 4.0 to 5.5 inches, and runoff is slow to medium. The surface layer is grayish brown and brown (32 inches). The underlying material is pale brown and light yellowish brown, loamy sand and extends to 60 inches or more.

148 – Urban land-Clear Lake complex – This complex is 55 percent Urban land and 35 percent Clear Lake clay on basin rims. Included in this unit are Omni silty clay loam and Marvin silty loam.

Urban land -- This area is covered by buildings and other structures. The soil material has been altered or mixed during urban development.

Clear Lake – This very deep, poorly drained soil formed in alluvium derived mainly from sedimentary rock. Permeability is slow, available water capacity is 7.0 to 9.5, and runoff is slow. The surface layer is very dark gray (37 inches). The underlying

material is dark gray and grayish brown, calcareous clay and silty clay and extends to depths of 60 inches or more.

149 – Urban land-Danville complex – This complex is 60 percent Urban land and 30 percent Danville silty clay loam. Included in this complex are small areas of Botella loam, Clear lake clay, and Tierra loam.

Urban land – This area is covered by buildings and other structures. The soil material has been altered or mixed during urban development.

Danville – This very deep, well-drained soil formed in alluvium derived mainly from sedimentary rock. Permeability is slow, available water capacity is 8.5 to 10.5 inches, and runoff is slow. The surface layer is grayish brown and dark gray silty clay loam (21 inches). The subsoil extends to a depth of 61 inches and is grayish brown, silty clay, silty clay loam, and heavy silty clay loam. The substratum is grayish brown, silty clay loam and extends to depths of 80 inches or more.

APPENDIX B

Example 1:

Select the 110km buffered interval. Convert the selected feature to a shapefile named 110km.shp. Next, use the geoprocessing wizard to clip bedrock.shp to the extent of 110km.shp, which results in a shapefile (110_bed.shp) that shows all the bedrock sites located between 108 and 110 km from the epicenter of the Loma Prieta quake. Then, highlight 110_bed.shp in the data menu and choose the summarize zones option. Select Ptype as the bedrock field for analysis and radial as the grid used for summarization. The result is a table showing statistics (std. deviation, mean, median, hi, lo, etc) for 110_bed. Determine the mean radial acceleration due to bedrock (98 cm/s/s). Convert 110km.shp to a grid. Set the 110km grid as a mask in the Surface menu option. Use the map calculator and type the formula ([Radial]/[98]) and click the button "calculate." The output is a grid showing the radial acceleration due to all the material located above the surface of the bedrock within the 110-108 km range. Rename this calculated grid as rad110. Highlight soils.shp in the data menu and choose summarize zones. Select "id" as the grid field for calculation and rad110 as the grid for summary. The result is a table showing statistics (std. Dev., mean, median, high, lo, etc.) for each polygon id found within the 110-108 km interval range. Highlight the id field in this summarization table. Pull up the soil data table. Highlight the id field in the soil data table. Use the join option to join the two tables. The resulting table shows the mean soil/bedrock radial acceleration for each polygon which contains fields texture, clay content, drainage, etc.). Export the table as an ASCII file named 110.txt. Display 110.txt in EXCEL. Delete all

unnecessary fields and clear contents of all values equal to zero. Save as 110.xls and open the data file in SPSS. Correlate mean soil/bed radial acceleration with texture, clay content, etc. Use Spearman's and Pearson's statistical tests with the "eliminate pairs list wise" option. This eliminates all pairs when at least one pair does not contain a value. Save results as SPSS files.

Example 2:

Purchase the maps from the USGS. Orient all maps to the same coordinate system using at least 5 control points. An accuracy of at least 10 meters should be achieved. For this work, maps were registered to the geographic lat/long coordinate system. Digitize each map using Capture 3.1 software. Set up the program to record point data along equal contour lines at a spacing of 1 millimeter. Set a dummy reference elevation to +10,000 feet to eliminate negative attribute values. For example, the surface contour is –250 feet with respect to mean sea level. The recorded attribute is 9750. Digitize all faults as separate point coverage's with attributes of latitude, longitude, and the name of the fault. The only faults in these maps occur on the San Francisco South quadrangle and are the San Andreas, San Bruno, and Serra Faults. Convert all points to the appropriate coordinate system. Because the program collected the data in degrees, the Blue Marble Calculator was used to convert the point coordinates from degrees to decimal degrees and saved as text files. Combine all the necessary text files to form one long list of points, with associated latitude, longitude, and elevation. Subtract 10,000 feet from all elevations. Import the text files into Surfer 7.0. Use the fault text files as blanking during the interpolation process. Chose an interpolation process. Kriging was implemented in this task. Download the appropriate Digital Elevation Models from a

free web site. For this project DEMs from the San Francisco North and San Francisco South Quadrangles were downloaded from the USGS web site. Import the DEMs into ArcInfo 8 using the Spatial Data Transfer System (SDTS) to Coverage Wizard. If necessary, convert the DEM from meters to feet using the following model in Imagine: Sfn*3.3 and SFS*3.3

Finally, subtract the interpolated elevation values from the DEM elevation values. The result is a grid showing the depth to the bedrock and is shown in Figure 20.

Example 3:

Using ArcView, buffer the Loma Prieta epicenter point coverage at 10 km intervals with 11 intervals (all soil data is <110 km from the epicenter). Add a numerical field to Age called polygon and assign each polygon a different number (i.e. 1, 2, 3, 4, etc). Select the 70-80 km interval and convert it to a shapefile called 80km. Use the geoprocessing wizard extension to clip both data layers Age and 1989 Intensity to the extent of the 80 km shapefile. Highlight the clipped Age coverage and chose from the menu Summarize Zones. Use the field "polygon" from Age as input values. When prompted for the second data layer for summarization, navigate to the clipped 1989 Intensity grid and use "intensity" as input values. The result of the summarization process is a table showing average intensity values for each different Age polygon. Highlight the field labeled "polygon." Next, pull up the original age table and highlight the polygon field. Join the two fields together and delete all fields except "Age" and "Intensity." Sort both columns together with respect to "Age". Delete all value pairs that reflect an age of "0" reflecting the age of water. Next sort both columns together with respect to "Intensity". Delete all value pairs that show intensity of "0" which also should reflect intensity measured at

water sites. The table now shows a list of different deposit ages and the corresponding average intensity calculated for the extent of each age polygon. Export the table as a text file named 1989Age_80. Open a statistical package such as SPSS. Import the data (1989Age_80). Chose the "correlate data" option and use Age and Intensity values as inputs. Choose both Spearman and Pearson's test with 95% confidence limits. The result is two correlation coefficients for the two input data layers.